Design of Two-dimensional TiO_2 based Nanomaterials for Sustainable Applications

Yuanwen Zhang

B. Eng & MA. Eng

Submitted in fulfilment of the requirements for the degree of

Doctor of Philosophy

School of Chemistry and Physics

Science and Engineering Faculty

Queensland University of Technology

2020

Keywords

Bio-inspired materials; Two-dimensional nanomaterials; Photonic structures; Energy materials; Titanium dioxide; Carbon nitride; Photocatalysis; Heterostructures; Thermal treatment; Sustainable application; Charge transfer; Nanostructures; Self-assembly; Hydrothermal.

Abstract

In the past decade, two-dimensional (2D) nanomaterials have drawn significant interests due to its salient physical, chemical and electronic properties aroused by the confined thickness and large surface area. Ultrathin two-dimensional (2D) nanomaterial is a big family representing a promising type of nanomaterials that possess sheet-like mophologies with only single- or few-atoms thickness. With such excellent features endowed by 2D structural characteristics, 2D nanomaterials have been proven to be successfully applied in a wide range of areas, including photocatalysis, electrocatalysis, energy storage and conversion devices, water splitting and so on.

In this thesis, the design of 2D TiO_2 based nanomaterials for sustainable applications such as photocatalysis, electrocatalysis, rechargeable batteries and bio-inspired applications are discussed in detail. Three research works "structure-induced charge unsaturation and wide-band light adsorption for enhanced photocatalytic performance", "strongly interfacial-coupled 2D-2D TiO_2/g-C_3N_4 heterostructure for enhanced visible-light induced synthesis and conversion" and "2D-TiO_2 nanosheets as substrates for Pt photocatalyst" are presented respectively.

Given their unique structural characteristics, superior properties and potential applications, 2D nanomaterials have become one of the most popular research hotspots in various fields. We believe that the research and investigations on 2D nanomaterials is of great significance for the further development of this promising field.

Table of Contents

List of Figures

Chapter 2.

Chapter 3.

Chapter 5.

List of Tables

List of Abbreviations

2D	Two-dimensional
3D	Three-dimensional
TMO	Transition metal oxide
TMD	Transition metal dichalcogenide
vdW	van der Waals
CVD	Chemical vapor deposition
SEM	Scanning electron microscope
TEM	Transmission electron microscope
EG	Ethylene glycol
XPS	X-ray photoelectron spectroscopy
BET	Brunauer-Emmett-Teller
GO	Graphene oxide
FT-IR	Fourier transform infra-red
AFM	Atomic force microscope
NPs	Nanoparticles
TGA	Thermal gravimetric analysis
OER	Oxygen evolution reaction
UV	Ultraviolet-visible
ORR	Oxygen reduction reaction
XRD	X-ray diffractometer
PL	Photoluminescence
TTIP	Titanium (IV) isopropoxide

List of Publications

[1] ***Y. Zhang****, J. Mei, C. Yan, T. Liao, J. Bell, Z. Sun*,* Bioinspired 2D nanomaterials for sustainable applications, ***Advanced Materials,*** 32 (2019) 1902806. *Selected and highlighted as Advanced Materials Frontispiece.*

[2] ***Y. Zhang****, J. Xu, J. Mei, S. Sarina, Z. Wu, T. Liao, C. Yan, Z. Sun*,* Strongly interfacial-coupled 2D-2D TiO_2/g-C_3N_4 heterostructure for enhanced visible-light induced synthesis and conversion, ***Journal of Hazardous Materials,*** 394 (2020) 122529.

[3] *J. Mei,* ***Y. Zhang,*** *T. Liao, X. Peng, G. A. Ayoko, Z. Sun*,* Black phosphorus promoted lithium storage for TiO_2-based anodes: widening potential window with enlarged capacity. ***Energy Storage Materials,*** 19 (2019) 424-431.

[4] *J. Mei,* ***Y. Zhang,*** *T. Liao, Z. Sun*, S. X. Dou,* Strategies for improving the lithium-storage performance of two-dimensional nanomaterials. ***National Science Review,*** 5 (2018) 389-416.

Statement of Original Authorship

The work contained in this thesis has not been previously submitted to meet requirements for an award at this or any other higher education institution. To the best of my knowledge and belief, the thesis contains no material previously published or written by another person except where due reference is made.

Signature: QUT Verified Signature

Date: 02/10/2020

Acknowledgements

I would like to express my deep gratitude to all the people and groups whoever have been helping me during my whole PhD study in QUT. I cannot finish my study successfully without their kind support.

Firstly, I want to thank the supervisor team: many thanks to my principle supervisor A/Prof. Ziqi Sun for his significance guidance, timely assistance and full support during my PhD study in QUT. Also, many thanks to my associate supervisor Prof. Chen Yan for his useful discussion and careful proof for my manuscripts.

Secondly, I want to express my thanks to the QUT technicians who have been helping me with all the experiments: Dr. Jamie Riches, Dr. Rachel Hancock, Dr. Elizabeth Graham, Dr. Josh Lipton-Duffin, Dr. Henry Spratt, Dr. Peter Hines, Dr. Llew Rintoul, Dr. Sanjleena Singh, and Dr. Tony Wang in the Central Analytical Research Facility (CARF) of QUT. Also, thanks to Peter Hegarty, Leonora Newby and Karen Rands-Trevor in the labs of E block of QUT.

Also I want to thank my group members and collaborators, thanks to the help from Mr. Jun Mei, Mr. Ziyang Wu. And thanks to the help and support from Prof. Huaiyong Zhu, A/Prof. Jingsan Xu, Dr. Sarina Sarina, A/Prof. Ting Liao, Prof. John Bell, A/Prof. Xiaomin Peng.

More importantly, I want to thank my parents and my wife for their kind support and encouragement in my life.

Lastly, special thanks are sent to QUT for the scholarship that support my living and studying in Australia.

Chapter 1. Introduction

This thesis mainly focuses on the design of 2D TiO_2-based nanomaterials for sustainable application such as photocatalysis, electrocatalysis, rechargeable batteries and bio-inspired applications. The emphasis of this thesis has been put on the design and synthesis of a serious of 2D nanomaterials including 2D-TiO_2, 2D-Co_3O_4, 2D-MnO_2, 2D-Fe_3O_4, g-C_3N_4 and the derived hybrids or compounds based on such 2D nanomaterials. The as-prepared 2D nanomaterials or 2D-based compounds have been characterised and applied in different sustainable applications and showed superior properties in photocatialysis, electrocatalysis or rechargeable batteries.

This chapter firstly outlines the background (section 1.1). Then the objectives and problems of the research are proposed in section 1.2. Section 1.3 further describes the significance and scope of this research. Finally, section 4 includes an outline of the remaining chapters of the thesis.

1.1 Research Background

In the past decade, two-dimensional (2D) nanomaterials have drawn significant interests due to its salient physical, chemical and electronic properties aroused by the confined thickness and large surface area.[1-3] With such excellent features endowed by 2D structural characteristics, 2D nanomaterials have been proven to be successfully applied in a wide range of areas, including photocatalysis, electrocatalysis, energy storage and conversion devices, water splitting and so on.[4-7] 2D metal oxides have been playing an important role in the family of 2D nanomaterials, as most of them are semiconductors and exhibit unique band structures which show great potential for optoelectronic devices and solar energy harvesting and conversion applications.[8-10]

Although extensive research progress has been achieved in the field of 2D nanomaterials, such as the development of different synthetic methods, discovery of their structures and properties, and exploration of their potential applications, challenges still remain.[11,12] Great efforts on pursuing precise control over their structures and properties and then realization of their practical applications never stop. Specifically, how to improve the existing synthetic approaches or develop new synthetic methods for scale-up production of 2D nanomaterials still requires great research efforts.[13] Besides, obtaining precise control over their compositions, thicknesses, lateral sizes, crystal phases, doping, defects, strains, vacancies and surface properties becomes increasingly important to unveil the correlations between the structural features and properties.[14, 15] Significantly, recent years have witnessed great research efforts in the interface, defect and crystal-phase engineering of 2D nanomaterials.[16-18] In addition, integration among various 2D nanomaterials to realize synergistic effects also deserves more research focus.

To better utilize the visible range of the solar spectrum for the photocatalytic reactions, modifying the chemical state and electronic structure of the catalysts has been identified as a desirable strategy.[19-21] Therein, the most important route is to introduce defects into the lattice structures of the catalysts by doping heteroatom elements or creating intrinsic vacancies.[22-25] Such defect center acting as an electron donor or acceptor can effectively adjust the electronic states of the catalysts, making the activated carries better contribute to the redox reactions.[26, 27] However, on the other hand, the created defects could also act as recombination centers for the excited charge carriers, which will lower the utilizing efficiency of the charge and result in relatively low catalytic activities.[28, 29] In addition, it is also challenging to incorporate dopants or vacancies into highly-crystalized catalytic materials by mild

synthetic methods and conditions, thus making the synthetic process less cost-effective.[30] Engineering the compressive strain of the catalyst surface is believed to be another effective way to realize some unconventional electronic structures and improve the catalytic performance of catalysts.[31] It is reported that the engineering of surface strain on the catalyst could result in different binding behavior between the oxygen species and the catalyst surface during the reaction process.[32, 33] Nevertheless, such strain engineering are usually constructed on the basis of ordered intermetallic phases with high transition metal component, and are not easy to be realized in homogeneous metal oxide semiconductor materials.

In 2009, Wang et al. found that graphitic carbon nitride (g-C_3N_4), a non-metal semiconductor material with van der Waals layered 2D nanostructure, could generate hydrogen from water under visible-light irradiation, ever since then, g-C_3N_4 has drawn dramatic attention in the field of photocatalysis.[34, 35] Pristine g-C_3N_4 is composed with two of the most earth-abundant elements, it is chemically and thermally stable, environmental friendly and cost-effective, and most importantly, it has a bandgap of 2.7 eV which is favourable for visible-light absorption.[36, 37] Although g-C_3N_4 has so many advantages, the high carrier recombination rate hinder it from being a perfect photocatalyst. In order to overcome this problem, researchers have developed a variety of modification strategies to improve the photocatalytic performance of g-C_3N_4, among which constructing g-C_3N_4 based heterojunctions has been considered as an effective approach to separate the photo-induced carries from recombination and thus enhance the photocatalytic activity.[38, 39] To date, many kinds of materials have been reported to be coupled with g-C_3N_4 and form heterojunctions which present improved photocatalytic activities, including but not limited to TiO_2, SnO_2, WO_3, ZnO, SnS_2, MOF, etc.[40, 41] As g-C_3N_4 itself is a typical 2D nanomaterial, the g-C_3N_4

based heterojunctions can be classified into three types on the basis of the geometry of the materials that are coupled with it, named “0D/2D”, “1D/2D” and “2D/2D” heterojunctions. Among them, the 2D/2D heterojunctions obviously have a significant advantage that the lager 2D/2D face-to-face interface will lead to higher contact area and better charge transfer efficiency compared to the point-to-face interface of 0D/2D heterojunctions and the line-to-face interface of 1D/2D heterojunctions.

1.2 Research Objectives and Problems

The premier goal of this research is to design optimized 2D titanium dioxide-based nanostructures with outstanding performance in various sustainable areas, such as photocatialysis, electrocatalysis, rechargeable batteries and bio-inspired applications. To achieve this objective, there are a serious of research problems that need to be solved in this project:

- What advantages do 2D nanomaterials have compared with other 0D, 1D or 3D materials?
- How to synthesize high-quality 2D TiO_2-based nanomaterials?
- How expand the application of TiO_2-based nanomaterials to visible-light driven photocatalysis?
- Which types of 2D nanomaterials are most suitable for a specific applications, i.e. photocatalysis, electrocatalysis or rechargeable batteries?
- How to design an optimised 2D nanostructure to improve its performance in photocatalysis, electrocatalysis or rechargeable batteries?
- How to design a 2D-2D heterostructured nanomaterials with high performance in photocatalysis?

1.3 Significance of Research

The significance of this research can be summarized into following points:

- A new strategy to modify the chemical state and electronic structure of metal oxide semiconductor are realized by manipulating the crystal structure of homogeneous 2D nanosheets.
- A further step towards visible-drive organic reaction using TiO_2 as photocatalyst.
- An intimately coupled 2D-2D heterostructured nanomaterials has been achieved by in situ wet-chemistry approach.
- The review of bio-inspired 2D nanomaterials for sustainable applications offer insights towards a green and sustainable society.

1.4 Thesis Outline

This report mainly include five chapters. Chapter 1 presents a brief introduction of the whole project. A summarized literature review including 2D nanomaterials for photocatalysis, electrocatalysis, rechargeable batteries and bio-inspired 2D materials are presented in chapter 2. Chapter 3, 4 and 5 present the research works of "structure-induced charge unsaturation and wide-band light adsorption for enhanced photocatalytic performance", "strongly interfacial-coupled TiO_2/g-C_3N_4 2D-2D heterostructured nanostructures for enhanced visible-light induced synthesis and conversion" and "2D-TiO_2 nanosheets as substrates for Pt photocatalyst" respectively. Finally, the conclusions and outlooks of this thesis are summarized in chapter 6.

Reference

[1] X. Xiao, H. Wang, P. Urbankowski, Y. Gogotsi, Chem Soc Rev 2018, 47, 8744.

[2] B. Liu, K. Zhou, Progress in Materials Science 2019, 100, 99.

[3] J. Mannix, B. Kiraly, M. C. Hersam, N. P. Guisinger, Nature Reviews Chemistry 2017, 1.

[4] J. Mei, T. Liao, G. A. Ayoko, Z. Sun, ACS Appl Mater Interfaces 2019, 11, 28205.

[5] Y. Zhang, J. Mei, C. Yan, T. Liao, J. Bell, Z. Sun, Adv Mater 2019, e1902806.

[6] J. Mei, Y. Zhang, T. Liao, X. Peng, G. A. Ayoko, Z. Sun, Energy Storage Materials 2019, 19, 424.

[7] J. Mei, T. Liao, L. Kou, Z. Sun, Adv Mater 2017, 29.

[8] S. Das, D. Pandey, J. Thomas, T. Roy, Adv Mater 2019, 31, e1802722.

[9] P. Xiong, R. Ma, N. Sakai, T. Sasaki, ACS Nano 2018, 12, 1768.

[10] M. P. Browne, Z. Sofer, M. Pumera, Energy & Environmental Science 2019, 12, 41.

[11] K. Geim, K. S. Novoselov, Nat. Mater. 2007, 6, 183.

[12] C. N. R. Rao, A. K. Sood, K. S. Subrahmanyam, A. Govindaraj, Angew. Chem., Int. Ed. 2009, 48, 7752.

[13] K. Geim, Science 2009, 324, 1530.

[14] R. Raccichini, A. Varzi, S. Passerini, B. Scrosati, Nat. Mater. 2015, 14, 271.

[15] M. Pumera, Chem. Soc. Rev. 2010, 39, 4146.

[16] Ambrosi, C. K. Chua, N. M. Latiff, A. H. Loo, C. H. A. Wong, A. Y. S. Eng, A. Bonanni, M. Pumera, Chem. Soc. Rev. 2016, 45, 2458.

[17] D. Wang, R. Kou, D. Choi, Z. Yang, Z. Nie, J. Li, L. V. Saraf, D. Hu, J. Zhang, G. L. Graff, J. Liu, M. A. Pope, I. A. Aksay, ACS Nano 2010, 4, 1587.

[18] P. Samor ̧ V. Palermo, X. Feng, Adv. Mater. 2016, 28, 6027.

[19] M. Li, Y. Chen, W. Li, X. Li, H. Tian, X. Wei, Z. Ren, G. Han, Small 2017, 13.

[20] Z. Lian, W. Wang, G. Li, F. Tian, K. S. Schanze, H. Li, ACS Appl Mater Interfaces 2017, 9, 16959.

[21] Y. H. Hu, Angew Chem Int Ed Engl 2012, 51, 12410.

[22] S. Na Phattalung, S. Limpijumnong, J. Yu, Applied Catalysis B: Environmental 2017, 200, 1.

[23] H. Hirakawa, M. Hashimoto, Y. Shiraishi, T. Hirai, J Am Chem Soc 2017, 139, 10929.

[24] L. W. Fan Zuo, Tao Wu, Zhenyu Zhang, Dan Borchardt, and Pingyun Feng, J Am Chem Soc 2010, 132, 11856.

[25] L. L. Xiaobo Chen, Peter Y. Yu, Samuel S. Mao, Science 2011, 331, 746.

[26] A. Naldoni, M. Allieta, S. Santangelo, M. Marelli, F. Fabbri, S. Cappelli, C. L. Bianchi, R. Psaro, V. Dal Santo, J Am Chem Soc 2012, 134, 7600.

[27] X. Xin, T. Xu, J. Yin, L. Wang, C. Wang, Applied Catalysis B: Environmental 2015, 176-177, 354.

[28] W. Li, A. Elzatahry, D. Aldhayan, D. Zhao, Chem Soc Rev 2018, 47, 8203.

[29] J. Wang, P. Zhang, X. Li, J. Zhu, H. Li, Applied Catalysis B: Environmental 2013, 134-135, 198.

[30] J. Xiong, J. Di, J. Xia, W. Zhu, H. Li, Advanced Functional Materials 2018, 28, 1801983.

[31] S. Zhang, X. Zhang, G. Jiang, H. Zhu, S. Guo, D. Su, G. Lu, S. Sun, J Am Chem Soc 2014, 136, 7734.

[32] N. Z. Lingzheng Bu, Shaojun Guo, Xu Zhang, Jing Li, Jianlin Yao, Tao Wu, Gang Lu, Jing-Yuan Ma, Dong Su,Xiaoqing Huang, Science 2016, 354, 1410.

[33] A. D. Caviglia, R. Scherwitzl, P. Popovich, W. Hu, H. Bromberger, R. Singla, M. Mitrano, M. C. Hoffmann, S. Kaiser, P. Zubko, S. Gariglio, J. M. Triscone, M. Forst, A. Cavalleri, Phys Rev Lett 2012, 108, 136801.

[34] W. J. Ong, L. L. Tan, Y. H. Ng, S. T. Yong, S. P. Chai, Chem Rev 2016, 116, 7159.

[35] X. Liu, M. C. Hersam, Adv Mater 2018, 30, e1801586.

[36] J. Fu, J. Yu, C. Jiang, B. Cheng, Advanced Energy Materials 2018, 8, 1701503.

[37] C. Yang, J. Qin, Z. Xue, M. Ma, X. Zhang, R. Liu, Nano Energy 2017, 41, 1.

[38] D. K. Bediako, M. Rezaee, H. Yoo, D. T. Larson, S. Y. F. Zhao, T. Taniguchi, K. Watanabe, T. L. Brower-Thomas, E. Kaxiras, P. Kim, Nature 2018, 558, 425.

[39] R. B. Pontes, R. H. Miwa, A. J. R. da Silva, A. Fazzio, J. E. Padilha, Physical Review B 2018, 97.

[40] R. Frisenda, E. Navarro-Moratalla, P. Gant, D. Perez De Lara, P. Jarillo-Herrero, R. V. Gorbachev, A. Castellanos-Gomez, Chem Soc Rev 2018, 47, 53.

[41] D. Unuchek, A. Ciarrocchi, A. Avsar, Z. Sun, K. Watanabe, T. Taniguchi, A. Kis, Nat Nanotechnol 2019, 14, 1104.

Chapter 2. Literature Review

2.1 Advances of ultrathin 2D nanomaterials

2D nanomaterials have attracted intensive research interest in recent years, due to their salient physical and chemical properties aroused by their unique structure and morphology compared to their bulk counterparts, such as good mechanical strength, excellent chemical activities, and large specific surface area, high thermal conductivity, and tunable electronic propertiesetc.[1] In the year 2004, Novoselov and co-workers successfully produced grephene by exfoliating from graphite suing plastic tape, [2] since then, the study of ultrathin 2D nanomaterials has become one of the most popular research areas in the academic society. The 2D nanomaterials possess unique physical, chemical and electronic properties due to their 2D structural feature.[3] Graphene is one of the most famous 2D nanomaterials, which possess a series of salient properties such as high charge mobility,[2] high conductivity,[4] ultrahigh surface-to-volune ratio,[5] high Young's modulus,[6] excellent optical transmittance,[7] etc. Since graphene has been one of the most popular research hotspot due to so many advantages, other grapheme-like 2D nanomaterials have also been drawing increasing research interest.[9−11] For example, layered metal oxides, transition metal dichalcogenides (TMDs), hexagonal boron nitride (h-BN), layered double hydroxides (LDHs), and graphitic carbon nitride (g-C_3N_4) are typical graphene-like ultrathin 2D nanomaterials that exhibit classic 2D properties due to their similar structural and morphological features to that of graphene.[12-16] Based on the extensive research on grapheme and grapheme-like 2D nanomaterials, many other 2D materials were discovered in the big family of 2D nanomaterials, such as MXenes, 2D-formed noble metals,[18] 2D metal−organic frameworks (2DMOFs), 2D covalent−organic frameworks (2DCOFs),

polymers, silicene, black phosphorus (BP) and perovskites.[17-25] Demands for ideal productivity of 2D nanomaterials greatly accelerated the development of synthetic and fabrication techniques to produce 2D nanomaterials, which can be classified as top-down and bottom-up methods.[27-33] Meanwhile, the material characterization technique is also developing very fast and can be very helpful in the research of 2D nanomaterilas. To date, a wide range of characterization techniques have been successfully utilized in ultrathin 2D nanomaterilas, such as Raman spectroscopy, scanning and transmission electron microscopy (SEM and TEM), optical microscopy, X-ray photoelectron spectroscopy (XPS), X-ray diffraction (XRD) and X-rayabsorption fine structure spectroscopy (XAFS).[35-39] More importantly, due to the appealing structural, physical and chemical properties of 2D nanomaterials, a wide range of applications have been developed in 2D nanomaterilas, such as photocatalysis, electrocatalysis, energy storage and conversion devices, sensors, and biomedicine.[40-44]

Over the last few years, 2D nanomaterials have been accepted as one of the most promising research areas in material science, nanotechnology as well as material physic and chemistry, owing to the salient physical and chemical properties, unique structural characteristics and wide range of applications of 2D nanomaterials.[45] Due to the ultrathin thickness of 2D nanoamaterials, they exhibited many unique properties compared to their 3D material counterparts. For example, the strong in-plane covalent bonds combined with the ultrathin thickness make these 2D materials extreme strong but still highly flexible.[46] Owing to the 2D nature, the phonons and electrons are confined in the two dimensions, a feature that is indispensable to the realization of many of the unprecedented thermal, electronic and magnetic properties.[47] A high exposure of atoms to the surface increases their sensitivities to various external

stimulations and also facilitates material property regulations through surface engineering.[48] With emerging synthesis and fabrication techniques, 2D nanomaterials can be produced with their sizes only growing in the lateral plane, and meanwhile maintain their ultrathin thickness unchanged, resulting in ultrahigh specific surface area which is very important in a wide range of applications.[49]

As mentioned above, there are incomputable kinds of materials in the big family of 2D materials. In this thesis, we mainly focus on 2D metal oxides and carbon nitride, as well as the multicomponent compounds composited by them. 2D metal oxides are an important member in the big family of 2D materials owing to a series of salient properties.[50] The branch of 2D metal oxides has played a key role in the successful implementation of a serious of sustainable applications including photocatalysis, electrocatalysis and rechargeable batteries. Graphite carbon nitride (g-C_3N_4) is also an important 2D materials since it has been found useful in photocatalytic reactions. In 2009, Wang et al. found that graphitic carbon nitride (g-C_3N_4), a non-metal semiconductor material with van der Waals layered 2D nanostructure, could generate hydrogen from water under visible-light irradiation, ever since then, g-C_3N_4 has drawn dramatic attention in the field of photocatalysis.[51] Pristine g-C_3N_4 is composed with two of the most earth-abundant elements, it is chemically and thermally stable, environmental friendly and cost-effective, and most importantly, it has a bandgap of 2.7 eV which is favourable for visible-light absorption.

In a word, 2D nanomaterials, especially 2D metal oxide based nanomaterials, due to their excellent chemical and physical properties, cost-effective synthetic processes and broad application extending to all kinds of sustainable fields, have been accepted as one of the most promising materials to face the increasingly serious environmental challenges.

Reference

[1] H. Zhang, ACS Nano 2015, 9, 9451−9469.

[2] K. S. Novoselov, A. K.Geim, S. V. Morozov, D. Jiang, Y. Zhang, S. V. Dubonos, I. V. Grigorieva, A. A.Firsov, Science 2004, 306, 666−669.

[3] A. K. Geim, K. S. Novoselov, Nat. Mater. 2007, 6, 183−191.

[4] Zhang, Y.; Tan, Y.-W.; Stormer, H. L.; Kim, P. Nature 2005, 438, 201−204.

[5] Stoller, M. D.; Park, S.; Zhu, Y.; An, J.; Ruoff, R. S. Nano Lett. 2008, 8, 3498−3502.

[6] Lee, C.; Wei, X. D.; Kysar, J. W.; Hone, J. Science 2008, 321, 385−388.

[7] Nair, R. R.; Blake, P.; Grigorenko, A. N.; Novoselov, K. S.; Booth, T. J.; Stauber, T.; Peres, N. M. R.; Geim, A. K. Science 2008, 320, 1308−1308.

[8] Balandin, A. A.; Ghosh, S.; Bao, W.; Calizo, I.; Teweldebrhan, D.; Miao, F.; Lau, C. N. Nano Lett. 2008, 8, 902−907.

[9] Xu, M. S.; Liang, T.; Shi, M. M.; Chen, H. Z. Chem. Rev. 2013, 113, 3766−3798.

[10] Gupta, A.; Sakthivel, T.; Seal, S. Prog. Mater. Sci. 2015, 73, 44−126.

[11] Ferrari, A. C.; Bonaccorso, F.; Fal'ko, V.; Novoselov, K. S.; Roche, S.; Bøggild, P.; Borini, S.; Koppens, F. H. L.; Palermo, V.; Pugno, N.; et al. Nanoscale 2015, 7, 4598−4810.

[12] Lin, Y.; Williams, T. V.; Connell, J. W. Soluble, J. Phys. Chem. Lett. 2010, 1,277−283.

[13] Weng, Q.; Wang, X.; Wang, X.; Bando, Y.; Golberg, D. Chem. Soc. Rev. 2016, 45, 3989−4012.

[14] Li, L. H.; Chen, Y. Adv. Funct. Mater. 2016, 26, 2594−2608.

[15] Tan, C. L.; Zhang, H. Chem. Soc. Rev. 2015, 44, 2713−2731.

[16] Chhowalla, M.; Shin, H. S.; Eda, G.; Li, L. J.; Loh, K.; Zhang, H. Nat. Chem. 2013, 5, 263−275.

[17] Huang, X.; Zeng, Z. Y.; Zhang, H. Chem. Soc. Rev. 2013, 42, 1934−1946.

[18] Lv, R.; Robinson, J. A.; Schaak, R. E.; Sun, D.; Sun, Y.; Mallouk, T. E.; Terrones, Acc. Chem. Res. 2015, 48, 56−64.

[19] Zhang, J.; Chen, Y.; Wang, X. Energy Environ. Sci. 2015, 8, 3092−3108.

[20] Ong, W.-J.; Tan, L.-L.; Ng, Y. H.; Yong, S.-T.; Chai, S.-P. Chem. Rev. (Washington, DC, U. S.) 2016, 116, 7159−7329.

[21] Zhi, C.; Bando, Y.; Tang, C.; Kuwahara, H.; Golberg, D. Adv. Mater. 2009, 21, 2889−2893.

[22] Osadaab, M.; Sasaki, T. J. Mater. Chem. 2009, 19, 2503−2511.

[23] Ma, R.; Sasaki, T. Acc. Chem. Res. 2015, 48, 136−143.

[24] Wang, Q.; O'Hare, D. Chem. Rev. 2012, 112, 4124−4155.

[25] Naguib, M.; Mochalin, V. N.; Barsoum, M. W.; Gogotsi, Y. Adv. Mater. 2014, 26, 992−1005.

[26] Fan, Z. X.; Huang, X.; Tan, C. L.; Zhang, H. Chem. Sci. 2015, 6, 95−111.

[27] Niu, J.; Wang, D.; Qin, H.; Xiong, X.; Tan, P.; Li, Y.; Liu, R.; Lu, X.; Wu, J.; Zhang, T.; et al. Nat. Commun. 2014, 5, 3313.

[28] Huang, X. Q.; Tang, S. H.; Mu, X. L.; Dai, Y.; Chen, G. X.; Zhou, Z. Y.; Ruan, F. X.; Yang, Z. L.; Zheng, N. F. Nat. Nanotechnol. 2011, 6, 28−32.

[29] Duan, H. H.; Yan, N.; Yu, R.; Chang, C. R.; Zhou, G.; Hu, H. S.; Rong, H. P.; Niu, Z. Q.; Mao, J. J.; Asakura, H.; et al. Nat. Commun. 2014, 5, 3093.

[30] Peng, Y.; Li, Y.; Ban, Y.; Jin, H.; Jiao, W.; Liu, X.; Yang, W. Science 2014, 346, 1356−1359.

[31] Rodenas, T.; Luz, I.; Prieto, G.; Seoane, B.; Miro, H.; Corma, A.; Kapteijn, F.; Llabrés i Xamena, F. X.; Gascon, J. Nat. Mater. 2015, 14, 48−55.

[32] Lu, Q. P.; Zhao, M. T.; Chen, J. Z.; Chen, B.; Tan, C. L.; Zhang, X.; Huang, Y.; Yang, J.; Cao, F. F.; Yu, Y. F.; et al. Small 2016, 12, 4669−4674.

[33] Colson, J. W.; Woll, A. R.; Mukherjee, A.; Levendorf, M. P.; Spitler, E. L.; Shields, V. B.; Spencer, M. G.; Park, J.; Dichtel, W. R. Science 2011, 332, 228−231.

[34] Kissel, P.; Murray, D. J.; Wulftange, W. J.; Catalano, V. J.; King, B. T. A. Nat. Chem. 2014, 6, 774−778.

[35] Kory, M. J.; Wörle, M.; Weber, T.; Payamyar, P.; van de Poll, S. W.; Dshemuchadse, J.; Trapp, N.; Schlüter, A. D. Nat. Chem. 2014, 6, 779−784.

[36] Tan, C. L.; Qi, X. Y.; Huang, X.; Yang, J.; Zheng, B.; An, Z. F.; Chen, R. F.; Wei, J.; Tang, B. Z.; Huang, W.; et al. Adv. Mater. 2014, 26, 1735−1739.

[37] Cai, S.-L.; Zhang, W.-G.; Zuckermann, R. N.; Li, Z.-T.; Zhao, X.; Liu, Y. Adv. Mater. 2015, 27, 5762−5770.

[38] Liu, H.; Du, Y.; Deng, Y.; Ye, P. D. Chem. Soc. Rev. 2015, 44, 2732−2743.

[39] Eswaraiah, V.; Zeng, Q.; Long, Y.; Liu, Z. Small 2016, 12, 3480−3502.

[40] Lalmi, B.; Oughaddou, H.; Enriquez, H.; Kara, A.; Vizzini, S.; Ealet, B.; Aufray, B. Appl. Phys. Lett. 2010, 97, 223109.

[41] Vogt, P.; Padova, P. D.; Quaresima, C.; Avila, J.; Frantzeskakis, E.; Asensio, M. C.; Resta, A.; Ealet, B.; Lay, G. L. Phys. Rev. Lett. 2012, 108, 155501.

[42] Tao, L.; Cinquanta, E.; Chiappe, D.; Grazianetti, C.; Fanciulli, M.; Dubey, M.; Molle, A.; Akinwande, D. Nat. Nanotechnol. 2015, 10, 227−231.

[43] Zhang, S.; Yan, Z.; Li, Y.; Chen, Z.; Zeng, H. Angew. Chem., Int. Ed. 2015, 54, 3112−3115.

[44] Ares, P.; Aguilar-Galindo, F.; Rodríguez-San-Migue, D.; Aldave, D. A.; Díaz-Tendero, S.; Alcamí, M.; Martín, F.; Gómez-Herrero, J.; Zamora, F. Adv. Mater. 2016, 28, 6332−6336.

[45] Singh, D.; Gupta, S. K.; Sonvane, Y.; Lukačević, I. J. Mater. Chem. C 2016, 4, 6386−6390.

[46] Shamsi, J.; Dang, Z.; Bianchini, P.; Canale, C.; Stasio, F. D.; Brescia, R.; Prato, M.; Manna, L. J. Am. Chem. Soc. 2016, 138, 7240−7243.

[47] Song, J.; Xu, L.; Li, J.; Xue, J.; Dong, Y.; Li, X.; Zeng, H. Adv. Mater. 2016, 28, 4861−4869.

[48] Dou, L.; Wong, A. B.; Yu, Y.; Lai, M.; Kornienko, N.; Eaton, S. W.; Fu, A.; Bischak, C. G.; Ma, J.; Ding, T.; et al. Science 2015, 349, 1518−1521.

[49] Liu, J.; Xue, Y.; Wang, Z.; Xu, Z.-Q.; Zheng, C.; Weber, B.; Song, J.; Wang, Y.; Lu, Y.; Zhang, Y.; Bao, Q. ACS Nano 2016, 10, 3536−3542.

[50] Novoselov, K. S.; Jiang, D.; Schedin, F.; Booth, T. J.; Khotkevich, V. V.; Morozov, S. V.; Geim, A. K. Proc. Natl. Acad. Sci. U. S. A. 2005, 102, 10451−10453.

[51] Chen, X.; Zhang, J.; Fu, X.; Antonietti, M.; Wang, X. J. Am. Chem. Soc. 2009, 131, 11658-11659.

2.2 Applications of ultrathin 2D nanomaterials

Photocatalysis

Photocatalysis for both organic transforming reactions and green solar energy generation is of great significance due to their promising potential to solve the increasingly serious challenge of environmental pollution and energy shortage. Generally, there are three main steps in a semiconductor-driven photocatalytic process: (i) the electron-hole pairs (charge carriers) are excited by the photon incident; (ii) the photo-excited electron-hole pair separate from each other and migrate to the surface of the catalysts; and (iii) the electrons and holes thus promote the corresponding oxidation and reduction reactions on the catalyst surface.[1, 2] Therefore, a good photocatalyst must meet several key conditions, including a suitable bandgap to collect sufficient photons, an efficient charge separation, as well as long lifetime of charge carries. However, very few materials could meet all of the afore-mentioned criteria and meanwhile being cost-effective and environmental-friendly. In the past few decades, great efforts have been made to developing photocatalysts with suitable band structures to absorb broad light spectrum.[3-5] Benefiting from the unique morphologies and electronic structures, ultrathin 2D nanomaterials exhibit distinct advantages in photocatalytic applications compared to their bulk counterparts. On the one hand, the enlarged surface area of ultrathin 2D nanomaterial is beneficial for the exposure of abundant surface active sites. On the other hand, the ultrathin nature of 2D materials make contribution to the charge migration from the bulk to the surface, avoiding the charge recombination and improving the charge lifetime. In addition, 2D nanomaterials can be employed as excellent substrates for constructing hybrid heterostructures or multicomponent composites to expand their applications in various photocatalytic reactions.

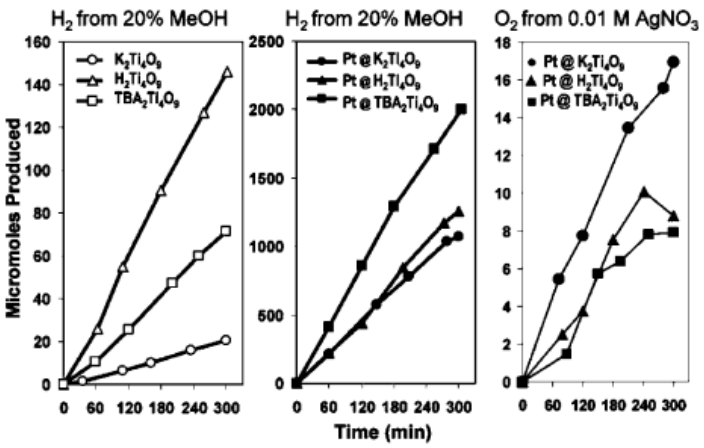

Figure 2-1 Photocatalytic H_2 and O_2 production over layered titanate, protonated titanate, and $Ti_4O_9^{2-}$ nanosheets.

Over the past decades, TiO_2 has been widely used as the photocatalyst due to its unique features including low cost, nontoxicity and high chemical and physical stability.[6-7] Osterloh et al. reported that the $Ti_4O_9^{2-}$ nanosheet loaded Pt as the cocatalyst exhibits a moderate hydrogen production yield using methanol as the sacrificial agent (**Figure 2-1**).[8] Rectanglar TiO_2 nanosheets with highly reactive (001) facets as the top and bottom surfaces have been successfully synthesized by a simple hydrothermal route with the assistance of hydrofluoric acid solution.[9] The percentage of (001) facets in the sheets was 89% with the optimal adjustment of the amount of hydrofluoric acid and reaction temperature. Such TiO_2 nanosheets show excellent photocatalytic efficiency, far exceeding that of commercially available Degussa P25, due to exposure of the high percentage of (001) facets.

Pt particles exhibit an absorption band in the visible region. Zhai et al. reported that Pt particles loaded on a TiO_2 thin film promote dehydrogenation of alcohols by visible light (λ>420 nm) under N_2 atmosphere.[10] Shiraishi and co-workers also reported that Pt particles with 3-4 nm diameter loaded on anatase TiO_2, when used for aerobic oxidation under visible light, facilitate direct e− transfer to anatase and promote the

reaction highly efficiently. The Pt/anatase catalysts promote aerobic oxidation of alcohols with an apparent quantum yield 7.1% (550 nm), which is much higher than that obtained with the Au/P25 catalyst (3.8%).[11]

Tu et al. reported hollow spheres made of exfoliated titanium dioxide/grapheme material assembled by a layer-by-layer method that can be used as the photocatalyst in CO_2 reduction reactions.[12] The TiO_2/grapheme hollow spheres showed a 9 fold increase for the photocatalytic CO_2 reduction than that of the commercial P25 TiO_2.[13] It is believed that the ultrathin nature of TiO_2 nanosheet composited with grapheme significantly increased the lifetime of photoexcited charge carriers, which leads to the large enhancement in the photocatalytic activity. In contrast to most reported nitrogen-doped titania photocatalysts with some localized states in the intrinsic band gap and small visible light absorption shoulders induced by inhomogeneous nitrogen doping near the particle surface, Liu et al. reported the homogeneous substitution of O by N in the whole particles of layered titanates which exhibited extraordinary band-to-band excitation in the visible-light ranging up to blue light. [15]

Electrocatalysis

In order to improve the next-generation energy devices, it is necessary to get a deeper understanding of the fundamental principles of electrocatalysis, which is responsible for accelerate electrochemical reactions on the electrode surface. The electrochemical water splitting is typically processed in an electrolyzer, which is composed by three component parts: an electrolyte (ionic conductor), a cathode, and an anode, through the application of an external voltage. However, the electrolysis of water is thermodynamically disfavored, requiring an input of energy to accelerate the reaction. This extra energy (overpotential) is due to the high activation energy required

to split water and the low conductivity of water and can be minimized by using efficient electrocatalysts and improving the conductivity of water. The electrochemical decomposition of water in an electrolyzer is composed of two half-reactions: hydrogen evolution reaction (HER) on the cathode and oxygen evolutionreaction (OER) on the anode. Inversely, in a hydrogen-air fuel cell, the hydrogen oxidation reaction (HOR) occurs at the anode and the oxygen reduction reaction (ORR) at the cathode. The hydrogen obtained through water electrolyzers has a high purity (99.999 vol.%), thus it can be used directly in fuel cells, being an ideal technological loop for the water cycle, where the hydrogen is produced by water splitting through the HER and OER for fuel generation, and then used by power generation through the ORR and HOR in fuel cells.[16]

2D nanomaterials possess unique features such as excellent mechanical properties, light transmittance, and electronic properties that make 2D nanomaterials very attractive in the fabrication of next-generation electronic/optoelectronic devices [17]. Compared to other dimensional nanomaterials, such asnanowires or nanoparticles, the two most important features of 2D nanomaterials for electrocatalysis are their uniformly exposed lattice plane and unique electronic state [18]. It is therefore that a magic combination of metal oxides and twodimensionality generates incredible synergetic effects beyond the material itself and thus boosts the performances in energy applications. It is believed that developing such an atomically-thin and mesoporous nanostructure should be of great benefit for OER catalysis. As a representative example, graphene-like holey Co_3O_4 nanosheets were successfully synthesized through a surfactant-assisted self-assembly approach and utilized as a catalyst for water oxidation. As expected, owing to its atomic thickness, mesoporous structure, and lattice structural distortion, which provide large amounts of catalytic

active sites, sufficient electrode/electrolyte contact, and facile mass conversion and transfer at the interface, the as-prepared raphene-like holey Co_3O_4 nanosheets exhibits superior OER catalytic performance with early onset potential, high current density, and long-term stability as compared with conventional Co_3O_4 nanostructures and commercial IrO_2.[19]

The ultrathin thickness of grephene-analogous 2D nanomaterials has led to superb and abnormal physical and chemical properties, endowing them with promising applications in many engineering fields.[20-25] Increasing edges or creating defects are beneficial for increasing the catalytic activity of grephene-like 2D nanomaterials. The density of states can be largely enhanced at the edges as compared with bulk graphene.[26] With the presence of defects such as vacancies and dislocations, additional electronic states can be induced and the electron transfer would be modified. Deng et al. demonstrated that the ORR could proceed with low energy barriers at these edges, particularly when these edges were functionalized with oxygen-containing chemical groups. Moreover, the ORR activity could be further enhanced by increasing the edge atoms via reducing the size of graphene nanosheets.[27]

Rechargeable batteries

It has been demonstrated that the integration of 2D nanomaterials with clean energy devices offers promising opportunities to address the major challenges driven by ever-growing global energy demands [27, 28]. Among these, graphene, transition metal oxide (TMO) nanosheets and transition metal dichalcogenide (TMD) nanosheets are three representative types of 2D nanomaterials, which have been extensively explored as promising electrode materials for LIBs.[29–43] The nanostructures of TMO nanosheets have great potential for lithium-ion storage, which is favorablefor charge transfer during the electrochemical reactions. Yang et al. developed a nanocasting

strategy for the synthesis of graphene-TiO_2 hybrid (G-TiO_2) nanosheets with graphene-based silica nanosheets as a sacrificial template.[44] This as-obtained nanostructure have many unique advantages to facilitate the insertion/deinsertion of Li ions, such as ultrathin thickness, mesoporous structure, high surface area and uniform dispersion of the graphene layers in between the TiO_2 nanosheets. In the traditional fabrication of graphene-based hybrid materials, the TMO nanosheets often only grow at the defect sites of the graphene surfaces and form discontinuous island-like domain arrays. Li et al. synthesized uniform mesoporous TiO_2/graphene/mesoporous TiO_2 sandwich-like nanosheets by slow hydrolysis and condensation of Ti precursor on graphene sheets in an ammonia solution with a following heating treatment at 500 ˚C in argon.[45] Recently, atomic layer-by-layer Co_3O_4/graphene (ATMCNs-GE) hybrid nanomaterial has been fabricated as anode materials for LIBs by Dou et al. via a surfactant-assisted self-assembly method together with a following calcination process.[46] Composites of TiO2-B nanosheet arrays on carbon nanotubes (CNTs@TiO2-B NSs) were prepared through a fast microwave-assisted solvothermal route by using an imidazolium-based ionic liquid, which served as a guiding agent to interact with CNTs via cation-π interactions and further guide the in-situ growth of TiO_2-B nanosheet arrays on the CNT surfaces. From a Brunauer-Emmett-Teller (BET) calculation, this hybrid showed a specific surface area as high as 151.2 $m^2 g^{-1}$. When fabricated as the working electrode for batteries, the CNTs@TiO_2-B composite maintained a reversible capacity of 147 mAh g^{-1} at the high current density of 6 A g^{-1}, which corresponds to ~36 C for anatase.[47] Another example of the facile fabrication of 2D nanosheets for high-capacity LIB cathode application was reported by Wang et al., where an ammonia-assisted hydrothermal method followed by calcination at 450 ℃ was employed.[48] During the hydrothermal process, ammonia played the

roles of both ligand and precipitating and structure directing agents for the controllable formation of the $Co(OH)_2$ nanosheets, which were further transformed into snowflakeshaped Co_3O_4 nanosheets by heat treatment. Electrochemical testing revealed that the snowflake-shaped Co_3O_4 electrode had a remarkable capacity with enhanced retention after 100 cycles and superior rate performance at various current densities, due to the greatly facilitated lithium-ion diffusion and electron transport contributed by the unique morphology.

Reference

[1] Chen, Z.; Jaramillo, T. F.; Deutsch, T. G.; Kleiman-Shwarsctein, A.; Forman, A. J.; Gaillard, N.; Garland, R.; Takanabe, K.; Heske, C.; Sunkara, M.; et al. J. Mater. Res. 2010, 25, 3−16.

[2] Chen, X.; Shen, S.; Guo, L.; Mao, S. S. Chem. Rev. 2010, 110, 6503−6570.

[3] Schneider, J.; Matsuoka, M.; Takeuchi, M.; Zhang, J.; Horiuchi, Y.; Anpo, M.; Bahnemann, D. W. Chem. Rev. 2014, 114, 9919−9986.

[4] Allen, M. R.; Thibert, A.; Sabio, E. M.; Browning, N. D.; Larsen, D. S.; Osterloh, F. E. Chem. Mater. 2009, 22, 1220−1228.

[5] Kim, H. N.; Kim, T. W.; Kim, I. Y.; Hwang, S. J. Adv. Funct. Mater. 2011, 21, 3111−3118.

[6] Han, X.; Kuang, Q.; Jin, M.; Xie, Z.; Zheng, L. S, J. Am. Chem. Soc. 2009, 131, 3152−3153.

[7] Yu, J.; Qi, L.; Jaroniec, M. J. Phys. Chem. C 2010, 114, 13118−13125.

[8] Oshima, T.; Ishitani, O.; Maeda, K. Adv. Mater. Interfaces 2014, 1, 1400131.

[9] Li, Y.; Wu, J.; Huang, Y.; Huang, M.; Lin, J. Int. J. Hydrogen Energy 2009, 34, 7927−7933.

[10] Hu, Y.; Guo, L. ChemCatChem 2015, 7, 584−587.

[11] Okamoto, Y.; Ida, S.; Hyodo, J.; Hagiwara, H.; Ishihara, T. J. Am. Chem. Soc. 2011, 133, 18034−18037.

[12] Li, X.; Kikugawa, N.; Ye, J. Adv. Mater. 2008, 20, 3816−3819.

[13] Hata, H.; Kobayashi, Y.; Bojan, V.; Youngblood, W. J.; Mallouk, T. E. Nano Lett. 2008, 8, 794−799.

[14] Matsumoto, Y.; Koinuma, M.; Iwanaga, Y.; Sato, T.; Ida, S. N. J. Am. Chem. Soc. 2009, 131, 6644−6645.

[15] Townsend, T. K.; Sabio, E. M.; Browning, N. D.; Osterloh, F. E. ChemSusChem 2011, 4, 185−190.

[16] Maeda, K.; Mallouk, T. E. C. J. Mater. Chem. 2009, 19, 4813−4818.

[17] Ebina, Y.; Sasaki, T.; Harada, M.; Watanabe, M. Chem. Mater. 2002, 14, 4390−4395.

[18] Kudo, A.; Tanaka, A.; Domen, K.; Maruya, K.-i.; Aika, K.-i.; Onishi, T. J. Catal. 1988, 111, 67−76.

[19] Dou, Y.; Liao, T.; Ma, Z.; Tian, D.; Liu, Q.; Xiao, F.; Sun, Z.; Kim, J. H.; Dou, S. H. Nano Energy 2016, 30, 267-275.

[20] Maeda, K.; Eguchi, M.; Oshima, T. Angew. Chem., Int. Ed. 2014, 53, 13164−13168.

[21] Silva, C. G.; Bouizi, Y.; Fornés, V.; García, H. J. Am. Chem. Soc. 2009, 131, 13833−13839.

[22] Lee, Y.; Choi, J. H.; Jeon, H. J.; Choi, K. M.; Lee, J. W.; Kang, J. K. Energy Environ. Sci. 2011, 4, 914−920.

[23] Zhao, Y.; Chen, P.; Zhang, B.; Su, D. S.; Zhang, S.; Tian, L.; Lu, J.; Li, Z.; Cao, X.; Wang, B. Chem. - Eur. J. 2012, 18, 11949−11958.

[24] Tu, W.; Zhou, Y.; Liu, Q.; Tian, Z.; Gao, J.; Chen, X.; Zhang, H.; Liu, J.; Zou, Z. Adv. Funct. Mater. 2012, 22, 1215−1221.

[25] Wang, G.; Shen, X.; Yao, J.; Park, J. Carbon 2009, 47, 2049−2053.

[26] Sheng, L.; Liao, T.; Kou, L. and Sun, Z., Mater Today Energy 2017, 3, 32–9.

[27] Deng, D.; Yu, L.; Pan, X.; Wang, S.; Chen, X.; Hu, P.; Chem Commun 2011, 47, 10016.

[28] Liao T., Sun Z, and Dou SX. ACS Appl Mater Interfaces 2017, 9, 8255–62.

[29] Zhao M, Lu Q and Ma Q et al. Small Methods 2017, 1, 1600030.

[30] Wu Z-S, Zhou G and Yin L-C et al. Nano Energy 2012, 1, 107–31.

[31] Sun Y,Wu Q and Shi G. Energ Environ Sci 2011, 4, 1113–32.

[32] Elshof JEt, Yuan H and Rodriguez PG. Adv Energy Mater 2016, 6, 1600355.

[33] Ding Y-L,Wen Y and Aken PAv et al. Small 2015, 11, 2011–8.

[34] Huang X, Zeng Z and Zhang H. Chem Soc Rev 2013, 42, 1934–46.

[35] Wang X, Weng Q and Yang Y et al. Chem Soc Rev 2016, 45, 4042–73.

[36] Du Y, Yin Z and Zhu J et al. Nat Commun 2012, 3, 1177.

[37] Mei J, Liao T and Kou L et al. Adv Mater 2017, 29, 1700176.

[38] Bonaccorso F, Colombo L and Yu G et al. Science 2015, 347, 1246501.

[39] Liu B, Zhang J-G and Shen G. Nano Today 2016, 11, 82–97.

[40] Cao X, Tan C and Zhang X et al. Adv Mater 2016, 28, 6167–96.

[41] Choi W, Choudhary N and Han HG et al. Mater Today 2017, 20, 116–30.

[42] Zhu J, Yang D and Yin Z et al. Small 2014, 10, 3480–98.

[43] Huang X, Zeng Z and Fan Z et al. AdvMater 2012, 24, 5979–6004.

[44] Yang S, Feng X and M ¨ullen K.. Adv Mater 2011, 23, 3575–9.

[45] Li W, Wang F and Liu Y et al. Nano Lett 2015, 15, 2186–93.

[46] Dou Y, Xu J and Ruan B et al. Adv Energy Mater 2016, 6, 1501835.

[47] Chen C, Hu X and Wang Z et al. Carbon 2014, 69, 302–10.

[48] B. Wang, X. Lu, Y. Tang, J. Mater. Chem. A 2015, 3, 9689.

2.3 Bio-inspired two-dimensional nanomaterials for sustainable applications

Millions of years of evolution has produced unique structures and specialized functions in all creatures on the earth to cope with the environment. Fascinating interfacial phenomena observed in various natural species, such as vivid iridescent colours, unique light-response behaviours, super-wetting properties, etc.,[1-4] offer excellent opportunities to develope artificial nanomaterials with similar functionalities, through manipulating the interface structures and chemistries based on inspirations from nature. To date, many bio-inspired structures or interfaces have been constructed, with some unique properties or functions which cannot be observed in their constitutent materials. For example, the exceptional mechanical, surface and optical properties observed in bone,[5, 6] nacre,[7, 8] gecko feet,[9] spider silk,[10] fish scales, butterfly wings,[11, 12] etc., have been attracting increasing research efforts. Recent advances include nacre inspired damage tolerant materials;[13, 14] fish scale and armadillo shell inspired artificial armours;[15, 16] lotus leaf and cicada wing inspired self-cleaning surfaces;[17-19] insect compound eye inspired anti-fogging coatings;[20, 21] gecko feet and mussels inspired super-adhesive materials;[22, 23] desert beetle and cactus inspired water harvesting;[24, 25] opal, butterfly wings, and chameleon inspired photonic materials;[26-29] insect-trapping plant (e.g., nepenthes and sarracenia) inspired ultrafast water transport;[30] fish-gill and cactus-needle inspired oil-water separation,[31] etc.. There is no doubt that learning from nature opens new doors for innovation in materials and sustainable technologies. Owing to the great diversity and complexity of nature, the well-evolved natural structures corresponding to specific functionalities may vary from 1D nanofibers or nanoneedles to 2D nanosheets or nanoplates or even 3D multiscale-ordered structures.[32] A good

understanding of the structure-property relationships is essential for bio-inspired nanomaterials design and fabrication.

Two-dimensional (2D) nanomaterials have achieved some significant triumphs in various applications, benefitting from their unique structural characteristics and relevant chemical and physical properties.[33-35] In fact, 2D nanostructures also widely exist in nature and generate some amazing functionalities, which offers us great opportunities to further expand the design and fabrication of 2D nanostructured materials, devices, and technologies.[36] By integrating 2D nanomaterials with the bio-inspired strategies, innovative materials and technologies have been proposed and realized. In this research news, recent progress in bio-inspired materials and technologies based on 2D nanomaterials for targeted sustainable energy and environmental technologies, such as energy conversion and storage and environmental remediation, etc., is reviewed and discussed. As shown in **Figure 2-2**, three topical subjects, including bio-inspired 2D photonic structures, bio-inspired 2D energy nanomaterials, and bio-inspired 2D super-wetting materials, along with the challenges and opportunities will be the focus of this article, and give an overall perspective to this emerging and promising research area.

Figure 2-2 Summary of bio-inspired 2D nanomaterials. Reproduced with permission.[35, 59, 82] Copyright 2017, 2019 American Chemical Society. Reproduced with permission.[20, 64, 67, 72] Copyright 2014, 2017, 2019 Wiley-VCH. Reproduced with permission.[68, 77] Copyright 2014, 2017 Nature Publishing Group. Reproduced with permission.[49] Copyright 2015, Royal Society of Chemistry. Reproduced with permission.[44] Copyright 2016, Elsevier. Reproduced under the terms of the Attribution 4.0 International license. [29, 34, 66, 81] Copyright 2015, 2016, 2017, 2018 Creative Commons.

Bio-inspired 2D photonic materials

To survive in the wild world, natural species have evolved various unique structures with fascinating optical functionalities, such as glitzy structural colours for attracting prey or mates,[37] tunable camouflage colours for escaping from predators,[38] antireflection function of compound eyes for weak light vision[36] and so on. These structures, as known as photonic crystal structures, have inspired the design of novel photonic micro/nano-structures and some smart optical devices.

Among the various natural photonic structures, one class consists of periodically stacked 2D multilayers, also known as Bragg Stacks, have been found in many natural organisms, such as plants, insects, and marine benthos.[39] Multiple pairs of 2D layers with different refractive indexes in Bragg Stacks can generate iridescent structural colours through constructive interference, when the optical thickness (nd) of a certain pair of AB layers meets the conditions of Equation 1,[40]

$$2(n_A d_A \cos\theta_A + n_B d_B \cos\theta_B) = m\lambda \quad (1)$$

where n is the refractive index, d is the physical thickness of each layer, θ is the angle of propagation in the corresponding layer, and λ is the wavelength of light giving the highest reflectivity, and m is an integer. Because of this interesting optical property, organisms with Bragg Stacks on their surfaces present a wide range of brilliant colours, creating a vivid world. Inspired by nature 2D photonic structures, many delicately designed 2D photonic materials with fluctuating structural colours have been developed with applications across broad areas.[41-45] Compared with pigment colour, structural colour can offer ultrahigh saturation, brightness, and vivid iridescence, or the change of colour with angle of incidence of the light.

One well-known case is the brilliant iridescent colours found in the elytra of some beetles. For example, buprestid beetles have beautiful green iridescence on their elytra (wing cases), which originates from multiple stacks of periodically ordered chitin-protein pairs.[46] The multilayers of chitin-protein pairs in beetles consist of a few thin layers of chitin in a proteinaceous matrix with different refractive indexes. When the optical thickness of the chitin layers genetically grow to approach one-quarter the wavelength of visible light (Equation 1), one or more colours will be generated by constructive interference. Inspired by the attractive structural colours of beetle elytra, nanoparticles which change colour with environment have been realized through a zinc

oxide (ZnO) flower-like structure using quasi-ordered scattering.[47] Similarly, an optical diode design was inspired by *Plusiotis batesi* beetles, which have a unique helix structure in their elytra for a conventional selective reflection.[48] Tzeng et al. fabricated a synthetic analogue with bio-inspired iridescent colours by mimicking the colour appearance of a *Chrysochroa rajah* beetle.[49] As shown in **Figure 2-3a**, the artificial Bragg Stack of optically reflective pairs with alternating low and high refractive indices were made from colloidal silica/cellulose nanocrystals and polyelectrolyte/clay thin layers assembled by a layer-by-layer deposition method, and the bio-inspired thin film showed similar iridescence as the beetle elytra.

By learning from the Bragg Stacks and the iridescent colour in biological species, some other artificial materials with well controlled thickness and refractive indices have been fabricated to realize structural colours, such as the spin-coated mesoporous titanium dioxide/silicon dioxide (TiO_2/SiO_2) multilayer stacks,[50, 51] layer-by-layer assembled TiO_2/SiO_2 nanoparticles,[52] thermally evaporated thin films of calcium fluoride (CaF_2) and zinc sulfide (ZnS),[53] polymers,[54] and so on, for the applications in sensors, smart windows, and soft robotic devices.[55] Besides the direct iridescent colours generated by reflection and interference, enhanced fluorescence emission properties have also been inspired by a *Hoplia coerulea* beetle, whose scales contain fluorescent molecules ingrained in 2D multilayers of thin flat chitin layers separated by air/chitin mixing layers.[56]

2D photonic structures based on guanine crystals have been observed in some hydrobios.[57] As shown in **Figure 2-3b**, tunable multilayer photonic structures in neon tetra fish can generate iridescent colours from blue to indigo with the change of light environment by tuning the tilt angle between guanine crystals and cytoplasm layers of the 2D guanine-cytoplasm pairs.[58] Based on this understanding, a dynamic

iridescence actuated by magnetic nanopillars has been fabricated, which allow the structure to tilt the substrate when the angle of the applied magnetic field is changed and this can lead to programmable iridescent display under ambient light.[59] This type of guanine-based photonic crystals has also been identified in different types of fishes, such as Japanese *Koi* fish and *Sardina pilchardus* fish. These fish are covered by a large area of guanine photonic crystal stacks with numerous reflecting units. These stacks generate a broadband, wavelength-independent reflector over the whole visible light spectrum when the incident angle approaches Brewster's angle.[60] In contrast to the above broadband reflectance, *sapphirinid* copepods, generate wavelength-independent reflectance in response to the luminous environment by controlling the thickness of the cytoplasm layers of the guanine-cytoplasm photonic crystal pairs.[61] Such tunable 2D photonic systems in *sapphirinid* copepods are rarely observed even in nature, and they have not yet been successfully mimicked in artificial systems. The major challenges in fabricating such a class of bio-inspired photonic structures are finding suitable 2D nanostructures and materials to replace the guanine crystals and cytoplasm layers and realizing the precisely controllable layer-by-layer assembly of the 2D crystals and layers. Although some pioneering studies have been performed on the guanine-based bio-inspired materials, for example, through the self-assembly of peptides or DNA to realize unique photonic performance,[62, 63] there is still a long way to go in developing this type of bio-inspired material.

Very recently, Sun et al. fabricated a sea-shell inspired 2D photonic nanostructure by using a facile vacuum-filtering technique to assemble graphene and atomically-thin 2D TiO_2 nanosheets in a layer-by-layer manner to mimic the iridescent, well-arranged, layered brick-and-mortar microstructures of natural sea-shells (**Figure 2-3c**).[64] The bio-inspired photonic structure with 16 alternating thin graphene layers and thick 2D

TiO_2 layers exhibited significant and beautiful green-red strip-like colours under both dispersion-dominated and reflection-dominated conditions, resulting from its well-designed thickness and well-aligned 2D interfaces. When this type of unique bio-inspired nanostructure is employed in optoelectronic devices, significantly enhanced photocurrent and much improved responsivity and sensitivity have been achieved, attributed to the significantly enhanced interlayer charge transfer formed between the 2D-2D heterostructure and the homostructure of the bio-inspired photoelectrode. Kolle and co-workers have fabricated a concave 2D photonic structure consisting of 2.5 mm thick concave gold layer and 20 nm thick carbon film with a conformal multilayer of thin titanium dioxide/alumium oxide (TiO_2/Al_2O_3) films to simulate the colour mixing effect resulting from deformed multilayer stacks in the wings of *Papilio blumei* butterfly. This proved that bio-inspired nanostructures could display the same optical features as the natural butterfly wing scale.[43] Furthermore, introducing stimuli-responsive materials into photonic structures can achieve colour shifting with the change of environments. For example, Wang et al. fabricated bio-inspired hybrid photonic crystals consisting of alternant thin films of TiO_2 and organic polymer layers, which have reversible colour shifting capacity over the full visible spectrum in response to different water-vapour concentrations as a result of swelling of the polymer layers.[65]

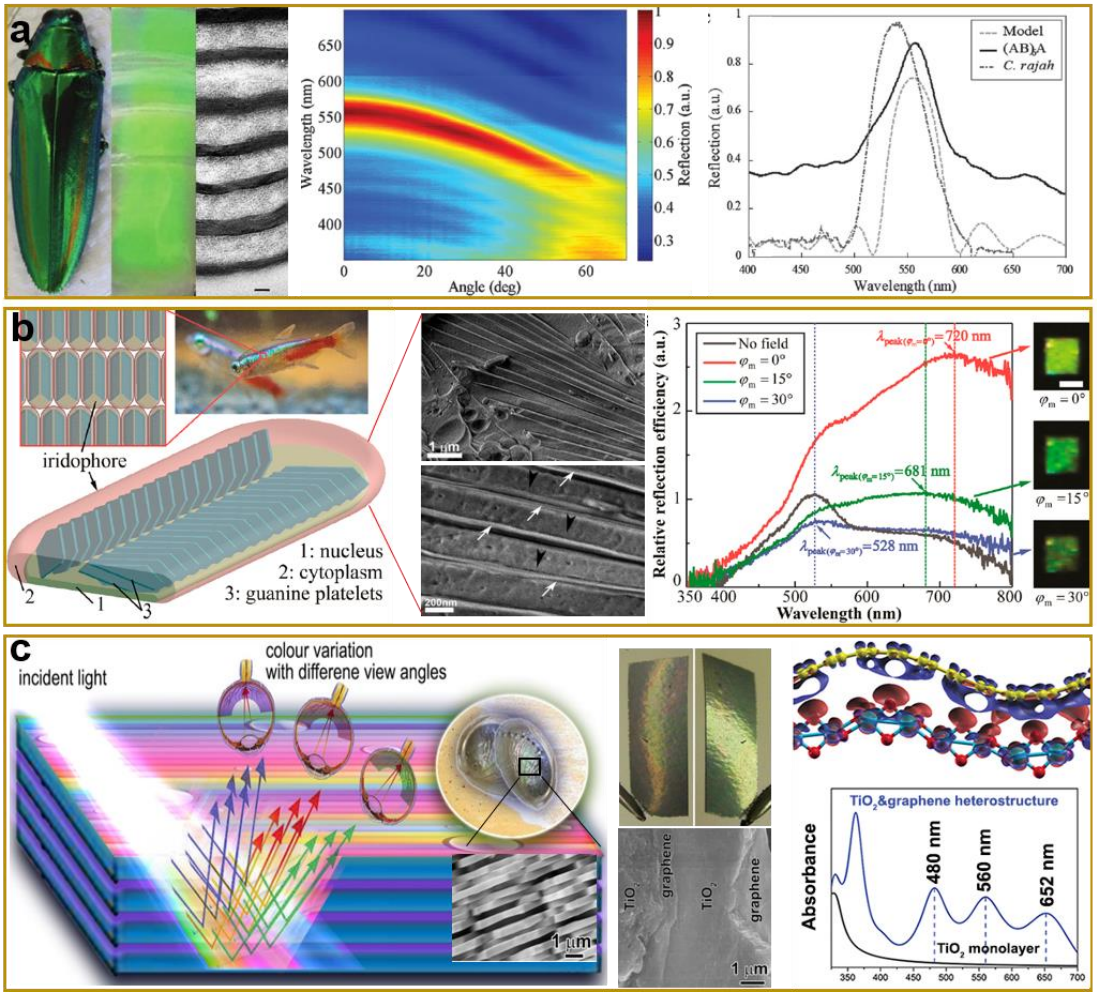

Figure 2-3 Bio-inspired 2D photonic nanomaterials. (a) The optical photographs and SEM image show the *C. rajah* beetle, the assembled artificial Bragg stacks with green color and the corresponding microstructure, the colour plots shows reflection-incidence angle spectrum for the artificial stacks, the right figure shows the reflection spectra of *C. rajah* elytron and the fabricated stack. Reproduced with permission.[49] Copyright 2015, Royal Society of Chemistry. (b) Schematic illustration of neon tetra and its photonic structures, the iridescence demonstration indicates colour variation from bright yellow to dark green with different magnetic alignment angles φ_m = 0−30°. Reproduced with permission.[59] Copyright 2019, American Chemical Society. The SEM images show the microstructures of the guanine crystals (with arrows) and cytoplasm layers (black arrows). Reproduced with permission.[58] Copyright 2015, Wiley-VCH. (c) Schematic illustation shows the angle-varing structural change of seashell structures, the inset shows the microstructure of natural sea-shell, the optical and SEM images show the seashell-inspired nanostructure made from graphene and 2D-TiO_2 nanosheets, the right part shows the interlayer electronic coupling and calculated light absorption spectrum of bio-inspired heterostructure. Reproduced with permission.[64] Copyright 2019, Wiley-VCH.

Therefore, based on the understanding on the structure-optical property relationships found in natural species, plenty of 2D bio-inspired photonic structures have been developed and fabricated. These bio-inspired 2D nanostructures presented mimicking extraordinary colours exhibited in natural species and are very promising in applications in optical displays, sensors, anti-counterfeit technologies, solar energy harvesting and conversion devices, etc.

Bio-inspired 2D energy materials

Development of high-efficiency energy conversion and storage devices has attracted great research interest, due to the urgent demand for green and sustainable energy supplies. To meet the increasing requirements on materials for high-performance energy devices, nanomaterials with precisely tailored structures and interfaces inspired from natural species have been created.[66] Bio-inspired nanomaterials have demonstrated some extraordinary properties, which are promising for enhancing the overall performance of energy conversion or storage devices.

Mei *et al*. proposed a honeycomb-inspired $CoMoO_x$ structures consisting of 2D nanosheets by learning from the robust mechanical stability and permeable channels and pores structures of natural honeycombs, which possess excellent structural robustness deriving from the elaborate structures.[67] The natural honeycomb or bee hive with cellular structures, composed of hexagonal channels and thin walls, as shown in **Figure 2-4a**, is well known for its excellent mechanical performances, highly-ordered cellular structures, and excellent ventilation capacity arising from the interconnected pore/channel structure. In this work, owing to the structural advantages derived from the natural honeycombs, the bio-inspired $CoMoO_x$ nanostructures consisting of interconnected pores and channels and ultrathin 2D walls exhibited much improved structural cycling stability and superior lithium storage capacity compared

to electrode materials with similar chemical compositions, but without the cellular nanostructure. This work confirms that bio-inspiration offers new insights into the design of novel electrode materials for high-efficiency energy devices.

Electric eel *Electrophorus electricus* is an amazing aquatic animal which can generate high voltages and currents from ion gradients through thousands of membranes with densely packed ion channels which separate long and thin electrically active cells stacked in parallel. Inspired by this power generation concept, a soft, flexible and transparent power source composed with polyacrylamide hydrogel and a repeated sequence of ion selective hydrogel membranes, similar to the repeated 2D compartments of electric eel, has been designed (**Figure 2-4b**). This has been shown to generate an open circuit voltage of 110 V or a power density of 27 mW m^{-2} per cell under mechanical contact activation of serially-stacked gel compartments.[68] This bio-inspired power system indeed opens a new window to design sustainable electrical generators. In addition to the ion-gradient power generator inspired by electric eel, novel triboelectric generators based on 2D materials have also been inspired by human skin,[69] Hummingbird wing,[70] and other natural structures.

It is interesting that nacre has also inspired the integration of 2D nanofluidic devices, where the mass and charge transport are confined in the interspace between 2D layers. Cheng et al. reported a bio-inspired 2D nanofluidic devices constructed from kaolinite-based Janus nanobuilding blocks. 2D Janus materials as a novel class of materials with distinct properties on each side have been considered as a promising material system in energy applications.[71] Unlike conventional 2D nanofluidics, the use of 2D Janus blocks in a nacre-mimicking assembly, delivers outstanding carrier transport mobility and almost perfect ion selectivity.[72]

The biological chain and the biocycle on the Earth all start from the energy supply from the sun, which have driven plenty of biological species to be extremely active for high-efficient solar energy harvesting or conversion. Recently, bio-inspired solar energy harvesting and conversion technologies, such as bio-inspired solar cells [73, 74] and bio-inspired carbon cycle processes,[75, 76] have achieved significant progress.

By learning from the 2D networks of leaf venation system of White Jade Orchid Tree Magnolia alba and spider web networks of a common spider *Agelena labyrinthica*, metallic networks featuring superior current delivery, minimal optical shading, and outstanding strength and flexibility have been designed for electro-optical devices, such as solar cells, light sources, touch screens, or flexible displays.[77] By directly mimicking the shape of a leaf, a bio-inspired flexible $Zn_{0.5}Cd_{0.5}S$@polyacrylonitrile photocatalyst in 2D leaf-like structure has been fabricated (**Figure 2-4c**). It shows enhanced photocatalytic hydrogen evolution activity compared to the pure $Zn_{0.5}Cd_{0.5}S$ nanoparticles with improved electrochemical cycling and structural stability in the photocatalytic hydrogen production processes, owing to the flat and flexible leaf-like structure and the superior light efficiency engendered by the hierarchical pore channels.[78] Also inspired by a leaf, 2D AgS_2 nanosheets with a leaf-like morphology with needle-like secondary structures have shown promise in solar cell applications.[79] Targetting a very different component of solar cells, Shams et al. extracted a transparent crab shell-inspired chitin nanofiber sheet by removing the inorganic calcium carbonate particles, proteins, lipids, and pigments from a real crab shell, and then impregnated a monomer to the sheet, followed by polymerization. This material has good transparency and very low coefficient of thermal expansion, and is an interesting candidate as a transparent substrate materials for flexible displays and solar cells.[80]

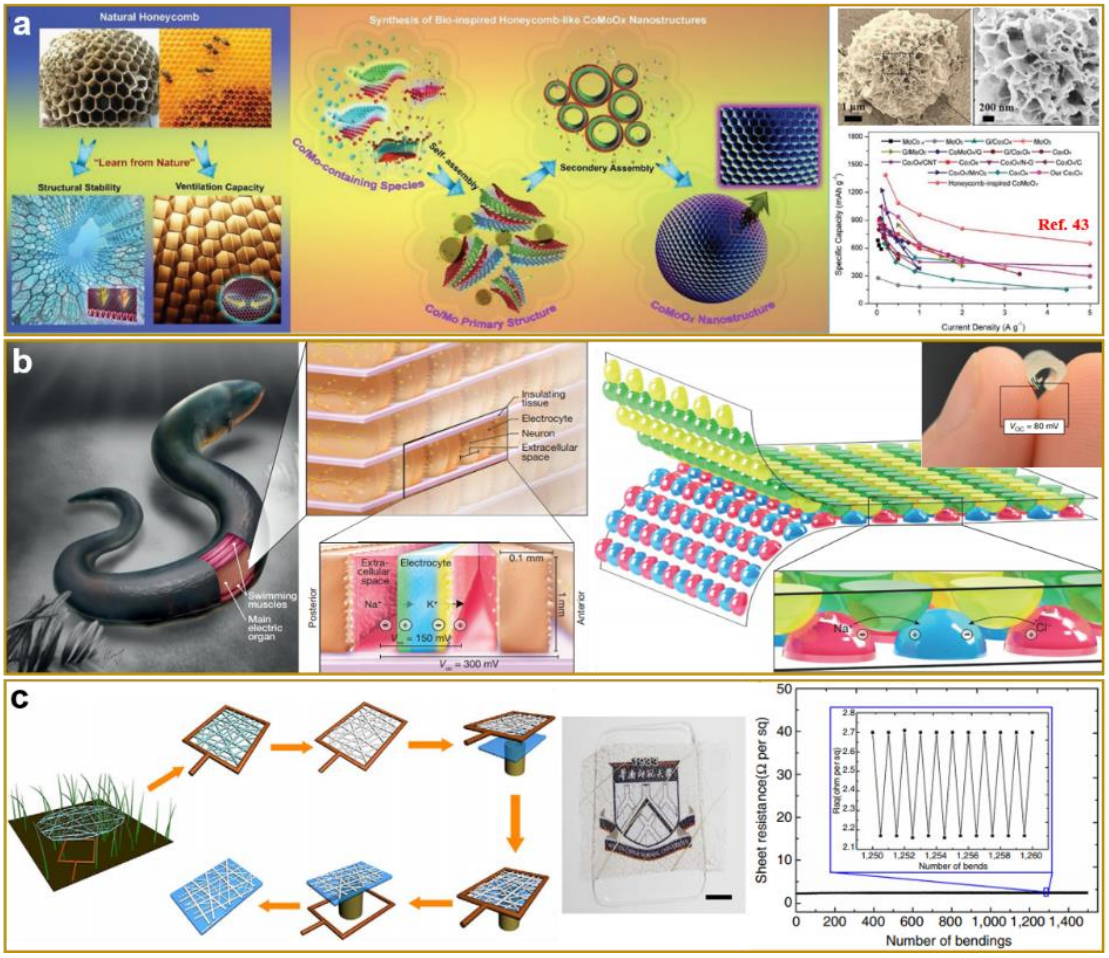

Figure 2-4 Bio-inspired 2D energy nanomaterials. (a) The photographs show a natural honeycomb and the inspired real-world construction with excellent structural stability and ventilation capacity, the schematic illustration shows the self-assembly route of honeycomb-inspired $CoMoO_x$ nanostructure, SEM images show the bioinspired $CoMoO_x$ microspheres composed of 2D nanosheets, and the comparison of rate capability and the capacity retention ratio of honeycomb-inspired $CoMoO_x$ nanostructure in a current density range between 0.2 and 5.0 A g^{-1} was summarized. Reproduced with permission.[67] Copyright 2019, Wiley-VCH. (b) The photographs show the *Electrophorus electricus* and the electrocytes in its organs, the right picture shows the artificial electric organ in its printed implementation and the inset shows the flexible artificial organ that produced an open-circuit voltage of 80 mV. Reproduced with permission.[68] Copyright 2017, Nature Publishing Group. (c) The schematic demonstrates the fabrication process of the silk spider web, the photograph shows the transparent leaf venation network, and the diagram illustrates the sheet network resistance oscillations. Reproduced with permission.[77] Copyright 2014, Nature Publishing Group.

Bio-inspired 2D super-wetting materials

Bio-inspired surfaces with superwettability have been intensively explored in past decades by inverstigating the super-wetting phenomenon in nature and this has

stimulated the applications of superwettability in liquid-proof textiles, oil-water separations, super/anti-adhesion surfaces, etc.[3] For example, water birds, both fresh water and salt water birds, such as the duck, goose, sea gull, pelican, etc., have superhydrophobic feathers to prevent wetting by water when they feed on lakes, rivers, beaches, etc.[17] Some birds, such as the cormorant, can even dive tens of meters deep into water to prey on fish while their feather remain unwetted by maintaining a thin layer of air on the surface of the feather. This superhydrophobic feature is due to both a 2D configuration of "quasi-hierarchical" microstructures and a specific greasy surface coating or preening oil secreted by the bird itself. Fish scales also exhibit self-cleaning and anti-fouling properties under water. Fish scale is an important organ as its role in protecting fish from contamination in the water environment.[17] By mimicking the natural 2D scale-like structure of the Asian *Arowana* fish scales, Sun *et al*. developed bio-inspired nanostructured coatings with tunable wettability in response to surface modification and scale-like structural orientation variation (**Figure 2-5a**).[81] In this study, the bio-inspired materials were fabricated in ZnO and the orientation of the scale-like nanostructures has been tailored to present different responses to water contact. Thin films with highly tilted scale structures have the capability to be tuned to exihibit either superhydrophilic or superhydrophobic. This interesting feature gives the bio-inspired materials the potential for many applications, such as marine antifouling, self-cleaning material, microfluidic regulation, bio-adhesion, etc.

Another example for natural super-wettability is the compound eye of flies. The unique surface structure gives the compound eye a superhydrophobic anti-fogging property, which allows them to maitain good functionality even in extreme environments. By learning from the biological structures and anti-fogging properties

of the fly eye, Sun et al. designed bio-inspired superhydrophobic antifogging ZnO nanomaterials with a low adhesion force to water drops, which effectively prevent the adhesion of water droplets on a tilted or curved surface.[20] **Figure 2-5b** shows artificial hierarchically-ordered ZnO microspheres that have a similar structure to the anatomical structure of the compound eye. Bio-inspired ZnO coatings can be easily fabricated by either brush-painting or spin coating of the fly-eye-inspired nanomaterials. As shown in the fogging test in Figure 4b, the fogging droplets on the bio-inspired coatings were in perfect spherical shapes due to the high contact angle and fully slid off a tilted substrate due to the low adhesive force. This bio-inspired antifogging coatings material is fabricated from low-cost material and is easy adapted for scalable production and large-scale painting, and thus has great potential for anti-fogging or anti-icing applications in some extreme environments.

Oil/water separation is another important application of bio-inspired super-wetting nanomaterials. It has been proved that the utilization of functional surfaces with both superoleophilic and superhydrophobic properties is an effective way to separate an oil-water mixture.[3] Dou et al. demonstrated a gradient porous separation mesh for one-step spilled oil collection and separation inspired by the crossflow filtration behaviour of fish gills (**Figure 2-5c**).[82] The key innovation of this technique is the growth 2D ultrathin cobalt oxide (Co_3O_4) nanosheets on metallic meshes, which turn the separation mesh from hydrophobic/oleophilic to hydrophilic/oleophobic. By using the innovative fsh-gill-inspired separation membrane, cross-flows formed on the membranes, in which the oil/water flows parallel to the bio-inspired 2D-Co_3O_4 membrane surface, and water is gradually filtered through the membrane, while oil is repelled and transported on the surface of membrane to the collection tank. Via this unique separation mechanism, the fish-gill inspired technology enables high-efficient

and continuous spilled oil collection and separation. This fish-gill inspired technology is therefore very promising for the clean-up of large-scale oil spills (**Figure 2-5c**). A shape-memory graphene film with electrothermally controlled surface wettability inspired by natural *Nepenthes* pitcher plant has been proposed by Wang et al. This bio-inspired thin film exhibited good electrical conductivity, superelasticity and high strength. The bio-inspired material possesses controllable slippery properties due to the reversible surface wettability, and thus can be used in various applications, including liquid harvesting devices, microfluidic channels, medical instruments, liquid handling robotic systems, etc.[83]

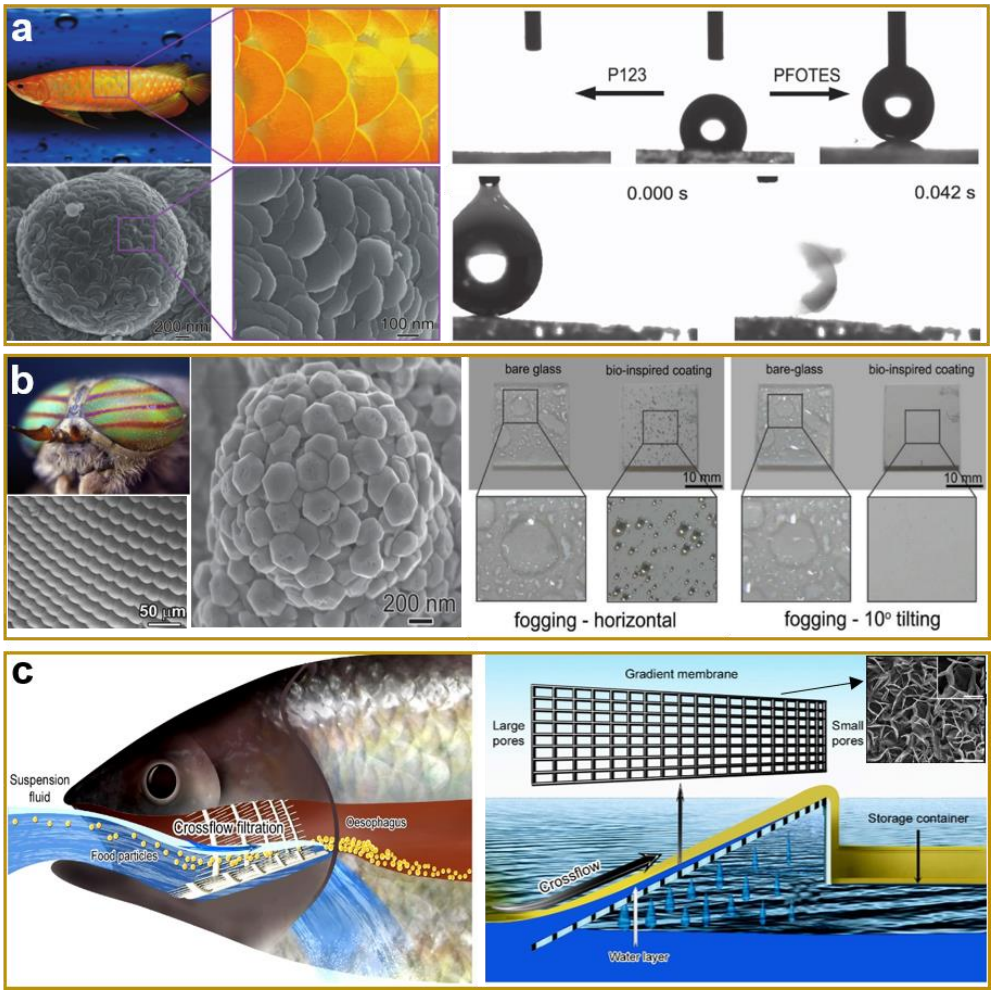

Figure 2-5 Bio-inspired 2D super-wetting nanomaterials. (a) Optic and SEM images of Asian Arowana fish scales, and the surface wettability modulation of the fish-scale-inspired nanostructured coatings,

showing the hydrophobic–superhydrophilic–superhydrophobic modulation of the water response. Reproduced with permission.[79] Copyright 2015, Nature Publishing Group. (b) Optical and SEM images of fly compound eyes, the microstructure of the fly-eye bio-inspired ZnO nanostructures shows the ommatidiumlens-like structures, the right pictures demonstrate the fogging test of the bare glass and bio-inspired coatings. Reproduced with permission.[20] Copyright 2014, Wiley-VCH. (c) Schematic illustration of crossflow filtration in fish gills and the demonstration of the bioinspired crossflow collection of spilled oil, the inset shows the ultrathin 2D-Co_3O_4 nanosheets coated on the wire surface. Reproduced with permission.[80] Copyright 2017, American Chemical Society.

Conclusions and Outlook

In summary, the well-evolved biological world, with its biodiversity and fascinating environmental responsive behaviour is a supremely effective materials-development laboratory to inspire our material and technology innovations. When science meets nature, a magic door opens to stimulate us to develop novel multifunctional nanomaterials beyond the present material systems. The combination of 2D nanomaterials with the concept of bio-inspiration, as we demonstrated above, has stimulated the development of novel materials and technologies.

On the other hand, there are still lots of grand challenges to be addressed, which limit the development of bio-inspired nanomaterials or technologies beyond 2D bio-inspired materials. Firstly, we need further efforts on discovering the phenomena and functionalities existing in natural species and gaining a better understanding of their structure-function relationships, which are fundamental but challenging two steps. Secondly, sophisticated synthetic methods or high-precise manufacturing techniques to achieve multiscale-ordering structures down to nanoscale are urgently needed to mimic complex natural structures or functions. In fact, some fascinating structures and

properties found in nature cannot be properly mimicked in our laboratories. For example, Dur et al. have revealed the unique tunable optical properties in the male sapphirinid copepods, which is very promising for advanced optical or light-harvesting devices.[61] However, due to the lack of proper material and fabrication method, such novel structures and properties have not been successfully mimicked yet. Thirdly, given that some biological systems present interesting properties themselves, the direct use of such bio-materials in functional devices would be an eco-friendly and efficient way to develop bio-inspired technologies. Recently, researchers discovered that biological materials directly derived from natural species exhibited outstanding performances in various energy applications such as photocatalysis, electrocatalysis and biomass conversion.[84-87] However, the precise and advanced biotechnology required in this route turns to be another major challenge. The last challenge is how to integrate multiple materials to realize desirable functions, such as well-designed heterostructures, organic-inorganic hybrid materials, etc. Apart from these challenges, the advances in developing 2D bio-inspired nanomaterials confirm that bio-inspiration is an effective approach to take the full advantages of the potential of materials for the design of mutifunctional smart devices. The development in this promising area thus paves a new way towards a green and sustainable society.

References

[1] A. R. Parker, C. R. Lawrence, Nature 2002, 414, 33.

[2] L. Wu, J. He, W. Shang, T. Deng, J. Gu, H. Su, Q. Liu, W. Zhang, D. Zhang, Adv. Opt. Mater. 2016, 4, 195.

[3] S. Wang, K. Liu, X. Yao, L. Jiang, Chem. Rev. 2015, 115, 8230.

[4] J. Aizenberg, P. Fratzl, Adv. Mater. 2009, 21, 387.

[5] X. Jin, B. Shi, L. Zheng, X. Pei, X. Zhang, Z. Sun, Y. Du, J. H. Kim, X. Wang, S. Dou, K. Liu, L. Jiang, Adv. Funct. Mater. 2014, 24, 2721.

[6] P. Westbroek, F. Marin, Nature 1998, 392, 861.

[7] J. H. Cartwrighta, A. G. Checa, B. Escribanoa, and C. I. Sainz-D áz, Proc. Natl. Acad. Sci. U. S. A. 2009, 106, 10499.

[8] F. Barthelat, Z. Yin, M. J. Buehler, Nat. Rev. Mater. 2016, 1, 16007.

[9] W. R. Hansen, K. Autumn, Proc. Natl. Acad. Sci. U. S. A. 2004, 102, 385.

[10] Y. Zheng, H. Bai, Z. Huang, X. Tian, F. Q. Nie, Y. Zhao, J. Zhai, L. Jiang, Nature 2010, 463, 640.

[11] Y. Zheng, X. Gao, L. Jiang, Soft Matter 2007, 3, 178.

[12] S. Kinoshita, S. Yoshioka, K. Kawagoe, Proc. R. Soc. Lond. B 2002, 269, 1417.

[13] U. G. Wegst, H. Bai, E. Saiz, A. P. Tomsia, R. O. Ritchie, Nat. Mater. 2015, 14, 23.

[14] A. Finnemore, P. Cunha, T. Shean, S. Vignolini, S. Guldin, M. Oyen, U. Steiner, Nat. Commun. 2012, 3, 966.

[15] B. J. Bruet, J. Song, M. C. Boyce, C. Ortiz, Nat. Mater. 2008, 7, 748.

[16] A. H. Barber, D. Lu, N. M. Pugno, Nature 2015, 519, s14.

[17] M. Liu, S. Wang, L. Jiang, Nat. Rev. Mater. 2017, 2, 17036.

[18] H. Xie, H. X. Huang, Y. J. Peng, Nanoscale 2017, 9, 11951.

[19] K. Liu, L. Jiang, Annu. Rev. Mater. Res. 2012, 42, 231.

[20] Z. Sun, T. Liao, K. Liu, L. Jiang, J. H. Kim, S. X. Dou, Small 2014, 10, 3001.

[21] Z. Han, X. Feng, Z. Guo, S. Niu, L. Ren, Adv. Mater. 2018, 30, e1704652.

[22] K. Liu, J. Du, J. Wu, L. Jiang, Nanoscale 2012, 4, 768.

[23] X. Jing, H. Y. Mi, Y. J. Lin, E. Enriquez, X. F. Peng, L. S. Turng, ACS Appl. Mater. Interfaces 2018, 10, 20897.

[24] Z. Yu, F. F. Yun, Y. Wang, L. Yao, S. Dou, K. Liu, L. Jiang, X. Wang, Small 2017, 13, 1701403.

[25] M. Cao, J. Ju, K. Li, S. Dou, K. Liu, L. Jiang, Adv. Funct. Mater. 2014, 24, 3235.

[26] R. A. Potyrailo, R. K. Bonam, J. G. Hartley, T. A. Starkey, P. Vukusic, M. Vasudev, T. Bunning, R. R. Naik, Z. Tang, M. A. Palacios, M. Larsen, L. A. Le Tarte, J. C. Grande, S. Zhong, T. Deng, Nat. Commun. 2015, 6, 7959.

[27] H. Zhou, J. Xu, X. Liu, H. Zhang, D. Wang, Z. Chen, D. Zhang, T. Fan, Adv. Funct. Mater. 2017, 28, 1705309.

[28] H. Kang, J. S. Lee, W. S. Chang, S. H. Kim, Adv. Mater. 2015, 27, 1282.

[29] R. Yan, M. Chen, H. Zhou, T. Liu, X. Tang, K. Zhang, H. Zhu, J. Ye, D. Zhang, T. Fan, Sci. Rep. 2016, 6, 20001.

[30] H. Chen, T. Ran, Y. Gan, J. Zhou, Y. Zhang, L. Zhang, D. Zhang, L. Jiang, Nat. Mater. 2018, 17, 935.

[31] K. Li, J. Ju, Z. Xue, J. Ma, L. Feng, S. Gao, L. Jiang, Nat. Commun. 2013, 4, 2276.

[32] N. Zhao, Z. Wang, C. Cai, H. Shen, F. Liang, D. Wang, C. Wang, T. Zhu, J. Guo, Y. Wang, X. Liu, C. Duan, H. Wang, Y. Mao, X. Jia, H. Dong, X. Zhang, J. Xu, Adv. Mater. 2014, 26, 6994.

[33] Z. Sun, T. Liao, Y. Dou, S. M. Hwang, M. S. Park, L. Jiang, J. H. Kim, S. X. Dou, Nat. Commun. 2014, 5, 3813.

[34] D. Xiang, T. Liu, J. Xu, J. Y. Tan, Z. Hu, B. Lei, Y. Zheng, J. Wu, A. H. C. Neto, L. Liu, W. Chen, Nat. Commun. 2018, 9, 2966.

[35] F. Zhang, J. Zhu, D. Zhang, U. Schwingenschlogl, H. N. Alshareef, Nano Lett. 2017, 17, 1302.

[36] P. Vukusic, J. R. Sambles, Nature 2003, 424, 852.

[37] P. Vukusic, J. R. Sambles, C. R. Lawrence, Nature 2000, 404, 457.

[38] J. Teyssier, S. V. Saenko, D. van der Marel, M. C. Milinkovitch, Nat. Commun. 2015, 6, 6368.

[39] Y. Zhao, Z. Xie, H. Gu, C. Zhu, Z. Gu, Chem. Soc. Rev. 2012, 41, 3297.

[40] S. Kinoshita, S. Yoshioka, J. Miyazaki, Rep. Prog. Phys. 2008, 71, 076401.

[41] C. Park, K. Koh, U. Jeong, Sci. Rep. 2015, 5, 8340.

[42] D. Wu, J. N. Wang, L. G. Niu, X. L. Zhang, S. Z. Wu, Q. D. Chen, L. P. Lee, H. B. Sun, Adv. Opt. Mater. 2014, 2, 751.

[43] M. Kolle, P. M. Salgard-Cunha, M. R. Scherer, F. Huang, P. Vukusic, S. Mahajan, J. J. Baumberg, U. Steiner, Nat. Nanotechnol. 2010, 5, 511.

[44] Z. Sun, T. Liao, L. Sheng, J. H. Kim, S. X. Dou, J. Bell, Mater. Today Chem. 2016, 1-2, 84.

[45] E. Fresta, V. Fernández-Luna, P. B. Coto, R. D. Costa, Adv. Funct. Mater. 2018, 28, 1707011.

[46] S. Yoshioka, T. Nakano, Y. Nozue, S. Kinoshita, J. R. Soc. Interface 2008, 5, 457.

[47] G. H. Kim, T. An, G. Lim, ACS Appl. Mater. Interfaces 2017, 9, 19057.

[48] J. Hwang, M. H. Song, B. Park, S. Nishimura, T. Toyooka, J. W. Wu, Y. Takanishi, K. Ishikawa, H. Takezoe, Nat. Mater. 2005, 4, 383.

[49] P. Tzeng, D. J. Hewson, P. Vukusic, S. J. Eichhorn, J. C. Grunlan, J. Mater. Chem. C 2015, 3, 4260.

[50] S. Y. Choi, M. Mamak, G. von Freymann, N. Chopra, and G. A. Ozin, Nano Lett. 2006, 6, 2456.

[51] B. Augui é, M. C. Fuertes, P. C. Angelom é, N. L. Abdala, G. S. Illia, A. Fainstein, ACS Photon. 2014, 1, 775.

[52] G. M. Nogueira, D. Banerjee, R. E. Cohen, M. F. Rubner, Langmuir 2011, 27, 7860.

[53] M. Muallem, A. Palatnik, G. D. Nessim, Y. R. Tischler, ACS Appl. Mater. Interfaces 2015, 7, 474.

[54] P. Lova, C. Bastianini, P. Giusto, M. Patrini, P. Rizzo, G. Guerra, M. Iodice, C. Soci, D. Comoretto, ACS Appl. Mater. Interfaces 2016, 8, 31941.

[55] F. Fu, L. Shang, Z. Chen, Y. Yu, Y. Zhao, Sci. Robot. 2018, 3, eaar8580.

[56] E. V. Hooijdonk, S. Berthier, J.-P. Vigneron, J. Appl. Phys. 2012, 112, 114702.

[57] A. Levy-Lior, E. Shimoni, O. Schwartz, E. Gavish-Regev, D. Oron, G. Oxford, S. Weiner, L. Addadi, Adv. Funct. Mater. 2010, 20, 320.

[58] D. Gur, B. A. Palmer, B. Leshem, D. Oron, P. Fratzl, S. Weiner, L. Addadi, Angew. Chem., Int. Ed. 2015, 54, 12426.

[59] Z. Luo, B. A. Evans, C. H. Chang, ACS Nano 2019, 13, 4657.

[60] T. M. Jordan, J. C. Partridge, N. W. Roberts, Nat. Photonics 2012, 6, 759.

[61] D. Gur, B. Leshem, V. Farstey, D. Oron, L. Addadi, S. Weiner, Adv. Funct. Mater. 2016, 26, 1393.

[62] O. Berger, L. Adler-Abramovich, M. Levy-Sakin, A. Grunwald, Y. Liebes-Peer, M. Bachar, L. Buzhansky, E. Mossou, V. T. Forsyth, T. Schwartz, Y. Ebenstein, F. Frolow, L. J. Shimon, F. Patolsky, E. Gazit, Nat. Nanotechnol. 2015, 10, 353.

[63] O. Berger, E. Yoskovitz, L. Adler-Abramovich, E. Gazit, Adv. Mater. 2016, 28, 2195.

[64] Z. Sun, T. Liao, W Li, Y Qiao, K. Ostrikov, Adv. Funct. Mater. 2019, 1901460.

[65] Z. Wang, J. Zhang, J. Xie, C. Li, Y. Li, S. Liang, Z. Tian, T. Wang, H. Zhang, H. Li, W. Xu, B. Yang, Adv. Funct. Mater. 2010, 20, 3784.

[66] L. V. Thekkekara, M. Gu, Sci. Rep. 2017, 7, 45585.

[67] J. Mei, T. Liao, H. Spratt, G. A. Ayoko, X. S. Zhao, Z. Sun, Small Methods 2019, 1900055.

[68] T. B. H. Schroeder, A. Guha, A. Lamoureux, G. VanRenterghem, D. Sept, M. Shtein, J. Yang, M. Mayer, Nature 2017, 552, 214.

[69] X. Wang, Y. Yin, F. Yi, K. Dai, S. Niu, Y. Han, Y. Zhang, Z. You, Nano Energy 2017, 39, 429.

[70] A. Ahmed, I. Hassan, P. Song, M. Gamaleldin, A. Radhi, N. Panwar, S. C. Tjin, A. Y. Desoky, D. Sinton, K. T. Yong, J. Zu, Sci. Rep. 2017, 7, 17143.

[71] Z. Wu, L. Li, T. Liao, X. Chen, W. Jiang, W. Luo, J. Yang, Z. Sun, Nano Today 2018, 22, 62.

[72] H. Cheng, Y. Zhou, Y. Feng, W. Geng, Q. Liu, W. Guo, L. Jiang, Adv. Mater. 2017, 29, 1700177.

[73] R. H. Siddique, Y. J. Donie, G. Gomard, S. Yalamanchili, T. Merdzhanova, U. Lemmer, H. Hölscher, Sci. Adv. 2017, 3, e1700232.

[74] R. Senthil, S. Yuvaraj, Int. J. Energy Res. 2019, 43, 1068.

[75] K. K. Sakimoto, N. Kornienko, P. Yang, Acc. Chem. Res. 2017, 50, 476.

[76] D. Kim, K. K. Sakimoto, D. Hong, P. Yang, Angew. Chem., Int. Ed. 2015, 54, 3259.

[77] B. Han, Y. Huang, R. Li, Q. Peng, J. Luo, K. Pei, A. Herczynski, K. Kempa, Z. Ren, J. Gao, Nat. Commun. 2014, 5, 5674.

[78] J. Fu, B. Zhu, W. You, M. Jaroniec, J. Yu, Appl. Catal., B 2018, 220, 148.

[79] I. Martínez-Ruvalcaba, J. F. Hernández-Paz, J. R. Mancilla, P. Ruiz, C. A. Pérez, P. E. García-Casillas, C. A. Rodríguez-González, J. Alloys Compd. 2014, 586, s526.

[80] M. I. Shams, M. Nogi, L. A. Berglund, H. Yano, Soft Matter 2012, 8, 1369.

[81] Z. Sun, T. Liao, W. Li, Y. Dou, K. Liu, L. Jiang, S.-W. Kim, J. H. Kim, S. X. Dou, NPG Asia Mater. 2015, 7, e232.

[82] Y. Dou, D. Tian, Z. Sun, Q. Liu, N. Zhang, J. H. Kim, L. Jiang, S. X. Dou, ACS Nano 2017, 11, 2477.

[83] J. Wang, L. Sun, M. Zou, W. Gao, C. Liu, L. Shang, Z. Gu, Y. Zhao, Sci. Adv. 2017, 3, e1700004.

[84] Z. Jiang, H. Sun, T. Wang, B. Wang, W. Wei, H. Li, S. Yuan, T. An, H. Zhao, J. Yu, P. K. Wong, Energy Environ. Sci. 2018, 11, 2383.

[85] H. Zhang, Y. Wang, D. Wang, Y. Li, X. Liu, P. Liu, H. Yang, T. An, Z. Tang, H. Zhao, Small. 2014, 10, 3371.

[86] S. Tian, Z. Wang, W. Gong, W. Chen, Q. Feng, Q. Xu, C. Chen, C. Chen, Q. Peng, L. Gu, H. Zhao, P. Hu, D. Wang, Y. Li, J. Am. Chem. Soc. 2018, 140, 11161.

[87] W. Gong, Y. Lin, C. Chen, M. Al-Mamun, H. Lu, G. Wang, H. Zhang, H. Zhao, Adv. Mater. 2019, 31, 1808341.

Chapter 3. Structure-induced Charge Unsaturation and Wide-band Light adsorption for Enhanced Photocatalytic Performance

Introductory Remarks

This chapter presents the work of a new strategy to modify the chemical state and electronic structure of metal oxide semiconductor realized by the structure-induced charge unsaturation in the homogeneous 2D-TiO_2 nanosheets. The crystallized 2D-TiO_2 nanosheets exhibited unconventional electronic states compared to its bulk counterparts, aroused by the 2D derived lattice distortion in the nanosheet structures. The structure-induced charge transfer from O atoms to Ti atoms resulted in reduced chemical states of the Ti metals in the 2D-TiO_2 nanosheet structures, which presented extraordinary optical and catalytic properties compared to those with conventional bulk crystal structures. Moreover, this structure also maintained the salient surface physical and chemical properties of 2D materials, such as the enlarged surface area which is beneficial for creating abundant surface active sites, leading to a better catalytic performance in the photocatalytic oxidation reactions of benzyl alcohol and benzylamine.

3.1 Introduction

Titanium dioxide (TiO_2) only absorbs ultraviolet light due to the wide band gap of semiconductor, which limits its application in visible light photocatalysis. Past researches mostly focus on doping hetero elements or creating vacancy defects to optimize the electronic band structure of TiO_2, however, the accompanying recombination centers could reduce the photonic efficiency in the photocatalytic reactions. Herein, we demonstrated a new strategy to modify the chemical state and electronic structure of metal oxide semiconductor realized by the structure-induced charge unsaturation in the homogeneous 2D-TiO_2 nanosheets. The lattice distortion occurring in the crystal structure of 2D-TiO_2 nanosheet resulted in unconventional charge transfer between Ti and O atoms, leading to improved light absorption in visible-light spectrum, which showed better photocatalytic performance in the aerobic oxidation reactions of benzyl alcohol and benzylamine.

Titanium dioxide (TiO_2) has been one of the most widely used materials in all kinds of catalytic applications due to its low cost, salient stability, and nontoxicity, which is in good alignment with the green concept of environmental protection and sustainable development [1-3]. However, as a member of semiconductor family, the chemical nature of TiO_2 determines that it can only be activated by ultraviolet-light irradiation, which has distinctly limited its application in visible-light photocatalysis areas [2, 4]. For example, TiO_2 photocatalysts have usually been reported to be successfully applied in the fields of dye degradation or pollutant treatment [5-7], while compared to its effectiveness in such systems, TiO_2 is not effective enough to perform organic syntheses with high productivity and selectivity, especially under visible-light irradiation [8, 9]. Conducting visible-light-driven selective organic reactions by TiO_2 photocatalysts remains yet a grand challenge [9, 10].

To better utilize the visible range of the solar spectrum for the photocatalytic reactions, modifying the chemical state and electronic structure of the catalysts has been identified as a desirable strategy [11-13]. Therein, the most important route is to introduce defects into the lattice structures of the catalysts by doping heteroatom elements or creating intrinsic vacancies [14-17]. Such defect center acting as an electron donor or acceptor can effectively adjust the electronic states of the catalysts, making the activated carries better contribute to the redox reactions [18, 19]. However, on the other hand, the created defects could also act as recombination centers for the excited charge carriers, which will lower the utilizing efficiency of the charge and result in relatively low catalytic activities [2, 20]. In addition, it is also challenging to incorporate dopants or vacancies into highly-crystalized catalytic materials by mild synthetic methods and conditions, thus making the synthetic process less cost-effective [21]. Engineering the compressive strain of the catalyst surface is believed to be another effective way to realize some unconventional electronic structures and improve the catalytic performance of catalysts [22]. It is reported that the engineering of surface strain on the catalyst could result in different binding behavior between the oxygen species and the catalyst surface during the reaction process [23, 24]. Nevertheless, such strain engineering are usually constructed on the basis of ordered intermetallic phases with high transition metal component, and are not easy to be realized in homogeneous metal oxide semiconductor materials.

To this end, we proposed a new strategy to modify the chemical state and electronic structure of metal oxide semiconductor realized by manipulating the crystal structure of homogeneous 2D-TiO_2 nanosheets, in which no foreign doping impurities nor inherent vacancy defects are included. The crystallized 2D-TiO_2 nanosheets exhibited unconventional electronic states compared to its bulk counterparts, aroused by the 2D

derived lattice distortion in the nanosheet structures [25-28]. The structure-induced charge transfer from O atoms to Ti atoms resulted in reduced chemical states of the Ti metals in the 2D-TiO_2 nanosheet structures, which presented extraordinary optical and catalytic properties compared to those with conventional bulk crystal structures. Moreover, this structure also maintained the salient surface physical and chemical properties of 2D materials, such as the enlarged surface area which is beneficial for creating abundant surface active sites, leading to a better catalytic performance in the photocatalytic oxidation reactions of benzyl alcohol and benzylamine.

3.2 Experimental

3.2.1 Materials

Titanium (IV) isopropoxide (TTIP, 97%), poly(ethylene glycol)-block-poly(propylene glycol)-block-poly(ethylene glycol) (PEO_{20}-PPO_{70}-PEO_{20}, Pluronic P123) and ethylene glycol (EG, anhydrous, 99.8%) were purchased form Sigma-Aldrich. Hydrochloric acid (HCl, 32%) and ethanol (absolute) were obtained from Ajax Finechem. All chemical reagents were used without further modification.

3.2.2 Synthesis of 2D-TiO_2 nanosheets

The synthetic method of 2D-TiO_2 nanosheets was reported in our previous paper. In a typical synthetic process, 1.05 g TTIP solution was added into 0.74 g HCl under vigorous stirring in bottle A, and in bottle B, 0.2 g P123 was dissolved in 3.0 g ethanol. After the P123 in bottle B was completely dissolved, the solution was mixed with the solution in bottle A and kept stirring for another 20 minutes. Then 2.5 mL of the mixture solution was transferred into a 45 mL autoclave along with 20 ml EG. The solvothermal process was conducted in an oven at 150 ℃ for 20 hours. The products were obtained by centrifuging and washed in water once and ethanol 3 times. The white powders of 2D-TiO_2 nanosheets were collected after drying at 120 ℃ for 8 hours.

The 2D-TiO_2 samples were further annealed in a Muffle furnace at 250-550 ℃ for 1 hour with a heating rate of 5 ℃/min, the obtained samples are denoted as 2D-TiO_2-T, where T refers to the annealing temperatures (℃).

3.2.3 Characterization

The morphologies of the samples were characterized by field emission scanning electron microscopy (FESEM, JEOL 7001F) and transmission electron microscopy (TEM, JEOL 2100). The accelerating voltage was 5 kV for SEM and 200 kV for TEM. X-ray photoelectron spectroscopy (XPS, Al Kα, 1486.6 eV) and ultraviolet photoelectron spectra (UPS, HeI, 21.22 eV) was recorded on a Kratos Axis Ultra photoelectron spectrometer. The electron paramagnetic resonance (ESR) spectrum was studied by MiniScope MS400 spektrometer (9.42GHz). The crystal information of the samples was obtained by X-ray diffraction facility (XRD, Philips Panalytical X'Pert MPD) using Co Kα radiation (λ=0.179 nm) at power source of 40 kV and 40mA. Raman spectra of the samples was studied by a laser Raman spectrometer (Renishaw inVia Raman Microscope) using an Ar+ laser (532 nm) as excitation source. Diffuse reflectance UV-visible spectra was collected on a Cary 5000 UV-Vis-NIR spectrometer (DRS UV-vis, Agilent) using $BaSO_4$ as reference. Brunauer-Emmett-Teller (BET) surface area of the samples was measured by N_2 adsorption/desorption isotherms (Micromeritics Tristar 3020) performed at 77 K.

3.2.4 Photocatalytic activity test

The photocatalytic activities of the as-prepared samples were estimated by the aerobic oxidation of benzyl alcohol and benzylamine in air under visible light irradiation. Oxidation of benzyl alcohol: 20 mg of catalyst was dispersed into 1 ml toluene containing 0.1 mmol benzyl alcohol in a 10 ml Pyrex glass tube. The reaction was conducted under irradiation of a 500 W halogen lamp (0.6 W/cm^2, $\lambda > 400$ nm) at

55 ℃ for 5-30 hours. The cycling test applied the same reaction condition as the original test, except that the reaction time was 20 hours for each cycle. After each cycle, the catalysts were recycled by centrifuging, washing and drying process. Oxidation of benzylamine: 10 mg of catalyst was dispersed into 2 ml toluene containing 0.2 mmol benzylamine in a 10 ml Pyrex glass tube. The reaction was conducted under irradiation of a 500 W halogen lamp (0.6 W/cm^2) at 45 ℃ for 5-20 hours. After the reaction, the aliquots were collected, centrifuged, and then filtered through a Millipore filter (pore size 0.45 μm) to remove the catalyst particles. The products were analyzed by gas chromatography (GC, Agilent).

3.3 Results and discussion

Figure 3-1a shows the schematic illustration of the 2D-TiO_2 structures changed with different temperatures. As the annealing temperature increase, the structures of 2D-TiO_2 transform from dispersed nanosheets to aggregated nanosheets and further to bulk nanoparticles. Transmission electron microscopy (TEM) analyses were performed on the synthesized 2D-TiO_2 and annealed 2D-TiO_2-T samples to examine their morphologies and crystal structures. As shown in Figure 1, the low-magnification TEM images of 2D-TiO_2 (**Figure 3-1b**) presents a well-dispersed graphene-like nanosheet structure with some of the edges rolling up caused by surface tension. The size of each 2D-TiO_2 nanosheet is around 100 nm. And in the case of 2D-TiO_2-250 (**Figure 3-1c**), after the heat-treatment process, the nanosheets were curled up to a larger extent and a small parts of the nanosheets were aggregated together due to the thermal effect, as a result, the size of the 2D-TiO_2-250 nanosheet shrinked to around 50 nm. The thermal effect appears to be more obvious in the 2D-TiO_2-350 samples. It can be seen from Figure 3-1d, some of the nanosheets were curled up completely to nanoscrolls and some others were sintered during the heating process. However, the

2D nanosheet structure can still be clearly distinguished in the TEM image. In this sample, the TiO_2 exists in forms of both sintered bulk phase and unfolded 2D nanosheet phase. When the annealing temperature increased beyond 450 ℃, a drastic change on the morphologies was observed. As clearly seen in Figure 1e and f, the major configuration of the samples changed from 2D nanosheets to bulk particles as a result of crystal growth under high temperature. The average particle size was 10-20 nm for 2D-TiO_2-450 and 20-30 nm for 2D-TiO_2-550, which increased with higher annealing temperature. Another feature that increased with annealing temperature was the crystallinity of the TiO_2 samples, as indicated by the high magnification TEM images in Figure 3-1 g-k. **Figure 3-S1** shows the TEM image of commercial TiO_2 P25 particles, presenting a similar morphology as those of 2D-TiO_2-450 and 2D-TiO_2-550 samples. Similar features can also been observed in the SEM images, as shown in **Figure 3-1** l-p, the morphologies changed obviously from dispersed nanosheets (**Figure 3-1** l, m and n) to solid particles (**Figure 3-1** o and p) as the annealing temperature varies. We believe that the various morphologies and crystallinities between these TiO_2 samples will induce interesting differences in their chemical states and catalytic performances.

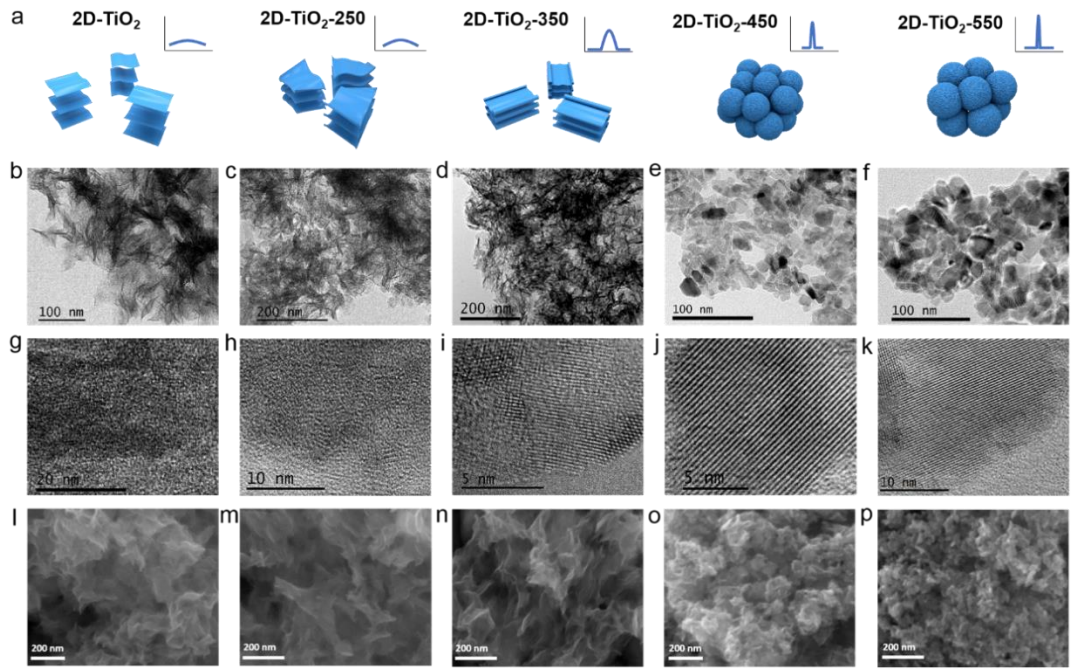

Figure 3-1 (a) Schematic illustration of the 2D-TiO_2 morphologies changed with different temperatures. (b-f) Low-magnification TEM images, (g-k) high-magnification TEM images and (l-p) SEM images of 2D-TiO_2, 2D-TiO_2-250, 2D-TiO_2-350, 2D-TiO_2-450 and 2D-TiO_2-550.

To investigate the phase composition and structural change of the samples, XRD and Raman spectroscopy was performed. As revealed by XRD patterns (**Figure 3-2a**), all as-prepared samples present a typical TiO_2 crystal structure without any foreign impurity phases, and the diffraction peak becomes stronger and sharper as the annealing temperature increases. In the pattern of 2D-TiO_2 sample, we observed a mixed crystal phase composite of both anatase and rutile phase, indicating a same phase composition with that of conventional P25 nanoparticles, except that the crystallinity of P25 is much better. The first two peaks lower than 20 degree are assigned to the structural thickness d of 1.2 and 0.62 nm, which are calculated by the Bragg equation $2d\sin\theta = n\lambda$. This should be attributed to the periodic stacking of the monolayers of the TiO_2 nanosheets, and the calculated values coincide well with the reported spacing of the monolayers in the stacked 2D-TiO_2 nanosheets. However,

these structural peaks in the XRD patterns can only be detected in the pure 2D-TiO_2 nanosheets rather than other annealed 2D-TiO_2-T samples, which indicates that the 2D monolayers were stacked into multilayer structures during the heat treating process. Such multilayer nanosheets had a higher thickness than before which could avoid the effect of quantum confinement and resulted in a narrower bank gap. It is also worth noting that, the trace of rutile phase disappears in the spectrums of 2D-TiO_2-450 and 2D-TiO_2-550 samples. We suspect that there should be a recrystallization and regrowth process of the TiO_2 nanocrystal accompanying the transformation from 2D phase to bulk phase. The Raman spectrums could be found in **Figure 3-2b**. The six (3Eg + 2B1g + A1g) Raman-active modes of anatase phase at frequencies of 144, 197, 397, 513, 519 and 639 cm-1 were detected in all samples. The unexpected Raman vibration at 260 cm-1 in the 2D-TiO_2 sample could be aroused by some organic species remained on the surface after the solvothermal synthesis, which were easily decomposed during the heat treatment. It is well known that Raman spectroscopy has been utilized as an efficient, accurate and well-established approach to investigate the structural changes in TiO_2 [29, 30]. The inset in Figure 3b shows an enlarged Raman spectrum from 100 to 200 cm-1. The Eg mode located at 143.4 cm-1 for commercial P25 nanoparticles undergoes a shift to higher frequencies of 150.2, 148.1 and 146.9 cm^{-1} for 2D-TiO2, 2D-TiO2-250 and 2D-TiO2-350 respectively, and such shift is not observed in the case of 2D-TiO2-450 and 2D-TiO_2-550 samples. Apparently, the blue shift of Eg mode is related to the 2D phases in the 2D-TiO_2, 2D-TiO_2-250 and 2D-TiO_2-350 samples, and the shift appears more significant as the proportion of 2D phase increases. It has been reported that the Eg mode shift can be caused by the lattice disorder of the TiO_2 crystals, which is exactly the important structural feature of the as-prepared 2D-TiO_2 nanosheets.

To further investigate how the chemical properties change with different morphologies of 2D-TiO_2 samples, we performed X-ray photoelectron spectroscopy (XPS) to study their surface chemical states. **Figure 3-2c** shows the Ti 2p spectrum of the 2D-TiO_2, 2D-TiO_2-T and P25 samples, which indicates a significant difference between those with 2D and bulk structures. In the Ti 2p spectrum of 2D-TiO_2 sample, the Ti 2p1/2 and Ti 2p3/2 spin-orbital splitting photoelectrons are assigned to the binding energy peaks of 463.2 and 457.6 eV, showing a 2.1 eV downshift to lower binding energy compared to the TiO2 samples with bulk crystal structures (2D-TiO_2-450, 2D-TiO_2-550 and P25). The shift of the 2D-TiO_2 binding energy is likely attributed to the extraordinary electron transfer between Ti atoms and O atoms caused by the crystal distortion in the nanosheet structures. In contrast to the traditional band engineering strategy based on the introduction of Ti^{3+} defects, such structure-induced electron transfer could avoid the formation of carrier recombination centers during the photocatalytic process and thus enhance their catalytic activities. It is noteworthy that, there are two groups of Ti 2p characteristic peaks coexisting in the spectrum of 2D-TiO_2-250 and 2D-TiO_2-350 samples, which are attributed to the 2D phase (463.2 eV for Ti $2p_{1/2}$ and 457.6 eV for Ti $2p_{3/2}$) and bulk phase (465.3 eV for Ti $2p_{1/2}$ and 459.7 eV for Ti $2p_{3/2}$) respectively. The detection of bulk phase in the XPS spectrum of these samples should be resulted from the aggregation and sintering of TiO_2 nanosheets under thermal effect, which is coincident with the observations in TEM characterization. In addition, the special 2D-structure-induced charge unsaturation in 2D-TiO_2 structure can also be confirmed by the electron paramagnetic resonance (ESR) spectrum. As shown in Figure 3-S2, the broad signal at g = 1.99 in 2D-TiO_2-350 should be assigned to the unpaired electrons around Ti atoms, which are aroused by the structure-induced charge transfer between Ti and O atoms. In contrast, such signal was

not detected in the bulk TiO_2 structures (P25 and 2D-TiO_2-550), indicating that no electron transfer behavior occurred in these structures, and the Ti atoms stayed at the normal Ti^{4+} states, which coincides well with the above XPS results.

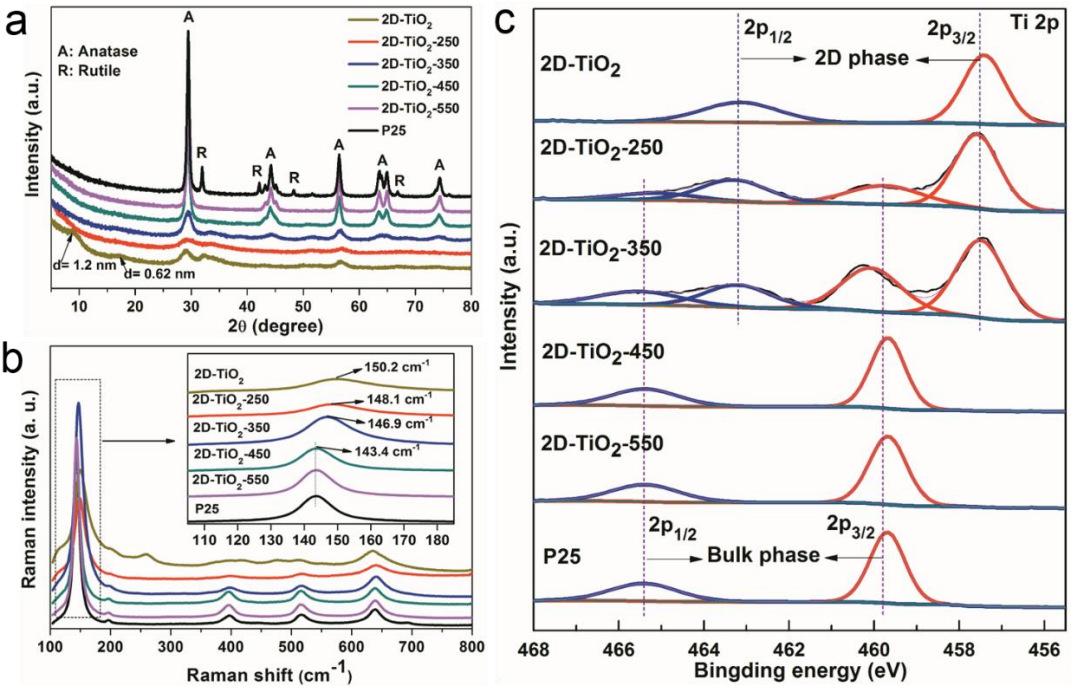

Figure 3-2 (a) XRD patterns of 2D-TiO_2 nanosheets, 2D-TiO_2-T and P25 samples. (b) Raman spectra of 2D-TiO_2 nanosheets, 2D-TiO_2-T and P25 samples. The inset shows the enlarged Eg mode of the samples. (c) XPS spectra of 2D-TiO_2 nanosheets, 2D-TiO_2-T and P25 samples.

UV-vis diffuse reflectance spectra (DRS) was studied to explore the optical properties of the 2D-TiO_2 nanosheets and annealed 2D-TiO_2-T samples (**Figure 3-3a**). The DRS spectra of P25 nanoparticles was also recorded as a reference. Due to the quantum confinement effect aroused by the ultrathin thickness of the nanaosheets, the optical absorbance of 2D-TiO_2 sample exhibits a blue shift to the UV region compared to that of P25. However, when the 2D-TiO_2 nanosheets were annealed at 250 and 350 ℃, the absorbance onset significantly shifted to the visible spectrum range due to the 2D-structure-induced charge unsaturation which changed the electronic band structure. Furthermore, the partly aggregated configurations and stacked multilayer structures of

the annealed nanosheets suppressed the quantum confinement effect, which allowed much more incident photons to be absorbed by the samples. When the annealing temperature was increased beyond 450 ℃, the nanaosheet structures all transformed to bulk nanoparticles, meanwhile the structure-induce charge unsaturation was recovered through the regrowth of TiO_2 crystals, as a result, the light absorbance of 2D-TiO_2-450 and 2D-TiO_2-550 have reduced to the same level as that of P25 nanoparticles.

Another remarkable feature of 2D-TiO_2 nanosheets is the high specific surface. As we known, the enlarged surface area is of great benefit for the exposure of abundant surface active sites in the photocatalytic reactions. The Brunauer-Emmett-Teller (BET) surface area of the samples was analyzed by N_2 adsorption/desorption isotherms, the results are presented in **Figure 3-3b**. The 2D-TiO_2 nanosheets have a very high BET surface area of 445.9 m^2/g contributed by their 2D nature and thin thickness, which is almost ninefold as that of commercial P25 (52.4 m^2/g). The surface areas of annealed 2D-TiO_2-250 (350.2 m^2/g) and 2D-TiO_2-350 (201.3 m^2/g) samples are lower due to thermal aggregation but still maintain at a relatively high level in the family of TiO_2 materials. However, the surface areas drop down drastically for 2D-TiO_2-450 and 2D-TiO_2-550 samples as the morphologies have transformed from 2D nanosheets to bulk crystals.

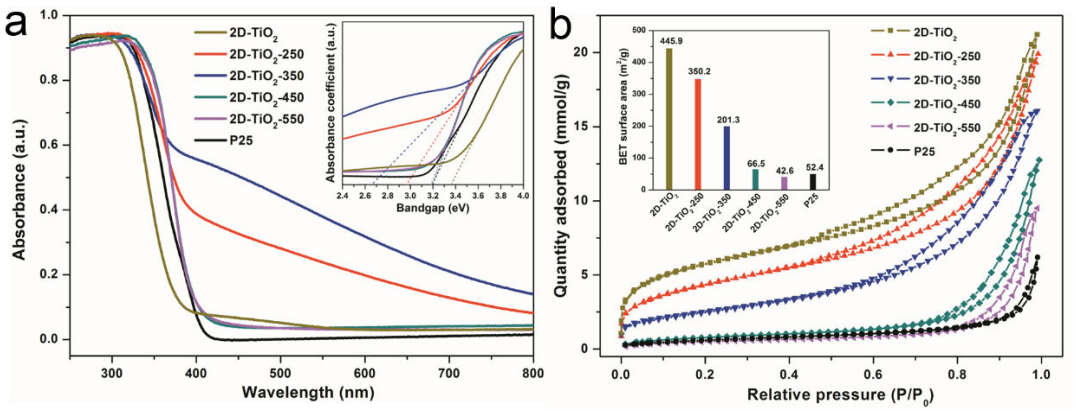

Figure 3-3 (a) UV-vis diffuse reflectance spectra and bandgap of 2D-TiO_2 nanosheets, 2D-TiO_2-T and P25 samples. (b) Nitrogen adsorption/desorption isotherms of 2D-TiO_2, 2D-TiO_2-T and P25 samples, the inset shows the BET surface area of 2D-TiO_2 nanosheets, 2D-TiO_2-T and P25 samples.

The photocatalytic properties of as-prepared 2D-TiO_2, 2D-TiO_2-T and P25 were evaluated by the aerobic oxidation of benzyl alcohol and benzylamine under visible light irradiation ($\lambda > 400$ nm), which are two typical photocatalytic aerobic oxidation reactions. **Figure 3-4** summarizes the yields of the product of the two reactions. Due to the poor crystallinity and wide bandgap of the 2D-TiO_2 nanosheets, this catalyst performed the lowest catalyticactivity in both reactions. Crystallinity is a very important factor that will influence the photocatalytic property as it determine the photo-excited carrier mobility and recombination rate. Therefore, despite the broadened visible light absorption, the catalytic activities of 2D-TiO_2-250 samples were still relatively low because the photo-excited carriers were not able to travel smoothly through the crystals due to their poor crystallinity. However, the 2D-TiO_2-350 catalysts exhibited the highest product yield in both reactions, which was one and a half times higher than that of commercial P25 catalyst. The reasons of the improvement could be attributed to several effects: 1. the narrowed bandgap aroused by the structure-induced charge unsaturation of the 2D-TiO_2 nanosheets afforded more carriers to be excited by the incident light; 2. the excited carries were more easily

migrated from the bulk to the surface due to the enhanced crystallinity and thin thickness of the 2D nanosheets; 3. the enlarged surface area contributed more active interfaces between the catalysts and the reactants. As can be seen in the result, when the 2D nanosheet structures transformed to bulk particles under higher annealing temperature in the 2D-TiO_2-450 and 2D-TiO_2-550 samples, the catalytic activities of both reactions suffered a decrease due to the structural changes. However it is interesting that the catalytic performances of these two samples were still competitive to that of commercial P25 TiO_2 catalysts, the possible reason could be that the pure anatase phases of 2D-TiO_2-450 and 2D-TiO_2-550 are more favorable to the aerobic oxidation reactions compared to the mixture phases of antase and rutile in P25 TiO_2. The cycling test of the photocatalytic activity of 2D-TiO_2-350 samples in the benzyl alcohol oxidation reaction are shown in **Figure 3-S3**. After six reaction cycles, the 2D-TiO_2-350 samples did not exhibit obvious decline, and the phase composition and crystal structure of the samples did not present any change compared to those before the reaction as indicated by the XRD test in **Figure 3-S4**, performing a good cycling stability in the photocatalytic oxidation process.

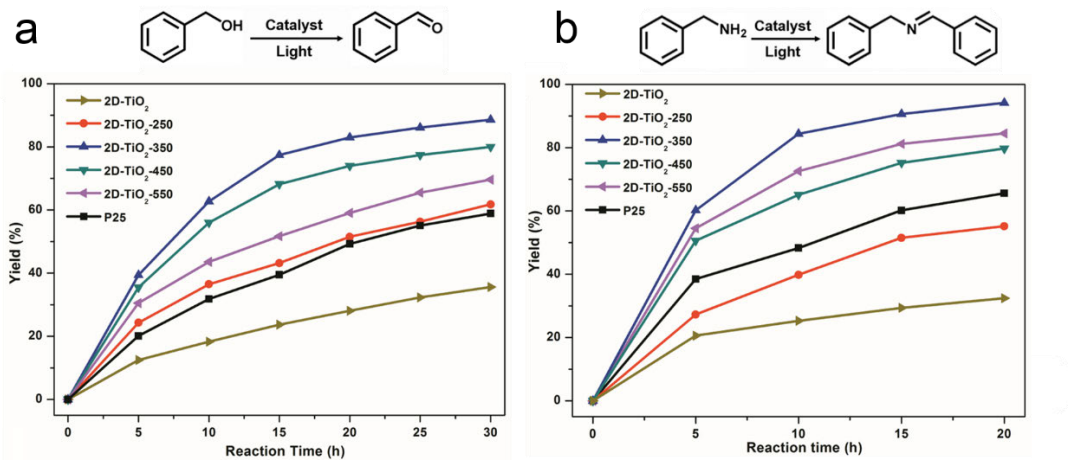

Figure 3-4 Photocatalytic performance of 2D-TiO_2 nanosheets, 2D-TiO_2-T and P25 catalysis under irradiation of visible light. (a) Photocatalytic oxidation of benzyl alcohol. (b) Photocatalytic oxidation coupling of benzylamine.

3.4 Conclusions

In summary, we demonstrated a strategy to modify the chemical state and electronic structure of metal oxide semiconductor realized by the structure-induced charge unsaturation in the homogeneous 2D-TiO_2 nanosheets. Compared to normal bulk structures of TiO_2, the modified homogenous 2D-TiO_2-350 nanosheet structure exhibited an unconventional electronic state, broadened visible-light absorption and boosted photocatalytic activity in the aerobic oxidation reactions. This work gives new insight on modifying the electronic band structure of metal oxide semiconductors towards efficient photocatalytic reactions driven by visible light.

Reference

[1] J. Schneider, M. Matsuoka, M. Takeuchi, J. Zhang, Y. Horiuchi, M. Anpo, D. W. Bahnemann, Chem Rev 2014, 114, 9919.

[2] W. Li, A. Elzatahry, D. Aldhayan, D. Zhao, Chem Soc Rev 2018, 47, 8203.

[3] Z. Luo, T. Wang, J. Zhang, C. Li, H. Li, J. Gong, Angew Chem Int Ed Engl 2017, 56, 12878.

[4] S. Selcuk, X. Zhao, A. Selloni, Nat Mater 2018, 17, 923.

[5] D. Kanakaraju, J. Kockler, C. A. Motti, B. D. Glass, M. Oelgemöller, Applied Catalysis B: Environmental 2015, 166-167, 45.

[6] C. Adán, J. Marugán, S. Mesones, C. Casado, R. van Grieken, Chemical Engineering Journal 2017, 318, 29.

[7] C. Athanasekou, G. E. Romanos, S. K. Papageorgiou, G. K. Manolis, F. Katsaros, P. Falaras, Chemical Engineering Journal 2017, 318, 171.

[8] S. Ramesh, F. Devred, D. P. Debecker, Applied Catalysis A: General 2019, 581, 31.

[9] X. Lang, J. Zhao, X. Chen, Angew Chem Int Ed Engl 2016, 55, 4697.

[10] Y. Li, Y. Bian, H. Qin, Y. Zhang, Z. Bian, Applied Catalysis B: Environmental 2017, 206, 293.

[11] M. Li, Y. Chen, W. Li, X. Li, H. Tian, X. Wei, Z. Ren, G. Han, Small 2017, 13.

[12] Z. Lian, W. Wang, G. Li, F. Tian, K. S. Schanze, H. Li, ACS Appl Mater Interfaces 2017, 9, 16959.

[13] Y. H. Hu, Angew Chem Int Ed Engl 2012, 51, 12410.

[14] S. Na Phattalung, S. Limpijumnong, J. Yu, Applied Catalysis B: Environmental 2017, 200, 1.

[15] H. Hirakawa, M. Hashimoto, Y. Shiraishi, T. Hirai, J Am Chem Soc 2017, 139, 10929.

[16] L. W. Fan Zuo, Tao Wu, Zhenyu Zhang, Dan Borchardt, and Pingyun Feng, J Am Chem Soc 2010, 132, 11856.

[17] L. L. Xiaobo Chen, Peter Y. Yu, Samuel S. Mao, Science 2011, 331, 746.

[18] A. Naldoni, M. Allieta, S. Santangelo, M. Marelli, F. Fabbri, S. Cappelli, C. L. Bianchi, R. Psaro, V. Dal Santo, J Am Chem Soc 2012, 134, 7600.

[19] X. Xin, T. Xu, J. Yin, L. Wang, C. Wang, Applied Catalysis B: Environmental 2015, 176-177, 354.

[20] J. Wang, P. Zhang, X. Li, J. Zhu, H. Li, Applied Catalysis B: Environmental 2013, 134-135, 198.

[21] J. Xiong, J. Di, J. Xia, W. Zhu, H. Li, Advanced Functional Materials 2018, 28, 1801983.

[22] S. Zhang, X. Zhang, G. Jiang, H. Zhu, S. Guo, D. Su, G. Lu, S. Sun, J Am Chem Soc 2014, 136, 7734.

[23] N. Z. Lingzheng Bu, Shaojun Guo, Xu Zhang, Jing Li, Jianlin Yao, Tao Wu, Gang Lu, Jing-Yuan Ma, Dong Su,Xiaoqing Huang, Science 2016, 354, 1410.

[24] A. D. Caviglia, R. Scherwitzl, P. Popovich, W. Hu, H. Bromberger, R. Singla, M. Mitrano, M. C. Hoffmann, S. Kaiser, P. Zubko, S. Gariglio, J. M. Triscone, M. Forst, A. Cavalleri, Phys Rev Lett 2012, 108, 136801.

[25] K. Lan, Y. Liu, W. Zhang, Y. Liu, A. Elzatahry, R. Wang, Y. Xia, D. Al-Dhayan, N. Zheng, D. Zhao, J Am Chem Soc 2018, 140, 4135.

[26] Q. K. Xiguang Han, Mingshang Jin, Zhaoxiong Xie, and Lansun Zheng, J Am Chem Soc 2009, 131, 3152.

[27] Z. Sun, T. Liao, Y. Dou, S. M. Hwang, M. S. Park, L. Jiang, J. H. Kim, S. X. Dou, Nat Commun 2014, 5, 3813.

[28] Y. Wang, C. Sun, X. Yan, F. Xiu, L. Wang, S. C. Smith, K. L. Wang, G. Q. Lu, J. Zou, J Am Chem Soc 2011, 133, 695.

[29] I. Tanabe, Y. Ozaki, Journal of Materials Chemistry C 2016, 4, 7706.

[30] X. X. Han, L. Chen, U. Kuhlmann, C. Schulz, I. M. Weidinger, P. Hildebrandt, Angew Chem Int Ed Engl 2014, 53, 2481.

Supporting information

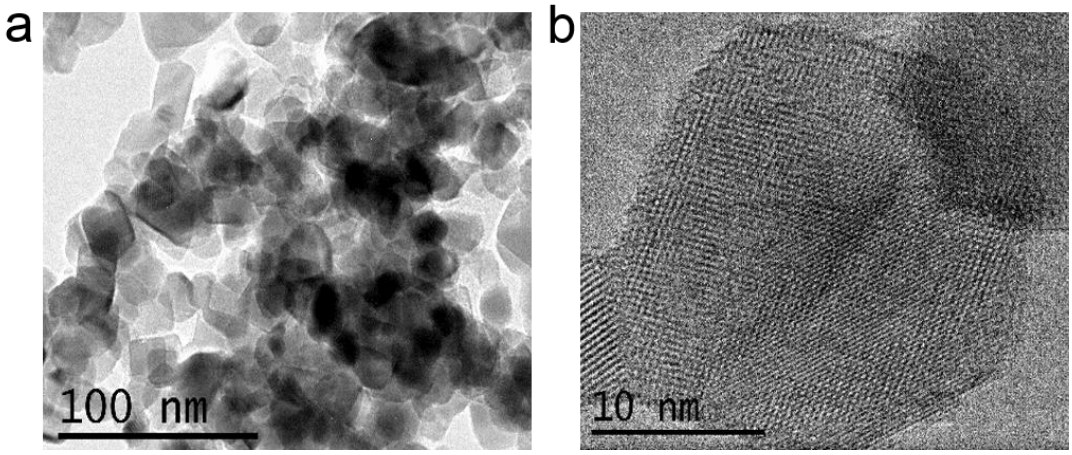

Figure 3-S1 Low (a) and high (b) magnification TEM image of P25.

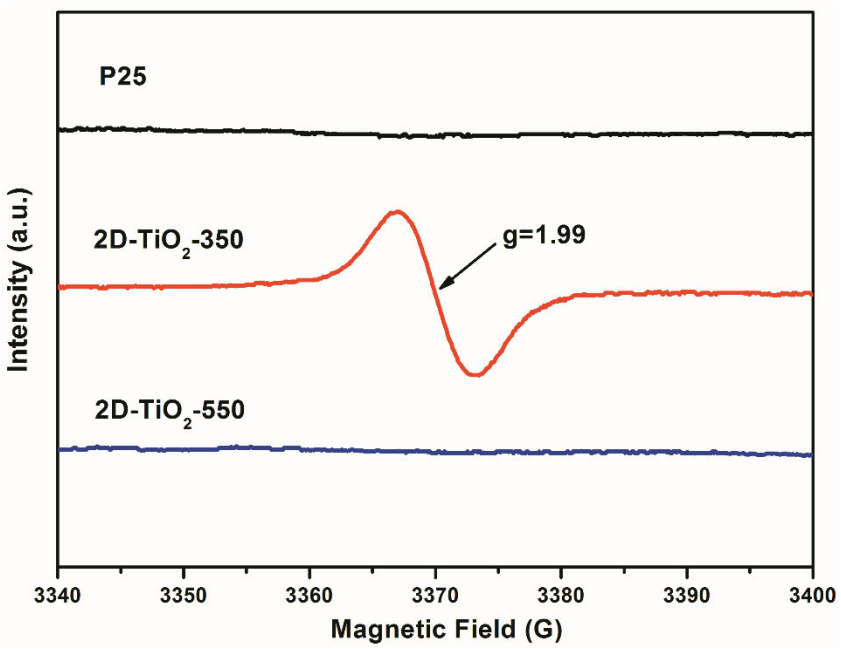

Figure 3-S2 EPR spectrum of P25, 2D-TiO_2-350 and 2D-TiO_2-550 samples.

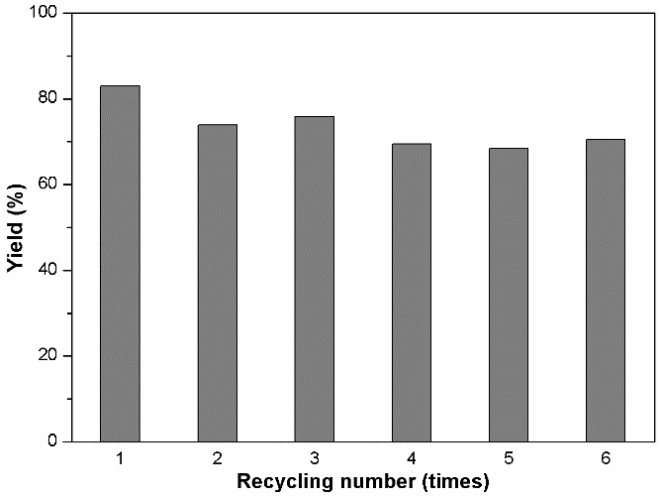

Figure 3-S3 Cycling test of aerobic oxidation reaction of benzyl alcohol for with 2D-TiO_2-350 catalysts under visible light irradiation, each cycle was conducted for 20 hours.

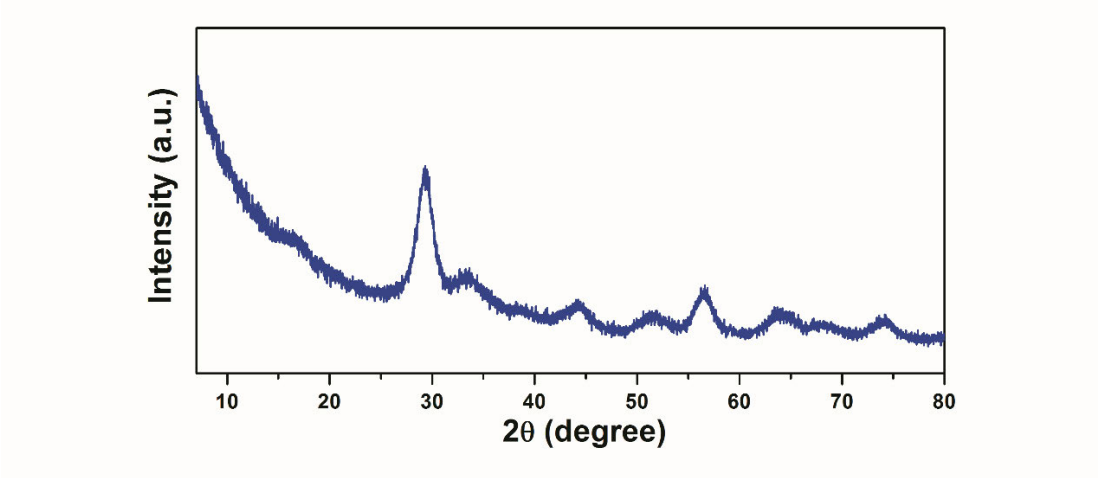

Figure 3-S4 XRD pattern of 2D-TiO_2-350 catalysts after 6 reaction cycles.

Chapter 4. Strongly interfacial-coupled 2D-2D TiO_2/g-C_3N_4 Heterostructure for Enhanced Visible-light Induced Synthesis and Conversion

Introductory Remarks

This chapter presents the work of an interfacially coupled TiO_2/g-C_3N_4 2D-2D heterostructure has been prepared via in situ growth of ultrathin 2D TiO_2 on dispersed g-C_3N_4 nanosheets. This strongly coupled 2D-2D TiO_2/g-C3N_4, different from the weakly bonded 2D-TiO_2/g-C_3N_4 heterostructures produced by mechanical mixing, has unique electronic structures and chemical states due to strong interlayer charge transfer, confirmed by both experimental and theoretical analyses. Significantly enhanced visible-light responses have been observed, indicating a great potential for visible-light induced photosynthesis and photocatalysis. For benzylamine oxidation coupling reactions under visible light irradiation for 20 h, 80% yield rate has been achieved, superior to ~30% yield rate when adopting either 2D-TiO_2 or g-C_3N_4, structure. The enhanced photocatalytic activity can be attributed to the adequate separation of photo-generated electrons at the strongly coupled 2D-2D interfacial heterojunctions.

4.1 Introduction

Two-dimensional (2D) nanosheet-based nanocomposites have attracted intensive interest owing to the unique electronic and optical properties from their constituent phases and the synergistic effect from the heterojunctions. In this study, an interfacially coupled TiO_2/g-C_3N_4 2D-2D heterostructure has been prepared via in situ growth of ultrathin 2D TiO_2 on dispersed g-C_3N_4 nanosheets. This strongly coupled 2D-2D TiO_2/g-C3N_4, different from the weakly bonded 2D-TiO_2/g-C_3N_4 heterostructures produced by mechanical mixing, has unique electronic structures and chemical states due to strong interlayer charge transfer, confirmed by both experimental and theoretical analyses. Significantly enhanced visible-light responses have been observed, indicating a great potential for visible-light induced photosynthesis and photocatalysis. For benzylamine oxidation coupling reactions under visible light irradiation for 20 h, 80% yield rate has been achieved, superior to ~30% yield rate when adopting either 2D-TiO_2 or g-C_3N_4, structure. The enhanced photocatalytic activity can be attributed to the adequate separation of photo-generated electrons at the strongly coupled 2D-2D interfacial heterojunctions.

Over the past decade, two-dimensional (2D) nanomaterials have drawn significant interests due to its salient physical, chemical, and electronic properties aroused by their confined thickness and large surface area.[1-3] With such excellent features endowed by 2D structural characteristics, 2D nanomaterials have been successfully applied in a wide range of areas, including photocatalysis, electrocatalysis, energy storage and conversion devices, sustainable fuel generation, and so on.[4-7] For example, 2D metal oxides, as most of them are semiconductors and exhibit unique band structures, have shown great potential for optoelectronic devices and solar energy harvesting and conversion.[8-10] Particularly, ultrathin 2D-TiO_2 nanosheets that possess the features

of atomic level thickness, significant quantum confinement effect, ultrafast interlayer transport properties, and extraordinary coupling behaviours with heterostructures have presented promoted performances in some typical applications, including solar cells, photodetectors, and rechargeable batteries.[11-13] As another example, graphitic carbon nitride (g-C_3N_4), a non-metal semiconductor material composed with two of the most earth-abundant elements, is chemically and thermally stable, environmentally friendly, cost-effective, and most importantly, a favourable bandgap of 2.7 eV, has been demonstrated to be an important metal-free catalyst for effective photocatalysis and electrochemical catalysis.[14]

Even though the unparalleled advantages endorse the 2D nanomaterials with promising potential for a wide range of applications, both the pristine 2D metal oxides and g-C_3N_4 suffer from some intrinsic defects, such as low electric conductivity and low visible light responsibility.[15, 16] To overcome these shortcomings of the pristine 2D metal oxides and g-C_3N_4, the formation of heterostructures that combines the merits of different 2D nanostructures have been developed.[17, 18] Very recently, the 2D-2D heterostructure bonded by weak van de Waals (vdW) forces have been found possessing superior performances than the individual constitutional 2D nanomaterials.[19-21] For example, the 2D vdW heterostructures with well-designed band alignment can boost the energy efficiency of optoelectronic devices.[22] Inspired by this, we are wondering that the 2D-2D heterostructures with stronger interfacial coupling could also achieve some incomparable properties as those weakly vdW bonded heterostructures.

In this work, 2D-2D TiO_2 nanosheet/g-C_3N_4 heterostructure with strongly interfacial coupling was synthesized by direct growth of ultrathin 2D-TiO_2 nanosheets on the 2D g-C_3N_4 templates. Different to the commonly used method for fabricating weakly

contact 2D-2D heterostructures through physically mixing two oppositely surface charged 2D nanosheets, this in-situ growth of 2D-TiO_2 nanosheet on 2D g-C_3N_4 allows the formation of strong chemical bonds between the nanosheets during the self-assembly. As a result we expected, much more significant charge transfer and stronger interfacial coupling occur of the in-situ grown, strongly bonded 2D-2D heterostructures than the corresponding physically mixed, weakly bonded 2D-2D heterostructures, and endorse the materials with much enhanced catalytic activities, particularly under visible light irradiations. We therefore proposed that the strongly coupled 2D-2D heterojunctions can further alter the interfacial electronic structure and much enhance visible light induced photosynthesis and photocatalysis activities, would provide us a new path for designing novel 2D based catalysts towards high-performance photocatalysis or electrochemical catalysis. .

4.2 Experimental

4.2.1 Materials

Cyanuric acid, melamine, Titanium (IV) isopropoxide (TTIP, 97%), poly(ethylene glycol)-block-poly(propylene glycol)-block-poly(ethylene glycol) (PEO_{20}-PPO_{70}-PEO_{20}, Pluronic P123) and ethylene glycol (EG, anhydrous, 99.8%) were purchased form Sigma-Aldrich. Hydrochloric acid (HCl, 32%) and ethanol (absolute) were obtained from Ajax Finechem. All chemical reagents were used without further modification.

4.2.2 Synthesis of g-C_3N_4

g-C_3N_4 was synthesized using the cyanuric acid−melamine supramolecular precursor according to a previous report. The typical synthetic procedure was as follow: First, a 1:1 molar ratio of cyanuric acid and melamine were mixed in water and shaken for 24 h at room temperature. Then, the obtained milky suspension was centrifuged and

washed with water three times and dried at 50 ℃ under vacuum. Afterward, the precursor powder was annealed in capped crucibles at 550 ℃ for 4 h at a heating rate of 2.3 ℃/min in nitrogen atmosphere. After cooling down, the yellow g-C_3N_4 powder was collected.

4.2.3 Synthesis of 2D-TiO_2/g-C_3N_4 composites

Firstly, suitable amount (5, 10, 50, 100 mg) of as-prepared g-C_3N_4 powder was dispersed in 20 ml EG solution and ultrasonic stirred for 60 min. In the meantime, 1.05 g TTIP solution was dissolved in 0.74 g concentrated HCl solution with vigorous stirring (bottle A); and 0.2 g Pluronic P123 was added into 3.0 g ethanol (bottle B). After stirring for 10 min, the solution in bottle B was poured into bottle A and stirred for another 20 min. 2.5 ml mixture solution of A and B was added in 20 ml g-C_3N_4/EG and then transferred into a 45 ml autoclave and heated at 150 ^oC for 20 h. The products of the hydrothermal reaction were washed with ethanol three times, and the yellow powders were collected after washing/centrifugation and drying at 80 ^oC for 24 h. The final products were calcined at 300 ℃ for 1 h before using as photocatalysts. The mechanically mixed 2D-TiO_2/g-C_3N_4 composites were synthesized via a simple solution mixing method. Firstly, 100 mg as-prepared 2D-TiO_2 and g-C_3N_4 powder were pretreated with diluted acid and alkali, respectively, and mixed in 100 ml deionized water. The mixed solution was further stirred for 2h at 600 rpm and then centrifuged and dried at 80 ^oC for 24 h. The as-prepared mechanically mixed 2D-TiO_2/g-C_3N_4 composites are named TC-33.3%-mix.

4.2.4 Characterization

The morphologies of the samples were characterized by field emission scanning electron microscopy (FESEM, JEOL 7001F) and transmission electron microscopy (TEM, JEOL 2100). The accelerating voltage was 5 kV for SEM and 200 kV for TEM.

X-ray photoelectron spectroscopy (XPS, Al Kα, 1486.6 eV) was recorded on a Kratos Axis Ultra photoelectron spectrometer. The crystal information of the samples was obtained by X-ray diffraction facility (XRD, Philips Panalytical X'Pert MPD) using Co Kα radiation (λ=0.179 nm) at power source of 40 kV and 40mA. Diffuse reflectance UV-visible spectra was collected on a Cary 5000 UV-Vis-NIR spectrometer (DRS UV-vis, Agilent) using $BaSO_4$ as reference. Brunauer-Emmett-Teller (BET) surface area of the samples was measured by N2 adsorption/desorption isotherms (Micromeritics Tristar 3020) performed at 77 K.

4.2.5 Photocatalytic activity test

Photocatalysis of dye degradation: 5mg of catalysts were dispersed in 10 ml of rhodamine 6G aqueous solution (10 mg/L). The suspended solution was stirred in the dark for 1 h to reach its adsorption equilibrium and then it was put under a 500W halogen lamp (400-750 nm) with illumination intensity of 0.5 W/cm^2. Degradation was monitored by taking aliquots every 10 minutes. These aliquots were centrifuged to remove the solid particles and then tested using a Cary 60 UV-vis spectrometer to get the absorption spectra. Photocatalysis of benzylamine oxidation: 10 mg of catalyst was dispersed into 2 ml toluene containing 0.2 mmol benzylamine in a 10 ml Pyrex glass tube. The reaction was conducted under irradiation of a 50 W halogen lamp (0.5 W/cm^2) at 35 ℃ for 200 hours. After the reaction, the aliquots were collected, centrifuged, and then filtered through a Millipore filter (pore size 0.45 μm) to remove the catalyst particles. The products were analyzed by gas chromatography (GC, Agilent).

4.3 Results and discussion

In this work, both the strongly coupled and the weakly coupled 2D-2D TiO_2-g-C_3N_4 heterostructures were fabricated respectively through an in-situ growth and physically

mixing methods. **Figure 4-1a** presents our concept for the in-situ synthesis of strongly coupled 2D-2D TiO_2/g-C_3N_4 heterojunctions via a wet-chemistry self-assemble approach. In a typical synthesis process, the as-prepared g-C_3N_4 powder was first dispersed in ethylene glycol (EG) and then mixed with the ethanol solution containing polyethylene oxide - polypropylene oxide - polyethylene oxide (PEO_{20}-PPO_{70}-PEO_{20}, Pluronic P123) surfactant and inorganic Titinum isopropoxide (TTIP) procursor. In this step, the surfactant molecules were supposed to be attached on the surface of g-C_3N_4 nanosheets to form a surfactant attached substrate, and then the hydrated titanium precursor oligomers were self-assembled into layered oligomer agglomerates guided by the lamellar micelles of surfactant. After the hydrothermal process and the removal of organic surfactants, the well-organized TiO_2 nanosheets were uniformly anchored to the surface of g-C_3N_4 substrates, leading to the formation of strongly bonded 2D-TiO_2-2D g-C_3N_4 heterojunctions. This method is adopted from the successful synthesis of atomically thin 2D-TiO_2 nanosheets from molecules developed in our previous report.[23] Via the wet-chemical synthesis approach, we prepared a series of 2D-TiO_2/g-C_3N_4 nanocomposites with different weight content of g-C_3N_4, namely TC-5%, TC-10%, TC-33.3%, and TC-50%, respectively, where the numbers stand for the weight percentage of g-C_3N_4 in the composites. It should be noted that the TC-33% sample corresponds to a 1:1 volume ratio of 2D ultrathin TiO_2 nanosheets (density is 4.23 g/cm^{-3}) to g-C_3N_4 (density is 2.18 g/cm^{-3}). As a comparison, weakly bonded 2D-2D TiO_2/g-C_3N_4 heterostructures were prepared by physically mixing the acid or alkali pretreated ultrathin 2D-TiO_2 nanosheets and g-C_3N_4 nanosheets into aqueous solvents, which adsorbed with each other through tailored surface electrostatic force. Typically, the sample donated as TC-33.3%-mixing was prepared for the purpose of comparison. The morphology and microstructures of the fabricated strongly coupled 2D-2D

TiO_2/g-C_3N_4 heterostructures were characterized by a transmission electron microscope (TEM). **Figure 4-1**b-d show the TEM images of TC-33.3%. As can be clearly observed in Figure 1b, the obtained nonaocomposite presents a typical "graphene-like" 2D nanaosheet morphology with the edges curled up aroused by high surface tension, which is a common phenomenon existed in 2D nanomaterials. The morphologies of 2D-TiO_2 and g-C_3N_4 can be clearly distinguished from each other as shown in the higher magnification TEM image (**Figure 4-1c**), and the 2D-TiO_2 and g-C_3N_4 nanosheets are stacked to form 2D-2D heterojunctions, where the darker parts in the middle of the image are the g-C_3N_4 ingredients according to the morphology of pure g-C_3N_4 shown in **Figure 4-S1**. The formation of 2D-TiO_2/g-C_3N_4 heterojunctions can be further identified in the HRTEM image. As shown in Figure 1d, the distinguished interface between the crystallized 2D-TiO_2 and the g-C_3N_4 is clearly observed. Furthermore, EDX mapping analysis of both TEM (**Figure 4-1e**) and SEM (**Figure 4-S2**) confirmed the distribution of C, N, Ti, and O elements corresponding to the uniform configuration of 2D-TiO_2 and g-C_3N_4 in the TC-33.3% sample.

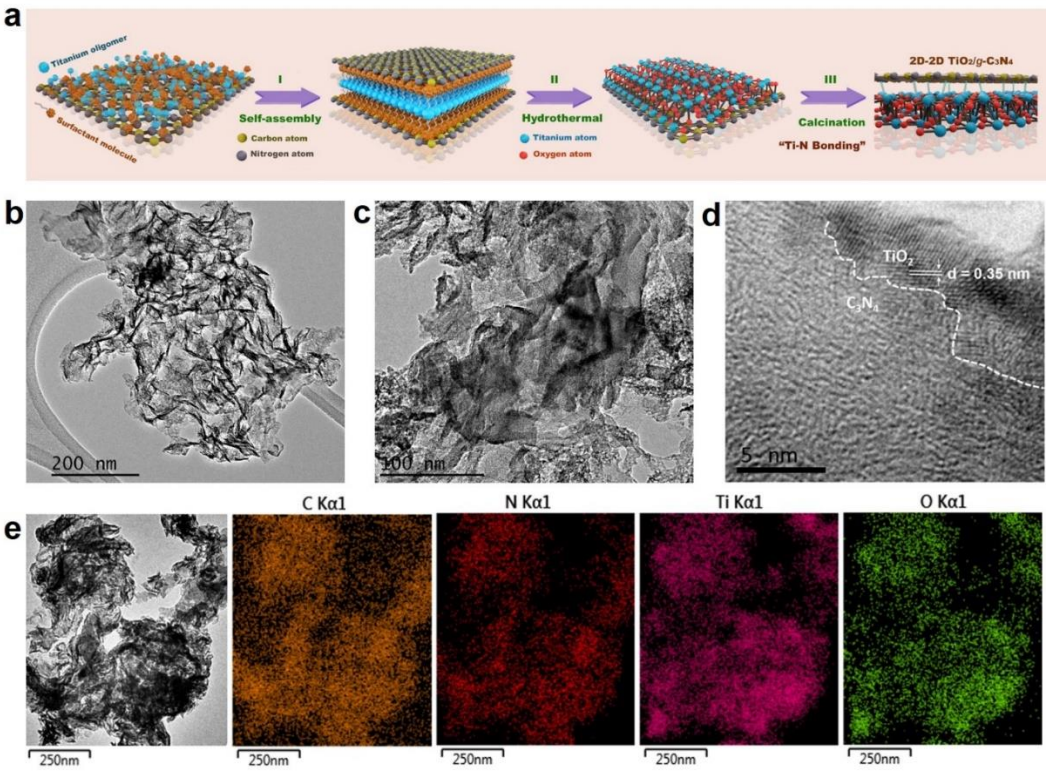

Figure 4-1 Synthetic process and morphological characterizations of 2D-TiO_2/g-C_3N_4 nanocomposites. (a) Schematic illustration of the synthesis of 2D-TiO_2/g-C_3N_4 heterojunctions via in situ self-assembly hydrothermal approach; (b, c) Low- and (d) high- resolution TEM images of TC-33.3% nanocomposites; (e) TEM EDX mapping images of TC-33.3% nanocomposites.

No distinct difference on the samples with different interfacial coupling states can be judged from the morphologies, but it can be clearly reflected from the chemical states and crystal structures of the bonding atoms and the constitutional nanosheets. **Figure 4-2a** and **Figure 4-S3** illustrate the crystal phase composition of the 2D-TiO_2/g-C_3N_4 nanocomposite identified by X-ray diffraction (XRD) characterization technique collected on pristine 2D-TiO_2, phase-pure g-C_3N_4, and as-synthesized TC-33.3% 2D-2D heterostructure. In the TC-33% heterostructure, the characteristic peaks from both the constitutional nanosheets were identified. For example, the peak at 32.1^o for the (002) facet diffraction arising from the stacking of conjugated aromatic layers of g-C_3N_4,[24, 25] and the peaks assigned to anatase (101) and rutile (110) and (200) of the 2D-TiO_2 nanosheets were observed in the TC-33% XRD patterns.[23] If we enlarge

the main peaks for those three sample, as shown in the inset of Figure 2a, the corresponding peaks for TC-33% were drafted to either lower or higher degrees. Compared to pristine 2D-TiO_2, the peaks of the heterostructure for TiO_2 shifted to lower degrees, indicating larger lattice parameters of the 2D-TiO_2 nanosheets in the strongly bonded heterostructure, while the peak for g-C_3N_4 shifted to a higher degree corresponding to smaller lattice parameters.[26] The drifting of the XRD patterns of the nanocomposite is definitely aroused by the strain of the heterostructure, where the 2D-TiO_2 is undergone a tensile stress and the g-C_3N_4 nanosheet is suffering from a compressive stress.[27] This lattice distortion identified by XRD is one concrete evidence of the formation of strongly bonded 2D-2D TiO_2/g-C_3N_4 heterostructure. In addition, there are two peaks at the lower degrees with *d* values of 1.2 and 0.62 nm, in the TC-33.3% patterns, which can be assigned to the structural periodicity of the nanosheets.[12]

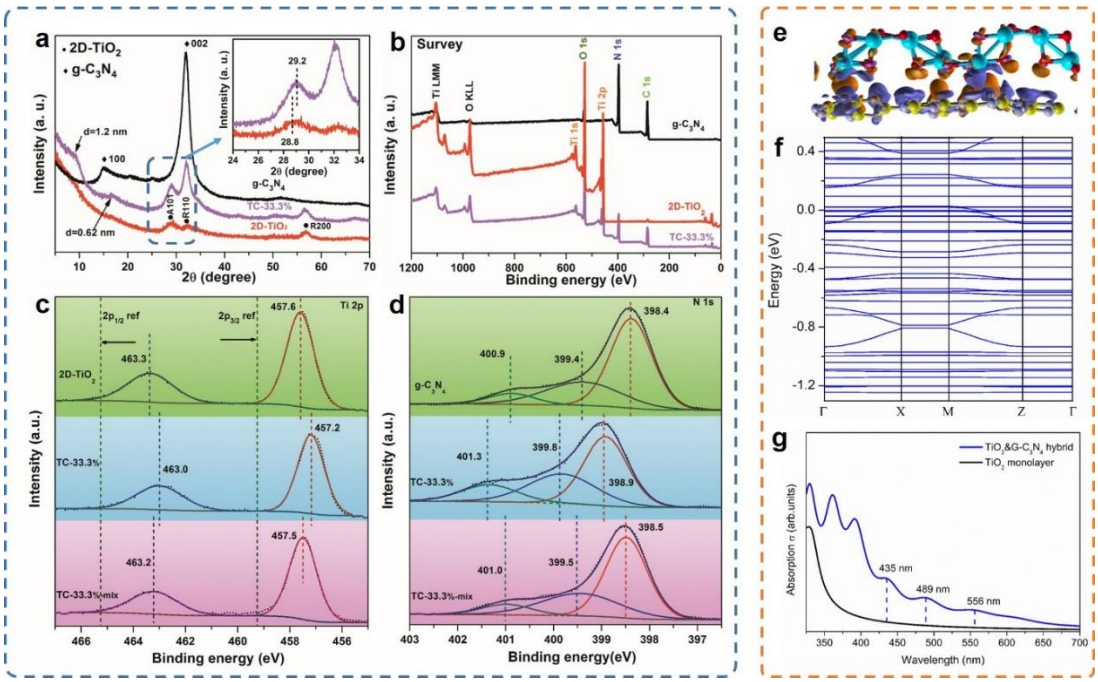

Figure 4-2 XRD, XPS pattern and DFT computational results of 2D-TiO_2/g-C_3N_4 nanocomposites composites. (a) XRD pattern of g-C_3N_4, 2D-TiO_2 and TC-33.3% samples; High resolution XPS spectra of (c) Ti 2p core level and (d) N 1s core level of TC-33.3% composites; (e) calculated charge transfer density plots along the interface of 2D-TiO_2/g-C_3N_4 nanocomposites; (f) calculated band structure of

2D-TiO_2/g-C_3N_4 nanocomposites; (g) calculated light absorption spectra of 2D-TiO_2/g-C_3N_4 nanocomposites.

The chemical states of 2D-TiO_2, g-C_3N_4, the strongly coupled TC-33.3%, and the physically mixed, weakly bonded TC-33%-mix samples were investigated by an X-ray photoelectron spectroscopy (XPS) technique (**Figure 4-2**b-d), which also directly reflected the difference between the strongly coupled TiO_2/C_3N_4 heterostructure and the weakly bonded TiO_2/C_3N_4 heterostructure. As can be seen in Figure 2b, all elements, including C, N, O, and Ti were detected in the survey spectra of TC-33.3%. It should be noted that O was also found in bulk-C_3N_4, attributed by the adsorbed hydroxyl groups and the formed defects,[28] and trace of C was identified in pristine TiO_2 aroused by the surface adventitious carbon from the surfactants.[29] **Figure 4-2c** presents the corresponding high-resolution Ti 2p spectra collected on 2D-TiO_2, strongly coupled TC-33%, and weakly bonded TC-33.3%-mix. As we previously reported, the Ti 2p core levels of the ultrathin 2D TiO_2 nanosheets present significant shifting towards bulk TiO_2 crystals, indicating a more reduced state of Ti in the nanosheets.[23] When strongly coupled with g-C_3N_4 nanosheets, the Ti 2p states further shifted to lower binding energy, which means that more electrons were transferred from g-C_3N_4 and made the Ti become more reduced compared to the pristine TiO_2 nanosheets, while this shifting was almost ignorable for the physically mixed, weakly bonded TC-33%-mix sample. The N 1s states shown in Figure 3-2d presented an opposite trend to Ti 2p, where those for TC-33% shifted to higher energy compare the pristine g-C_3N_4, indicating the transfer of electrons outwards N after coupling, and no significant change for the weakly bonded heterostructures. Based on the XPS results, it is very clear that there are obvious charge transfers from N to Ti in the strongly coupled 2D-2D heterostructures, while these charge transfers are much less in the weakly bonded 2D-2D TiO_2/g-C_3N_4 heterostructures. The XPS data are thus

another solid evidence in confirming the formation of strongly coupled 2D-2D TiO_2/g-C_3N_4 heterostructure.

In order to provide a deep understanding on the interfacial coupling state of the strongly bonded 2D-2D TiO_2/g-C_3N_4 heterostructures, density functional theory (DFT) calculations were performed to investigate the coupling behaviours and the interfacial charge transfers along the heterojunction interface. As shown in Figure 2e, the atomic configuration and the calculated interfacial charge transfers were illustrated. The charge density difference at the interface of 2D-TiO_2/g-C_3N_4 heterojunctions was investigated to reveal the interaction mechanism between g-C_3N_4 and 2D-TiO_2. The charge density difference, $\Delta\rho(r)$, of 2D-TiO_2/g-C_3N_4 heterostructure was calculated as

$$\Delta\,\rho(r) = \rho(r)_{2D-TiO2/g-C3N4} - [\rho(r)_{2D-TiO2} + \rho(r)_{g-C3N4}] \quad (1)$$

where $\rho(r)_{2D\text{-}TiO2/g\text{-}C3N4}$ is the charge density of the heterojunction system and $\rho(r)_{2D\text{-}TiO2}$ and $\rho(r)_{g\text{-}C3N4}$ are the charge densities of the individuals of 2D-TiO_2 and g-C_3N_4, respectively. Owing to the strongly coupled interface of the heterojunctions, the charge transfer occurs sufficiently along the whole interface through the N-O-Ti bonds and results in much a significant gain of electrons in Ti atoms and the loss of electrons in N atoms, which consist with the experimental XPS data presented in Figure 2c-d. It has been reported that the electron unsaturation strongly correlates with the chemical reactivity of the materials,[30] and this significant interfacial charge transfer will definitely dramatically increase the activity of the 2D-2D TiO_2/g-C_3N_4 heterostructures. Such efficient interfacial charge transfer induced by strong 2D-2D coupling will also alter the electronic structure of the materials.[31] The band structure of the strongly coupled 2D-TiO_2/g-C_3N_4 heterostructure was further calculated. As shown in Figure 2f, it is noted that some gap states formed in the band structure of 2D-TiO_2/g-C_3N_4, arising by the close interaction of the heterostructures. As a result, the

visible-light absorption of the heterostructures is much improved compared with that of individual 2D-TiO_2 monolayer (**Figure 4-2g**). It is believed that the significant charge transfer and gap states induced by the strongly coupled 2D-2D heterostructures exhibit extraordinary interfacial coupling states, significantly enhanced interfacial charge transfer behaviors, and thus much improved electron unsaturation and visible-light responsibility.

The optical properties and the associated spectroscopy characterizations of the strongly coupled 2D-2D TiO_2/g-C_3N_4 heterostructures have been performed on either the strongly coupled heterostructures with different ratios, the weakly bonded TC-33%-mixing, or individual nanosheets (**Figure 4-3** and **Figure 4-S4**). **Figure 4-3a** presents the UV-Vis diffuse reflectance absorption spectroscopy (DRS) measurements. It showed that the absorption onset is 380 and 465 nm for 2D-TiO_2 and g-C_3N_4, respectively, corresponding to a band gap of 3.25 and 2.65 eV. For the strongly coupled 2D-TiO_2/g-C_3N_4 heterojunctions, the DRS absorption edges of TC-5%, TC-10%, TC-33.3%, and TC-50% showed a significant red shift from UV region to visible-light region compared to that of the 2D-TiO_2, and the extent of red shift gets larger with the increase of g-C_3N_4 amount in the composites, indicating the significant influences of g-C_3N_4 in 2D-TiO_2 on the band structure. The red shift of UV-vis absorption wavelength in the strongly coupled 2D-TiO_2/g-C_3N_4 allows more photos to be absorbed by the materials and thus enhance the light utilizing efficiency. We also measured the UV-Vis absorption spectrum of the weakly bonded 2D-TiO_2/g-C_3N_4, TC-33%-mix, as shown in **Figure 4-S4a**. It is very clear that this red shift of UV-vis absorption is much less significant for the weakly bonded heterostructures. The calculated band gap for the strongly bonded TC-33% reached 2.75 eV, while the band

gap for weakly bonded TC-33%-mix was 2.90 eV. This is another direct evidence on the much-enhanced interfacial charge transfers achieved by the formation of strongly coupled heterostructures. The photoluminescence spectra were recorded to reveal the migration of photo-generated carriers in the 2D-TiO_2/g-C_3N_4 nanocomposites. **Figure 4-3b** shows the photoluminescence (PL) spectra of 2D-TiO_2, TC-5%, TC-10%, TC-33.3%, TC-50%, and g-C_3N_4 samples at the excitation wavelength of 320 nm. Pristine g-C_3N_4 has a strong peak around 460 nm in the PL spectrum, which can be attributed to the band-band PL phenomenon, i.e. the emission light energy is approximately equal to the bandgap energy of g-C_3N_4.[32] Once 2D-TiO_2 were coupled on the g-C_3N_4 nanosheet, the emission intensity of PL spectra decreases significantly, suggesting that the g-C_3N_4/TiO_2 nanosheet has a lower recombination rate of photo-generated electron–hole pairs than g-C_3N_4, which is favourable for the photocatalytic reactions. The FT-IR spectra of 2D-TiO_2, g-C_3N_4, and TC-x nanocomposites are shown in **Figure 4-3c**. The spectra shows that all the spectra of TC-x samples are combination of the characteristic peaks of 2D-TiO_2 and g-C_3N_4. Specifically, the absorption band between 600 and 800 cm^{-1} denotes the stretching vibration of Ti-O-Ti. The sharp absorption peak at 808 cm^{-1} is attributed to the out-of-plane bending vibration of tri-s-triazine units of g-C_3N_4. The intense absorption band between 1240 and 1640 cm^{-1} is ascribed to the typical C-N and C=N stretching vibration of tri-s-triazine rings, and the wide absorption band between 3000 and 3600 cm^{-1} is due to the stretching vibration of terminal NH groups of g-C_3N_4.[33, 34] Owing to that the characteristic vibration bands associating with heavy metal atoms are usually located in the wavelength range lower than 500 cm^{-1}, no significant interfacial N-O-Ti vibrations can be identified in the FTIR spectra except for the minor changes observed in the range of 800-500 cm^{-1}.[35] As can be seen in **Figure 4-3**a-c, the characterization results of TC-x samples show a

very close relationship with the addition amount of g-C_3N_4 in the heterostructures. In **Figure 4-3d**, the data of the UV-vis DRS absorption onset, PL intensity, and FTIR transmission rate of the TC-x sample were collected to draw a variation tendency graph as a function of the g-C_3N_4 weigh percentage. From this graph it can be noted that a liner relation to the g-C_3N_4 amount in the heterostructures has been observed, suggesting that the g-C_3N_4 are well incorporated into the heterojunctions in a similar bonding state. In addition, the results of Brunauer-Emmett-Teller (BET) surface areas of the heterostructures are also proportional to the g-C_3N_4 amount. As shown in **Figure 4-S5**, the BET surface areas of 2D-TiO_2, TC-5%, TC-10%, TC-33.3%, TC-50%, and g-C_3N_4 are 385.6, 355.1, 325.9, 249.4, 169.1, and 43.4 m^2/g, respectively, as determined by N_2 adsorption/desorption isotherms, presenting a linear decreasing trend with the increase of g-C_3N_4 amount in the heterostuctures. The weakly bonded 2D-2D TC-33%-mix, however, does not share similar trends to the strongly bonded counterpart, TC-33%, as the data shown in **Figure 4-3d**, which again real the differences brought by the interfacial coupling states.

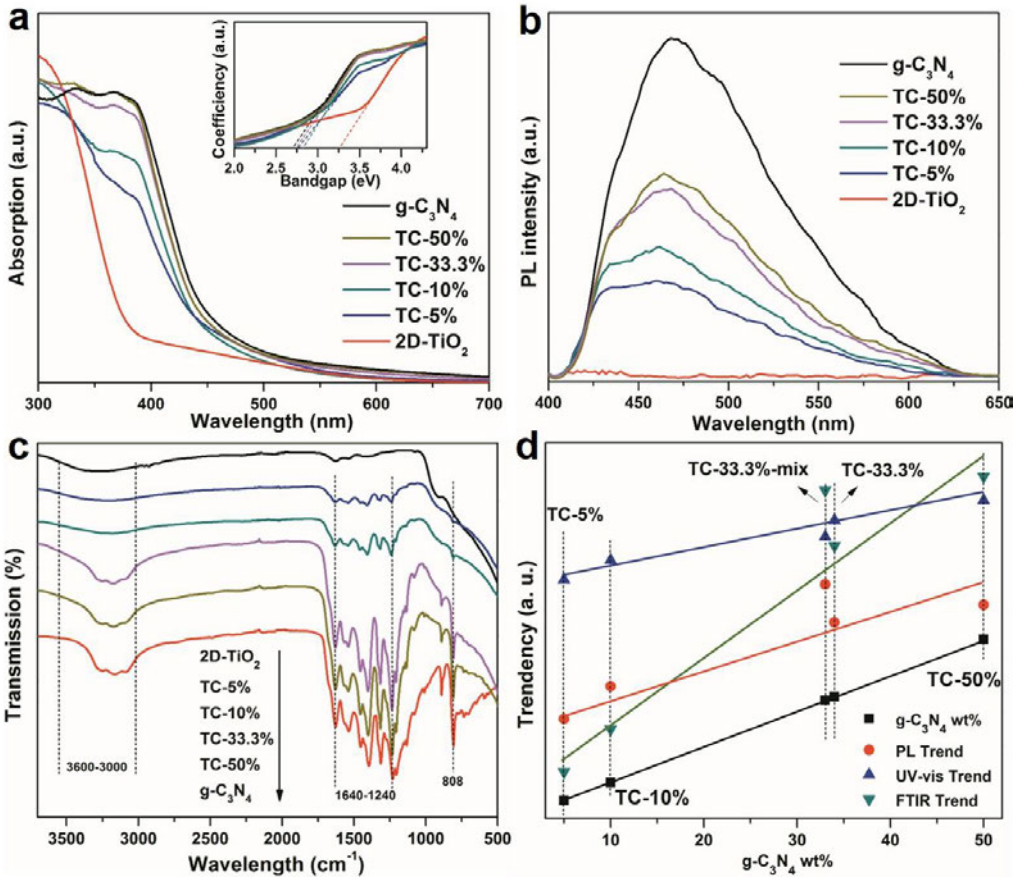

Figure 4-3 Optical properties and FTIR spectra of 2D-TiO_2/g-C_3N_4 nanocomposites. (a) UV-vis diffuse reflectance spectra, (b) PL spectra and (c) FTIR spectra of 2D-TiO_2, TC-5%, TC-10%, TC-33.3%, TC-50% and g-C_3N_4, with the inset in (a) showing the bandgap of corresponding samples; (d) the change of UVvis absorption, PL intensity and FTIR transmission as a function with the increase of the weight percentage of g-C_3N_4 in the TC composites.

It is obvious that the formation of strongly coupled 2D-2D heterostructures has significantly enhanced the interfacial chemical coupling, the extraordinary interfacial charge transfers, and the visible light responsibility. To confirm the unique bonding states on the chemical reactivity of the heterostructures, the catalytic activities of the 2D-2D TiO_2/g-C_3N_4 heterostructures driven by visible light have been examined systematically.

The typical visible light driven photosynthesis reaction, the oxidation and coupling of benzylamine into dibenzulamine, catalyzed by either the strongly coupled

heterostructures or the pristine 2D-TiO_2 or g-C_3N_4 nanosheets, were investigated under visible light irradiation. As shown in **Figure 4-4a**, the pristine g-C_3N_4 presented the lowest activity towards benzylamine oxidation and coupling, and only ~30% of product was detected after 20 hours visible light irradiation. The pristine 2D-TiO_2 is a little bit better than g-C_3N_4 nanosheets, which gives a 40% conversion after 20 hours. It is interesting that the highest conversion of 80% after 20 h was reached by the addition of strongly coupled TC-33% catalyst, which corresponding to 100% coverage of the nanosheets by its counterpart or 1:1 in terms of volume ratio of g-C_3N_4 to TiO_2. The inferior photocatalytic reactivity of the pristine nanosheets can be attributed to the wide bandgap of 2D-TiO_2 or the high carrier recombination rate of g-C_3N_4. By constructing strongly coupled heterostructures, both the band gap and carrier recombination issues can be solved. The reason why TC-33.3% showed the highest activity than other TC-x heterostructures is that this composition reaches 1:1 in volume and can give 100% match of these two nanosheets to form heterostructures. As we mentioned above, the strongly coupled heterostructures exhibited extraordinary interfacial coupling and charge transfer behoviors, and thus the 100% matched hetoerstructure achieves the highest visible-light absorption and lowest carrier recombination rate. The impact of the light intensity on the photocatalytic reaction rate over 2D-TiO_2, g-C_3N_4, and TC-33.3% was evaluated by varying the light intensity while maintaining other conditions unchanged. As shown in **Figure 4-4b**, it clearly seen that the increase in light intensity resulted in a linear increase in the reaction rate for all three catalysis, due to more photo-induced electrons and holes could promote the oxidation and coupling reactions.

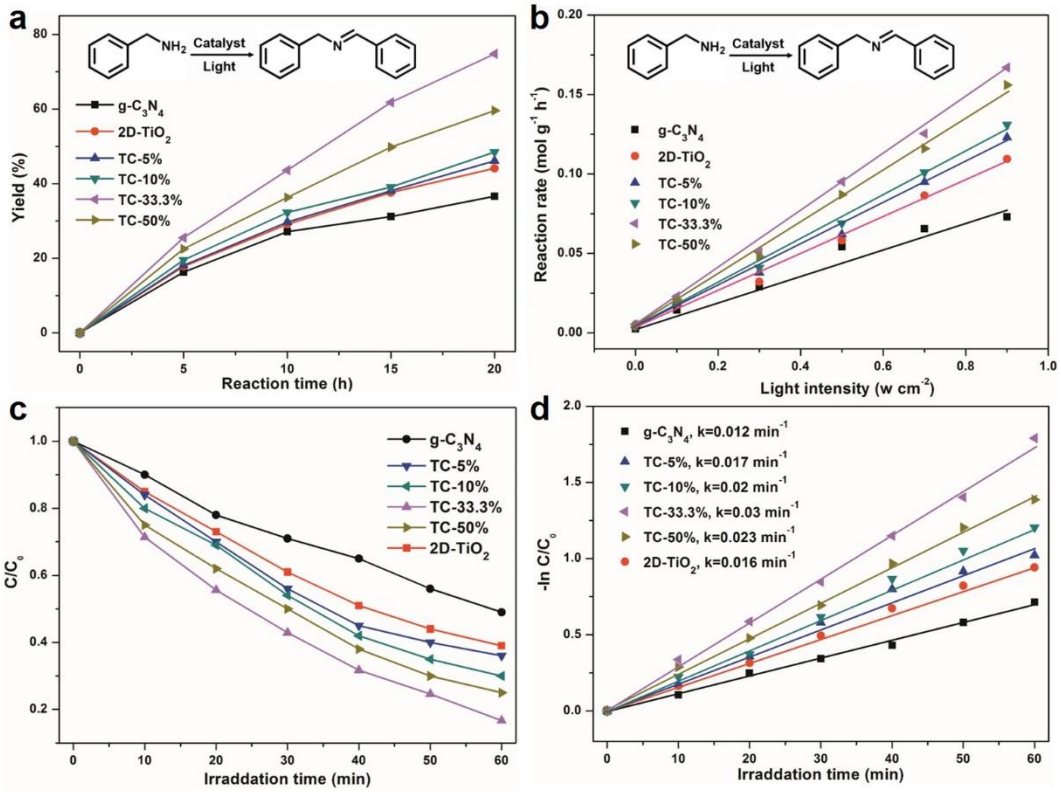

Figure 4-4 Photocatalytic performance of organic reaction and dye degradation over 2D-TiO_2/g-C_3N_4 nanocomposites. (a) Photocatalytic activity and (b) the reaction rate of the benzylamine oxidation coupling over 2D-TiO_2, g-C_3N_4 and TC-x samples under visible-light irradiation; (c) catalytic activity and (d) kinetic curves of the rhodamine 6G photodegradation tests over 2D-TiO2, TC-5%, TC-10%, TC-33.3%, TC-50% and g-C_3N_4.

To demonstrate the visible light driven reactivity of the heterostructures, the photocatalytic activities of 2D-TiO_2, g-C_3N_4, and the strongly coupled heterostructures were further evaluated by the Rhodamine 6G dye degradation test under visible-light irradiation (**Figure 4-4c**). As demonstrated in **Figure 4-S6**, it can be calculated that 60% and 50% of the dye was degraded after 60 min with the addition of pristine 2D-TiO_2 and g-C_3N_4, respectively, while all the strongly coupled 2D-TiO_2/g-C_3N_4 heterostructures presented higher photodegradation rate than both of 2D-TiO_2 and g-C_3N_4, confirming the synergistic effect of the heterojunctions. Similar to the benzylamine oxidation and coupling reations, TC-33.3% exhibited the highest

photocatalytic activity and 85% of the dye degraded after 60 min visible light irradiation, owing to the 100% coverage of the heterostructures. The kinetic curves for the Rhodamine 6G dye degradation over 2D-TiO_2, g-C_3N_4, and TC-x heterostructures are plotted and displayed in **Figure 4-4d**. They can be fit well with the pseudo-first order correlation, ln (C_0/C) = kt, where k is the apparent reaction rate constant, C_0 and C are the initial and instantaneous concentrations of Rhodamine 6G, respectively. One can easily compare the photocatalytic performance of different photocatalysts, based on the k values. In contrast to pristine g-C_3N_4 (k = 0.012 min^{-1}) and 2D-TiO_2 (k = 0.016 min^{-1}), the TC-33% heterostructure presented a two-fold enhancement in terms of the reaction kinetics (k = 0.03 min^{-1}). It is very clear that the TC-33% heterostructure provides the highest reactivity towards the visible-light driven dye degradation. The enhanced visible light induced photosynthesis and conversion, as we demonstrated in this article, is from the unique coupling states of the heterostructures. Compared to the widely studied weakly bonded heterostructures, these strongly coupled heterostructures prepared through in-situ self-assembly presented extraordinary bonding states, much enhanced interfacial charge transfers, improved electron unsaturation, and superior visible-light responses, and thus exhibited enhanced visible-light driven catalytic activity.

4.4 Conclusions

In this work, we successfully constructed strongly interfacially bonded 2D-2D ultrathin TiO_2/g-C_3N_4 heterostructures via an in situ molecular self-assembly routine. The as-prepared strongly coupled nanojunctions have a uniform 2D morphology with very distinct features as compared to the weakly bonded counterparts prepared by mechanical mixing. For example, significantly drifted peaks are observed in various spectroscopy analyses, attributed to interfacial charge transfers. The strongly coupled

2D-2D TiO_2/g-C_3N_4 heterostructures thus exhibit much narrowed band structures, enhanced visible light absorption, and superior chemical reactivity. When used as photocatalyst, the strongly coupled heterostructures present almost two-fold efficiency in visible light driven photosynthesis or conversion reactions compared to either 2D-TiO_2 or g-C_3N_4, structure. This work thus demonstrates a possibility of designing new, and 2D heterojunction based catalysts.

References

[1] X. Xiao, H. Wang, P. Urbankowski, Y. Gogotsi, Chem Soc Rev 2018, 47, 8744.

[2] B. Liu, K. Zhou, Progress in Materials Science 2019, 100, 99.

[3] A. J. Mannix, B. Kiraly, M. C. Hersam, N. P. Guisinger, Nature Reviews Chemistry 2017, 1.

[4] J. Mei, T. Liao, G. A. Ayoko, Z. Sun, ACS Appl Mater Interfaces 2019, 11, 28205.

[5] Y. Zhang, J. Mei, C. Yan, T. Liao, J. Bell, Z. Sun, Adv Mater 2019, e1902806.

[6] J. Mei, Y. Zhang, T. Liao, X. Peng, G. A. Ayoko, Z. Sun, Energy Storage Materials 2019, 19, 424.

[7] J. Mei, T. Liao, L. Kou, Z. Sun, Adv Mater 2017, 29.

[8] S. Das, D. Pandey, J. Thomas, T. Roy, Adv Mater 2019, 31, e1802722.

[9] P. Xiong, R. Ma, N. Sakai, T. Sasaki, ACS Nano 2018, 12, 1768.

[10] M. P. Browne, Z. Sofer, M. Pumera, Energy & Environmental Science 2019, 12, 41.

[11] Y. Zhu, L. Peng, Z. Fang, C. Yan, X. Zhang, G. Yu, Adv Mater 2018, 30, e1706347.

[12] L. Sheng, T. Liao, L. Kou, Z. Sun, Materials Today Energy 2017, 3, 32.

[13] W. Zhang, T. Xu, Z. Liu, N. L. Wu, M. Wei, Chem Commun (Camb) 2018, 54, 1413.

[14] A. Mishra, A. Mehta, S. Basu, N. P. Shetti, K. R. Reddy, T. M. Aminabhavi, Carbon 2019, 149, 693.

[15] W. J. Ong, L. L. Tan, Y. H. Ng, S. T. Yong, S. P. Chai, Chem Rev 2016, 116, 7159.

[16] X. Liu, M. C. Hersam, Adv Mater 2018, 30, e1801586.

[17] J. Fu, J. Yu, C. Jiang, B. Cheng, Advanced Energy Materials 2018, 8, 1701503.

[18] C. Yang, J. Qin, Z. Xue, M. Ma, X. Zhang, R. Liu, Nano Energy 2017, 41, 1.

[19] D. K. Bediako, M. Rezaee, H. Yoo, D. T. Larson, S. Y. F. Zhao, T. Taniguchi, K. Watanabe, T. L. Brower-Thomas, E. Kaxiras, P. Kim, Nature 2018, 558, 425.

[20] R. B. Pontes, R. H. Miwa, A. J. R. da Silva, A. Fazzio, J. E. Padilha, Physical Review B 2018, 97.

[21] R. Frisenda, E. Navarro-Moratalla, P. Gant, D. Perez De Lara, P. Jarillo-Herrero, R. V. Gorbachev, A. Castellanos-Gomez, Chem Soc Rev 2018, 47, 53.

[22] D. Unuchek, A. Ciarrocchi, A. Avsar, Z. Sun, K. Watanabe, T. Taniguchi, A. Kis, Nat Nanotechnol 2019, 14, 1104.

[23] Z. Sun, T. Liao, Y. Dou, S. M. Hwang, M. S. Park, L. Jiang, J. H. Kim, S. X. Dou, Nat Commun 2014, 5, 3813.

[24] T. Di, B. Zhu, B. Cheng, J. Yu, J. Xu, Journal of Catalysis 2017, 352, 532.

[25] A. Cao, L. Zhang, Y. Wang, H. Zhao, H. Deng, X. Liu, Z. Lin, X. Su, F. Yue, ACS Sustainable Chemistry & Engineering 2018, 7, 2492.

[26] Y. Tan, Z. Shu, J. Zhou, T. Li, W. Wang, Z. Zhao, Applied Catalysis B: Environmental 2018, 230, 260.

[27] Z. Tong, D. Yang, T. Xiao, Y. Tian, Z. Jiang, Chemical Engineering Journal 2015, 260, 117.

[28] Y. Wang, W. Yang, X. Chen, J. Wang, Y. Zhu, Applied Catalysis B: Environmental 2018, 220, 337.

[29] K. Lan, Y. Liu, W. Zhang, Y. Liu, A. Elzatahry, R. Wang, Y. Xia, D. Al-Dhayan, N. Zheng, D. Zhao, J Am Chem Soc 2018, 140, 4135.

[30] L. Shen, Y. Xia, S. Lin, S. Liang, L. Wu, Nanoscale 2017, 9, 14654.

[31] Q. Wang, W. Wang, L. Zhong, D. Liu, X. Cao, F. Cui, Applied Catalysis B: Environmental 2018, 220, 290.

[32] Z.-H. Z. Meng-Yang Ye, Zhuo-Feng Hu, Le-Quan Liu, Hui-Ming Ji, Zhu-Rui Shen, and Tian-Yi Ma, Angew Chem Int Ed Engl 2017, 56, 1.

[33] P. Xia, B. Zhu, B. Cheng, J. Yu, J. Xu, ACS Sustainable Chemistry & Engineering 2017, 6, 965.

[34] J. Fu, Q. Xu, J. Low, C. Jiang, J. Yu, Applied Catalysis B: Environmental 2019, 243, 556.

[35] M. F. Atitar, R. Dillert, D. W. Bahnemann, The Journal of Physical Chemistry C 2017, 121, 4293.

Supporting Information

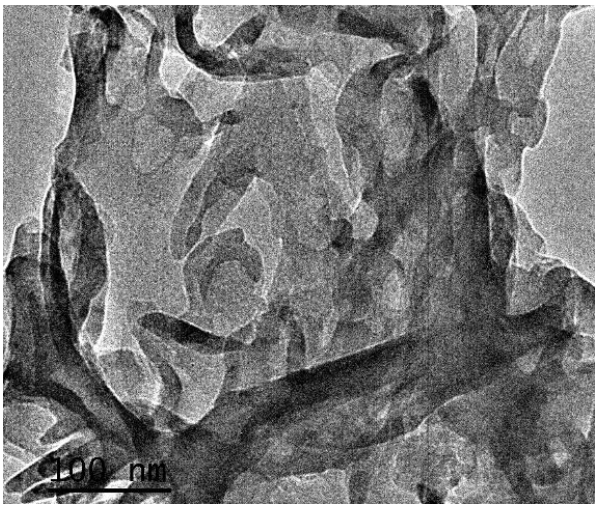

Figure 4-S1 TEM image of as-prepared g-C_3N_4 nanosheets.

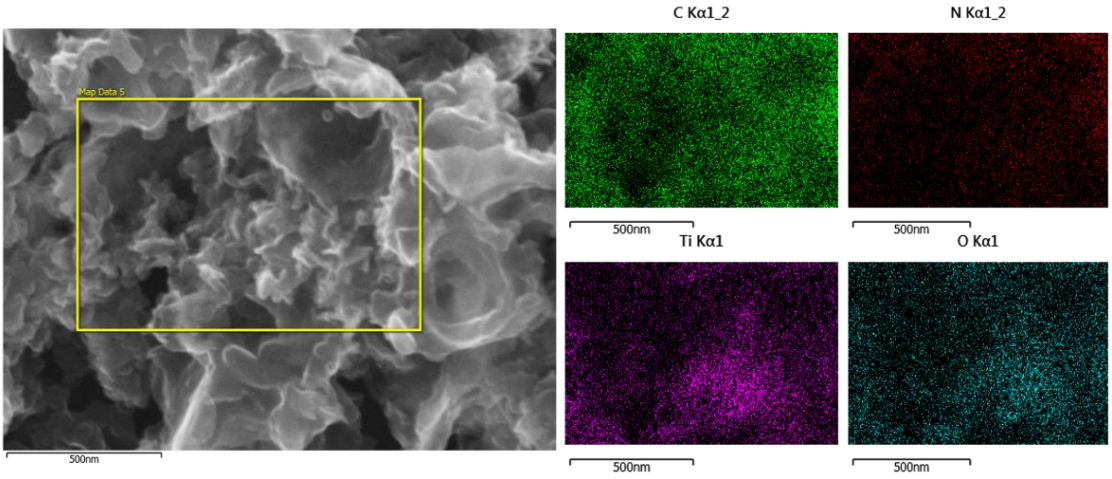

Figure 4-S2 SEM EDX mapping images of TC-33.3% nanocomposites.

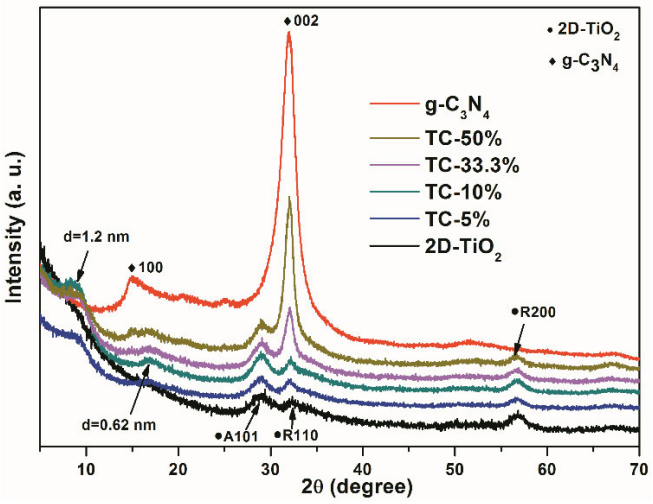

Figure 4-S3 XRD pattern of 2D-TiO_2, TC-5%, TC-10%, TC-33.3%, TC-50% and g-C_3N_4 samples.

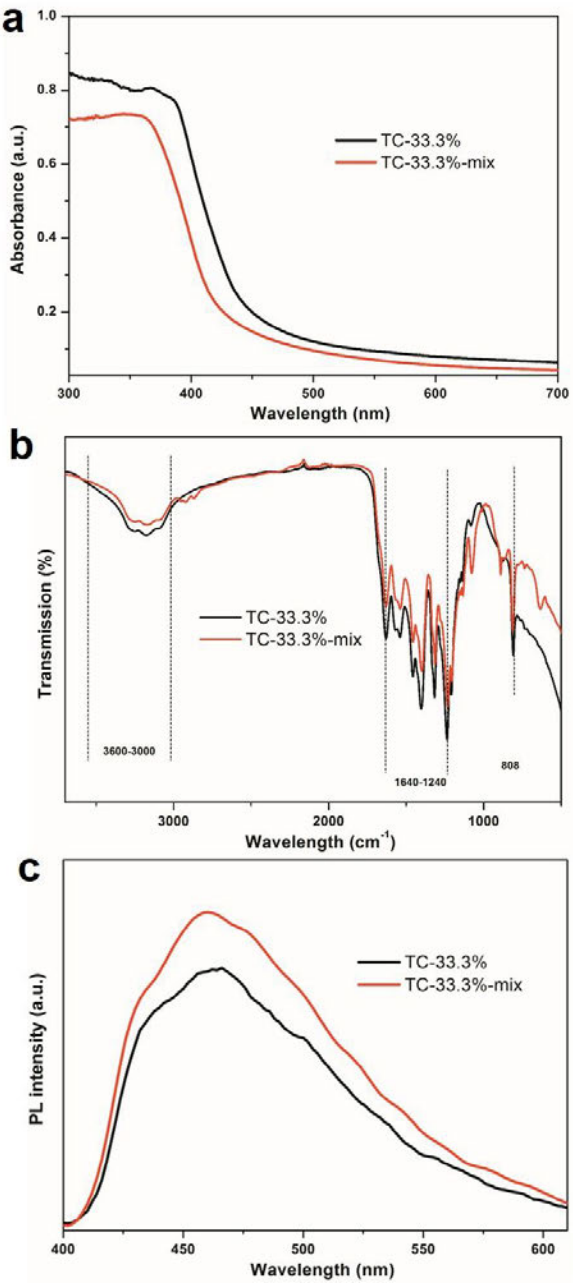

Figure 4-S4 (a) UV-vis diffuse reflectance spectra, (b) FTIR spectra and (c) PL spectra of TC-33.3% and TC-33.3%-mix.

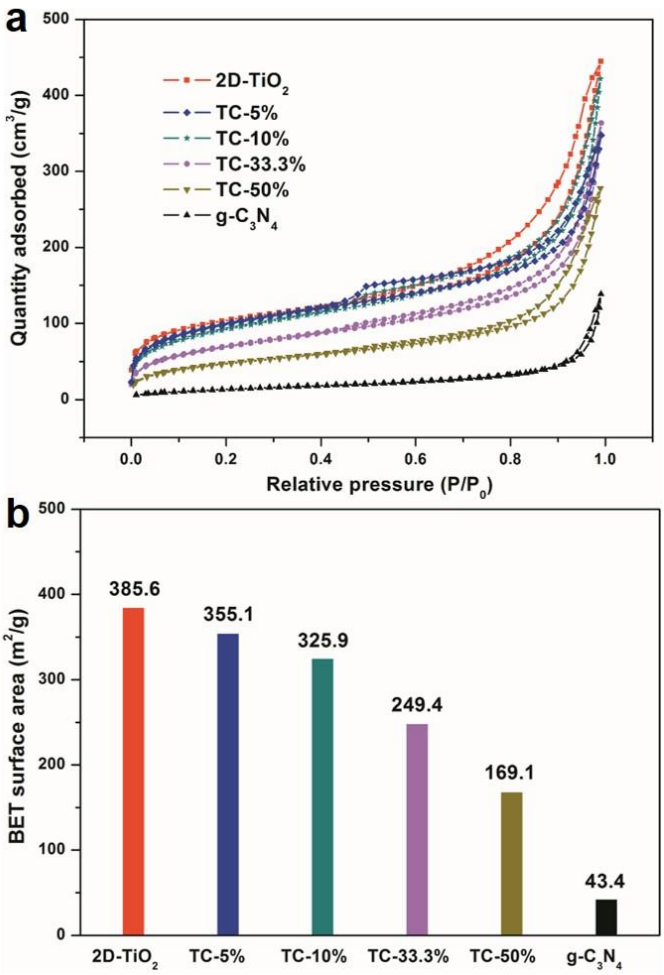

Figure 4-S5 (a) Nitrogen adsorption/desorption isotherms and (b) the BET surface area of 2D-TiO_2, TC-5%, TC-10%, TC-33.3%, TC-50% and g-C_3N_4 samples.

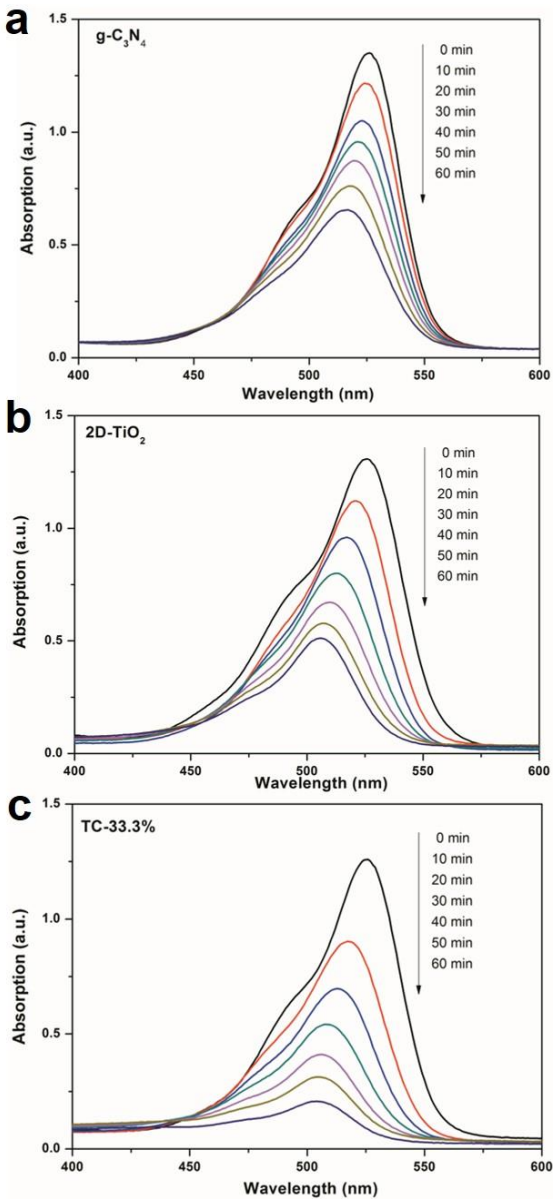

Figure 4-S6 UV-visible spectrum changes of Rhodamine 6G dye over g-C3N4, 2D-TiO2 and TC-33.3% under visible-light irradiation.

Chapter 5. 2D-TiO_2 nanosheets as substrates for Pt photocatalyst

Introductory Remarks

This chapter presents the work of novel 2D-TiO_2 nanosheets as the substrate to load noble metal Pt particles, which showed superb photocatalytic performance in a series of organic transforming reactions. When used for aerobic oxidation under visible light, the Pt loading on 2D-TiO_2 substrates (Pt/2D-TiO2) promote the reaction more efficiently than the Pt loading on commercial P25 (Pt/P25). Such improvement could be attributed to the abundant surface active sites of 2D-TiO_2 aroused by its large surface area and the uniform distribution of noble metal particles on 2D surfaces. This research indicates the advantages of 2D nanomaterial as substrates in metal-loading catalysts, and could provide some beneficial reference for the field of visible-light driven photocatalyst.

5.1 Introduction

Due to the daily increasing energy and environmental challenge around the global society, people are seeking scientific solutions to increase the energy utilizing efficiency and reduce the environmental pollution. Semiconductor photocatalysts have been accepted as a good solution due to their potential applications in photocatalytic water splitting and organic pollution degradation via a sustainable routine.[1-6] Given a wide range of photocatalysts that have been reported to be successfully employed in photocatalytic reactions, TiO_2 has been one of the most widely investigated photocatalyst due to its salient physical and chemial stability and relatively low cost.[7-8] However, as a member of semiconductor family, the chemical nature of TiO_2 determines that it can only be activated by ultraviolet-light irradiation, which has distinctly limited its application in visible-light photocatalysis areas.[9] For example, TiO_2 photocatalysts have usually been reported to be successfully applied in the fields of dye degradation or pollutant treatment, while compared to its effectiveness in such systems, however TiO_2 is not effective enough to perform organic syntheses with high productivity and selectivity, especially under visible-light irradiation.[10] Conducting visible-light-driven selective organic reactions by TiO_2 photocatalysts remains yet a grand challenge.

To solve the low light absorption efficiency of single-phase TiO_2 photocatalyst, constructing TiO_2 with other narrow band gap semiconductor or noble metal to form TiO_2-based heterostructures has been considered as an effective method to promote its photocatalytic performance,[10-11] as the TiO_2-based heterostructures could significantly enhance the light absorption in visible region and meanwhile reduce the charge recombination rate. [12-13] The constructing of TiO_2-based heterostructures with noble metals can improve the photocatalytic properties in two aspects. Firstly, the

loaded noble metals on the TiO_2 surfaces can induce an electron trap to avoid the electrons form recombination with holes.[14-15] More importantly, the loading of noble metals such as Pt on TiO_2 can generate a Schottky barrier at the interface between Pt and TiO_2, which effectively captures the photo-generated electrons and reduces the rate of electron-hole recombination and promotes the organic transforming reactions.[16-17] Recently, loading noble metal atoms on TiO_2 substrates to boost the photocatalytic activities has attracted significant attention. For example, Chung et. al reported a one-pot synthesis approach to prepare Pt-containing TiO_2 materials which showed superior properties in photo-reforming of methanol.[18] Matsubara and co-workers prepared the Pt/TiO_2 catalysts by the polygonal barrel-sputtering method and compared their photocatalytic water splitting performances to those prepared by the conventional photodeposition method.[19]

It is reported that Pt particles exhibited an absorption band in the visible region, arising by the inter band transition of electrons inside the Pt atoms.[20-22] In this work, we demonstrated novel 2D-TiO_2 nanosheets as the substrate to load noble metal atoms, which showed superb photocatalytic performance in a series of organic transforming reactions. When used for aerobic oxidation under visible light, the Pt loading on 2D-TiO_2 substrates (Pt/2D-TiO_2) promote the reaction more efficiently than the Pt loading on commercial P25 (Pt/P25). Such improvement could be attributed to the abundant surface active sites of 2D-TiO_2 aroused by its large surface area and the uniform distribution of noble metal particles on 2D surfaces.

5.2 Experimental

5.2.1 Materials

Titanium (IV) isopropoxide (TTIP, 97%), poly(ethylene glycol)-block-poly(propylene glycol)-block-poly(ethylene glycol) (PEO_{20}-PPO_{70}-PEO_{20}, Pluronic P123),

chloroplatinic acid, L-ascorbic acid and ethylene glycol (EG, anhydrous, 99.8%) were purchased form Sigma-Aldrich. Hydrochloric acid (HCl, 32%) and ethanol (absolute) were obtained from Ajax Finechem. All chemical reagents were used without further modification.

5.2.2 Synthesis of 2D-TiO2 nanosheets

The synthetic method of 2D-TiO_2 nanosheets was reported in our previous paper. In a typical synthetic process, 1.05 g TTIP solution was added into 0.74 g HCl under vigorous stirring in bottle A, and in bottle B, 0.2 g P123 was dissolved in 3.0 g ethanol. After the P123 in bottle B was completely dissolved, the solution was mixed with the solution in bottle A and kept stirring for another 20 minutes. Then 2.5 mL of the mixture solution was transferred into a 45 mL autoclave along with 20 ml EG. The solvothermal process was conducted in an oven at 150 ℃ for 20 hours. The products were obtained by centrifuging and washed in water once and ethanol 3 times. The white powders of 2D-TiO2 nanosheets were collected after drying at 120 ℃ for 8 hours.

5.2.3 Synthesis of Pt/2D-TiO_2 and Pt/P25 catalysts

100 mg P25 TiO_2 or as-prepared 2D-TiO_2 powders were add into 10 ml water, the solution was ultrasonic stirred for 10 min to disperse the powder. Then appropriate amount chloroplatinic acid (40 mM) were added in to TiO_2 water solution. After stirring for 15 h under room temperature, excessive amounts of L-ascorbic acid water solution were added dropwise into the solution. The mixture solution was kept stirring for another 4. The products were washed with deionized water and ethanol for 3 times. The Pt/TiO_2 powders were collected after drying at 120 ℃ for 4 h. All the catalysts were calcined at 350 ℃ for 1 h before use.

5.2.4 Characterization

The morphologies of the samples were characterized by field emission scanning electron microscopy (FESEM, JEOL 7001F) and transmission electron microscopy (TEM, JEOL 2100). The accelerating voltage was 5 kV for SEM and 200 kV for TEM. Diffuse reflectance UV-visible spectra was collected on a Cary 5000 UV-Vis-NIR spectrometer (DRS UV-vis, Agilent) using $BaSO_4$ as reference.

5.2.5 Photocatalytic activity test

The photocatalytic activities of the as-prepared samples were estimated by the aerobic oxidation of benzyl alcohol, methoxybenzyl alcohol and nitrobenzyl alcohol in air under visible light irradiation. Oxidation of benzyl alcohol: 20 mg of catalyst was dispersed into 1 ml toluene containing 0.1 mmol benzyl alcohol in a 10 ml Pyrex glass tube. The reaction was conducted under irradiation of a 500 W halogen lamp (0.6 W/cm^2, $\lambda > 400$ nm) at 55 ℃ for 20 hours. Oxidation of methoxybenzyl alcohol and nitrobenzyl alcohol: 10 mg of catalyst was dispersed into 2 ml toluene containing 0.2 mmol methoxybenzyl alcohol or nitrobenzyl alcohol in a 10 ml Pyrex glass tube. The reaction was conducted under irradiation of a 500 W halogen lamp (0.6 W/cm^2) at 45 C for 20 hours. After the reaction, the aliquots were collected, centrifuged, and then filtered through a Millipore filter (pore size 0.45 μ m) to remove the catalyst particles. The products were analyzed by gas chromatography (GC, Agilent).

5.3 Results and discussion

The morphologies of as-prepared Pt/P25 and Pt/2D-TiO_2 catalysts were characterized by SEM and TEM technics. The SEM images of Pt/P25 samples are shown in **Figure 5-1**. It can be seen that all the Pt/P25 samples presented a well-organized P25 particle distribution, however the Pt particles loading on the P25 surfaces suffered from a serve agglomeration. As the Pt loading was higher, the more particles were aggregated to form Pt clusters. As it can be seen in Figure 1, the aggregated Pt clusters in $Pt_{0.25}$/P25

are in sizes of several nanometers (**Figure 5-1a, b**), with higher Pt loadings, the sizes of Pt clusters get larger and reach about 20 nm in Pt_2/P25 (**Figure 5-1g, h**). Such aggregation of Pt particles will badly reduce the total active sites of the catalysts and thus leads to a poor catalytic performance.

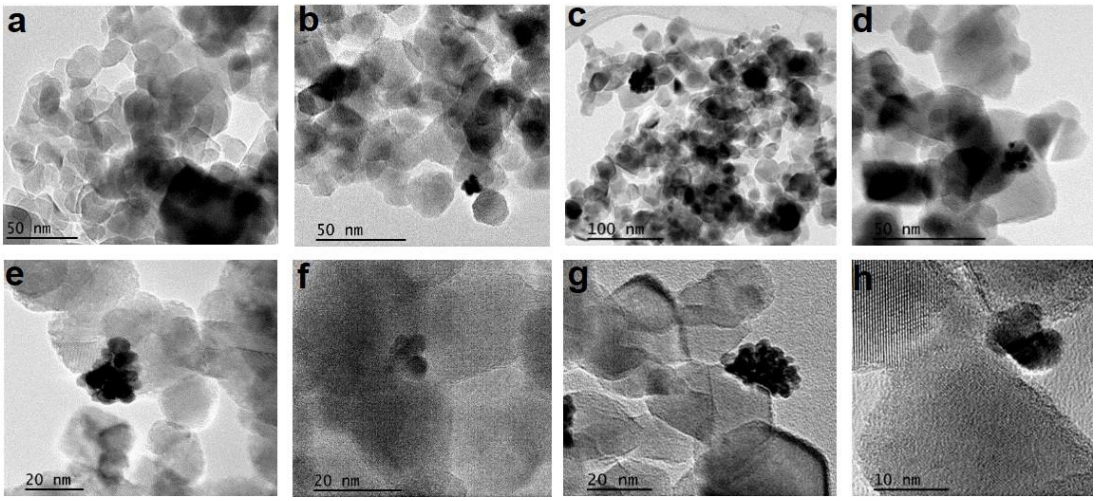

Figure 5-1 Morphologies of Pt/P25 catalysts. (a, b) Low and high resolution SEM images of $Pt_{0.25}$/P25 catalysts; (c, d) Low and high resolution SEM images of $Pt_{0.5}$/P25 catalysts; (e, f) Low and high resolution SEM images of Pt_1/P25 catalysts; (g, h) Low and high resolution SEM images of Pt_2/P25 catalysts.

The morphologies and particle distributions of Pt/2D-TiO_2 samples were also investigated by electron microscope. Due to the relative small particle size, we performed TEM on these samples to better observe the distribution of Pt particles on 2D-TiO2 surfaces. As shown in **Figure 5-2**, the 2D-TiO_2 were clearly observed in all the samples, and some of the nanosheets were curled up completely to nanoscrolls and some others were sintered during the heating process. However, the 2D nanosheet structure can still be clearly distinguished in the TEM image. In the $Pt_{0.25}$/2D-TiO_2 sample (**Figure 5-2a**), it can be seen that some small Pt particles with sizes about 2-3 nm are dispersed uniformly on the 2D-TiO_2 substrate. While the Pt loading increased to 0.5% and 1%, as demonstrated in **Figure 5-2** b and c, the Pt particles are still well-

dispersed, with their sizes being larger to about 3-5 nm. However, in the Pt_2/2D-TiO_2 sample (**Figure 5-2d**), it is clearly seen that several Pt clusters with sizes larger than 10 nm formed due to the aggregation. From these results, it is believed that the Pt loading amounts will have influence on the their distribution sizes and morphologies of the final catalysts.

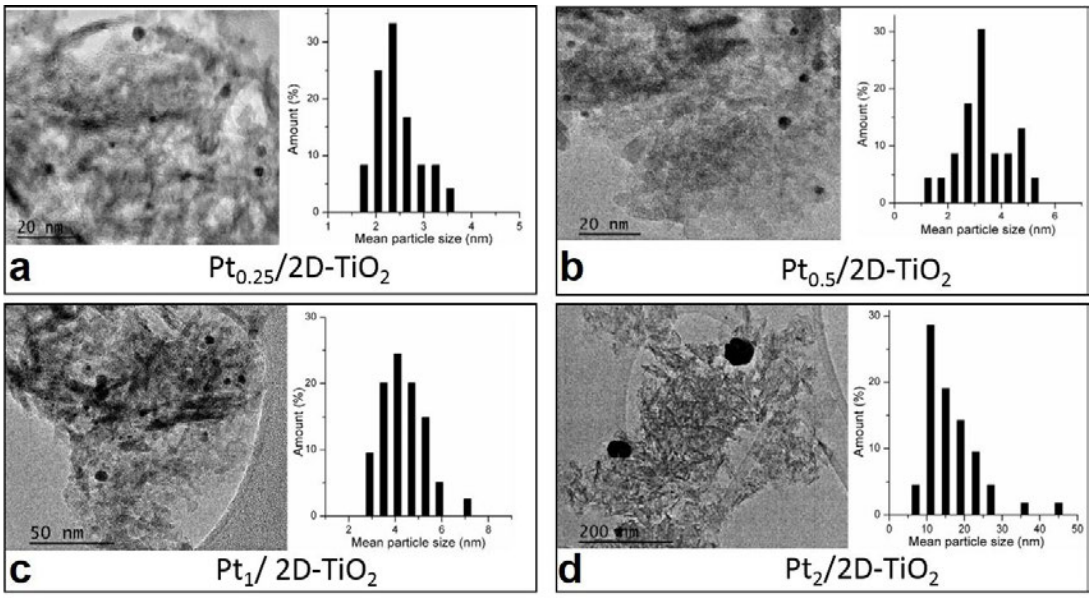

Figure 5-2 Morphologies of Pt/2D-TiO_2 catalysts. TEM image and particle size distribution of (a) $Pt_{0.25}$/2D-TiO_2, (b) $Pt_{0.5}$/2D-TiO_2, (c) Pt_1/2D-TiO_2 and (d) Pt_2/2D-TiO_2 catalysts.

To better characterize the Pt distribution on the 2D-TiO2 surfaces, High-angle annular dark field (HAADF) TEM was performed on $Pt_{0.25}$/2D-TiO_2 and $Pt_{0.5}$/2D-TiO_2 samples. As can be seen in **Figure 5-3**, some small bright dots are uniformly distributed on the 2D-TiO2 substrates, which are referred to the Pt particles. Compared to the normal TEM characterizations, HAADF TEM technic has much higher resolutions, as a result, some Pt particles with sizes even smaller than 1 nm can be distinguished as indicated by the red marks in **Figure 5-3a**. With such small size distribution of Pt particles, the total active sites of the catalyst will increase a lot, thus leading to better catalytic performances.

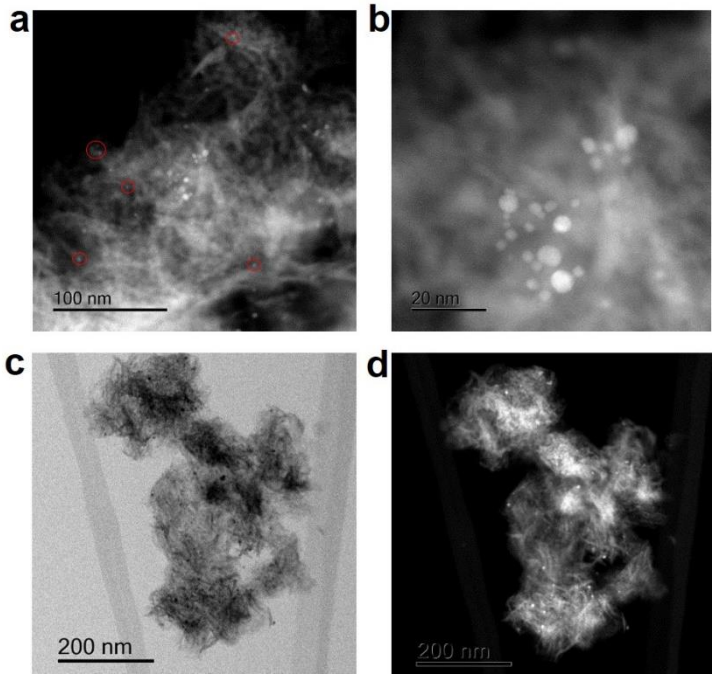

Figure 5-3 High-angle annular dark field (HAADF) TEM images of Pt/2D-TiO_2 catalysts. (a, b) HAADF images of $Pt_{0.25}$/2D-TiO_2, (c, d) HAADF images of $Pt_{0.5}$/2D-TiO_2.

To comfirm the loading amount of Pt on the TiO_2 substrates, we conducted conductively coupled plasma optical emission spectrometer (ICP-OES) test to check the metal content in the as-prepared Pt/2D-TiO_2 and Pt/P25 catalysts. As shown in **Table 5-1**, the Ti weight content of all 8 samples are about 20%, which is matching with the natural content ration in TiO_2. The Pt content in Pt/P25 samples are 0.25%, 0.52%, 0.98%, and 1.96% for $Pt_{0.25}$/P25, $Pt_{0.5}$/P25, Pt_1/P25 and Pt_2/P25, respectively, which is perfectly matching with the designed Pt loading amount. The Pt content in Pt/2D-TiO_2 samples are 0.33%, 0.74%, 1.37%, and 2.56% for $Pt_{0.25}$/2D-TiO_2, $Pt_{0.5}$/2D-TiO_2, Pt_1/2D-TiO_2 and Pt_2/2D-TiO_2, respectively, which is a bit higher than the designed amount, this could be attributed to the residual water and organic content in the 2D-TiO_2. The ICP-OES test evidently confirmed the Pt loading amount in the as-prepared catalysts, and indicated that the Pt loading amount in the final product basically accord with the previously designed amount.

Table 5-1 Conductively coupled plasma optical emission spectrometer (ICP-OES) test on Pt/2D-TiO_2 and Pt/P25 catalysts

Samples	Relative amount (mg/L)		Pt loading (wt %)
	Pt	Ti	
Pt0.25/2D-TiO2	0.118	21.27	0.33
Pt0.5/2D-TiO2	0.263	21.19	0.74
Pt1/2D-TiO2	0.462	20.18	1.37
Pt2/2D-TiO2	0.846	19.80	2.56
Pt0.25/P25	0.095	22.99	0.25
Pt0.5/P25	0.182	21.07	0.52
Pt1/P25	0.383	23.44	0.98
Pt2/P25	0.705	21.56	1.96

UV-vis diffuse reflectance spectra (DRS) was studied to explore the optical properties of the Pt/2D-TiO_2 and Pt/P25 samples (**Figure 5-4**). The DRS spectra of P25 nanoparticles and 2D-TiO2 nanosheets were also recorded as a reference. As shown in **Figure 5-4**, it can be seen that, after loading Pt particles on TiO2, the light absorption of both Pt/2D-TiO_2 and Pt/P25 enhanced very obviously, and both of them presented an increasing trend with higher Pt loading. To be noted, the light absorption of all Pt/2D-TiO_2 catalysts are higher than that of Pt/P25 catalysts, especially in the region from 380 to 500 nm. The absorption onsets of Pt/2D-TiO_2 are also lower than that of Pt/P25, indicating better light absorption in UV region. Such improvement could be caused by the better particle distribution and finer particle size of Pt/2D-TiO_2. The insets show the optical colour of the as-prepared samples, it is clearly seen that the Pt/2D-TiO_2 samples are more colourful than Pt/P25 samples, which means a better visible light absorption.

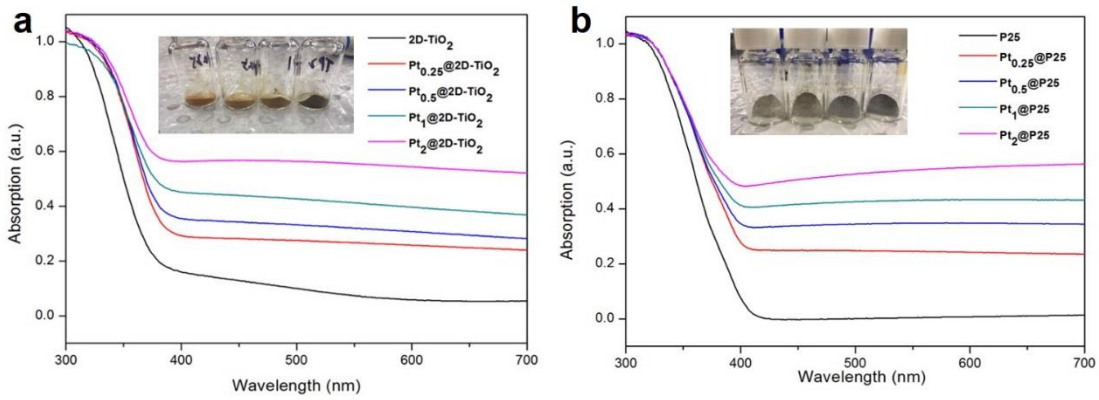

Figure 5-4 Optical properties of Pt/2D-TiO_2 and Pt/P25 catalysts. (a) UV-vis diffuse reflectance spectra (DRS) of Pt/2D-TiO_2, the inset shows the optical images of $Pt_{0.25}$/2D-TiO_2, $Pt_{0.5}$/2D-TiO_2, Pt_1/2D-TiO_2 and Pt_2/2D-TiO_2, from left to right, repectively; (b) UV-vis diffuse reflectance spectra (DRS) of Pt/2D-P25, the inset shows the optical images of $Pt_{0.25}$/P25, $Pt_{0.5}$/P25, Pt_1/P25 and Pt_2/P25, from left to right, repectively;

The photocatalytic properties of Pt/2D-TiO_2 and Pt/P25 were investigated by the light-promoted organic reaction of oxidation of benzylalcohol. From **Figure 5-5a**, it is clearly seen that the Pt/2D-TiO_2 catalyst exhibits higher reactive activity than Pt/P25 do in converting benzylalcohol into corresponding aldehyde with high selectivity (> 90%), however they both presented very low activity in the absence of visible light. However, in dark condition, the Pt/2D-TiO_2 catalysts presented much higher activity than Pt/P25 catalysts. As shown in **Figure 5-5b**, all the Pt/2D-TiO_2 catalysts exhibited much higher turnover number than Pt/P25 catalysts, and the $Pt_{0.5}$/2D-TiO_2 catalyst presented the highest activity, with a turnover number of 90, which is 8 folds higher than that of $Pt_{0.5}$/P25. Such improvement in dark reactions indicates better thermal activity of Pt/2D-TiO_2 catalysts.

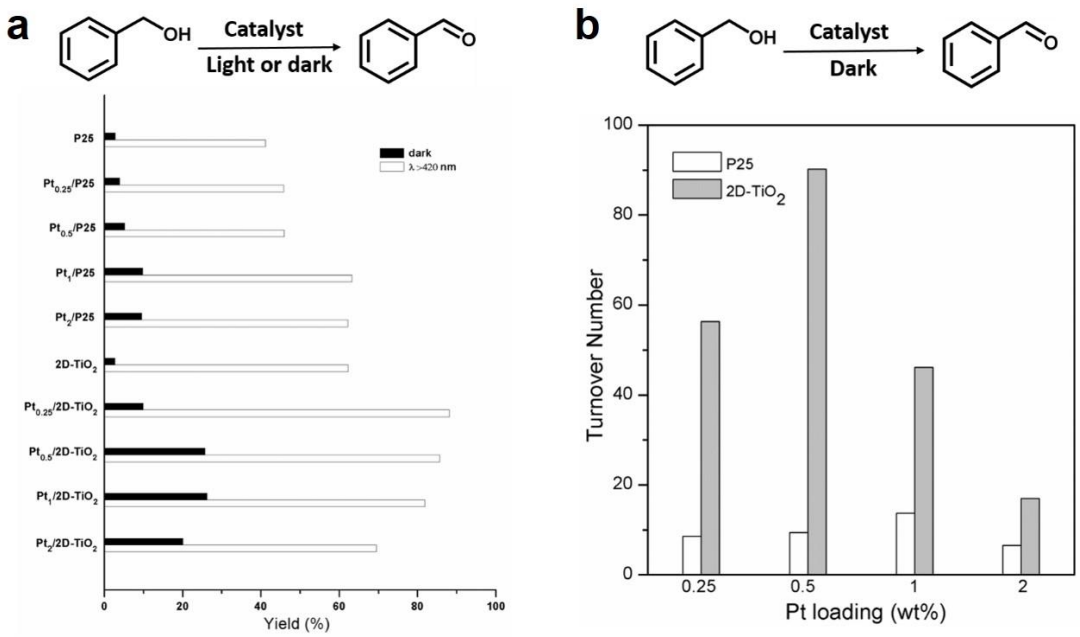

Figure 5-5 Photocatalytic performances of Pt/2D-TiO_2 and Pt/P25 catalysts. (a) Photocatalytic performances of Pt/2D-TiO_2 and Pt/P25 catalysts over benzylalcohol oxidation reacitons; (b) Turnover number of Pt/2D-TiO_2 and Pt/P25 catalysts over benzylalcohol oxidation reacitons.

The photocatalytic performance of as-prepared Pt/2D-TiO_2 and Pt/P25 were also tested over other series of organic transforming reactions including the aerobic oxidation of methoxybenzyl alcohol and nitrobenzyl alcohol. As shown in **Figure 5-6**, the photocatalytic activities of the catalysts exhibited a similar trend as that of benzyl alcohol oxidation reaction. All the Pt/2D-TiO_2 catalysts presented higher activity in processing corresponding reactions. The higher photocatalytic activity of Pt/2D-TiO_2 should mainly be attributed to three reasons. Firstly, the large surface area associated with the ultrathin thickness of the 2D-TiO_2 substrate is of beneficial for the obtaining sufficient active sites on the surfaces. Secondly, the ultrathin thickness of 2D-TiO_2 nanosheets could significantly improve the charge separation due to the reduced charge transfer distance from the centre of bulk to the surface. Thirdly, the better distribution and fine particle size of loaded Pt on 2D-TiO_2 contribute to more active sites and higher visible light absorption.

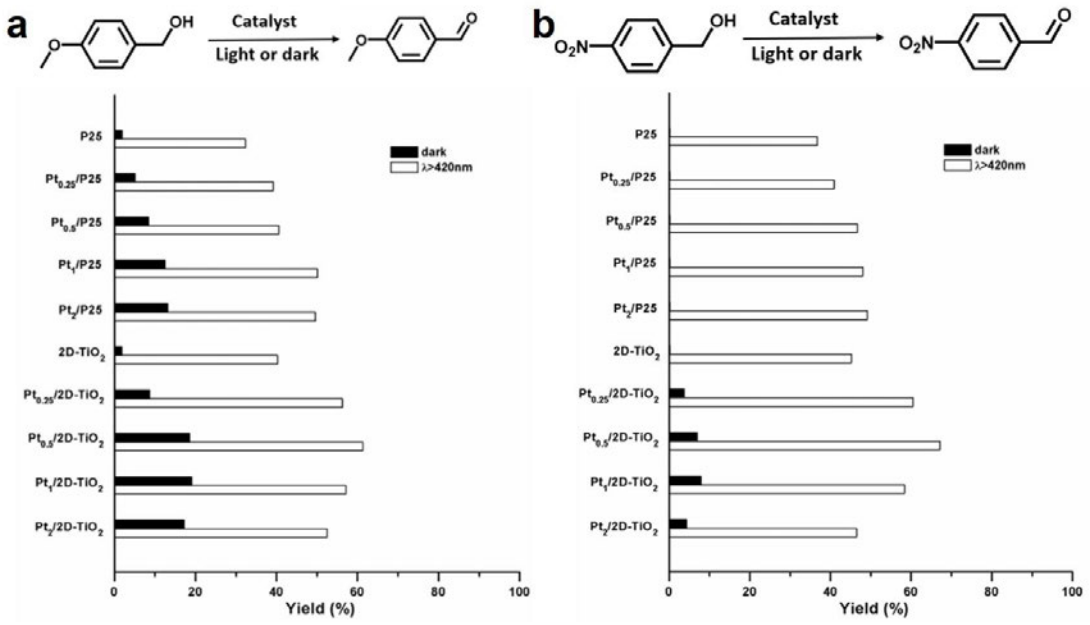

Figure 5-6 Photocatalytic performances of Pt/2D-TiO_2 and Pt/P25 catalysts over (a) methoxybenzyl alcohol and (b) nitrobenzyl alcohol.

5.4 Conclusion

In this work, we demonstrated novel 2D-TiO_2 nanosheets as the substrate to load noble metal Pt particles, which showed superb photocatalytic performance in a series of organic transforming reactions. When used for aerobic oxidation under visible light, the Pt loading on 2D-TiO_2 substrates (Pt/2D-TiO_2) promote the reaction more efficiently than the Pt loading on commercial P25 (Pt/P25). Such improvement could be attributed to the abundant surface active sites of 2D-TiO_2 aroused by its large surface area and the uniform distribution of noble metal particles on 2D surfaces. This research indicates the advantages of 2D nanomaterial as substrates in metal-loading catalysts, and could provide some beneficial reference for the field of visible-light driven photocatalyst.

References

[1] L. Buzzetti, G. E. M. Crisenza and P. Melchiorre, Angew Chem Int Ed Engl, 2019, *58*, 3730-3747.

[2] H. Kisch, Acc Chem Res, 2017, *50*, 1002-1010.

[3] L. Marzo, S. K. Pagire, O. Reiser and B. Konig, Angew Chem Int Ed Engl, 2018, *57*, 10034-10072.

[4] A. Meng, L. Zhang, B. Cheng and J. Yu, Adv Mater, 2019, *31*, e1807660.

[5] M. Xiao, Z. Wang,M. Lyu,B. Luo,S. Wang, G. Liu,H. M. Cheng and L. Wang, Adv Mater, 2019, *31*, e1801369.

[6] C. Xu, P. Ravi Anusuyadevi, C. Aymonier, R. Luque and S. Marre, Chem Soc Rev, 2019, *48*, 3868-3902.

[7] Q. Guo, C. Zhou, Z. Ma and X. Yang, Adv Mater, 2019, *31*, e1901997.

[8] X. Li, J.-L. Shi, H. Hao and X. Lang, Applied Catalysis B: Environmental, 2018, *232*, 260-267.

[9] V. Likodimos, Applied Catalysis B: Environmental, 2018, *230*, 269-303.

[10] M. E. Aguirre, R. Zhou, A. J. Eugene,M. I. Guzman and M. A. Grela, Applied Catalysis B: Environmental, 2017, *217*, 485-493.

[11] L. Guo, Z. Li,K. Marcus, S. Navarro, K. Liang, L. Zhou, P. D. Mani, S. J. Florczyk, K. R. Coffey, N. Orlovskaya,Y. H. Sohn and Y. Yang, ACS Sens, 2017, *2*, 621-625.

[12] A. Cabrera-Reina, A. B. Martinez-Piernas, Y. Bertakis, N. P. Xekoukoulotakis, A. Aguera and J. A. Sanchez Perez, Water Res, 2019, *166*, 115037.

[13] L. Zheng, F. Teng, X. Ye,H. Zheng and X. Fang, Advanced Energy Materials, 2019, *10*, 1902355.

[14] X. Zhou, V. Haublein, N. Liu, N. T. Nguyen, E. M. Zolnhofer,H. Tsuchiya,M. S. Killian, K. Meyer, L. Frey and P. Schmuki, Angew Chem Int Ed Engl, 2016, *55*, 3763-7.

[15] E. Antolini, Applied Catalysis B: Environmental, 2018, *237*, 491-503.

[16] S. Kattel, B. Yan, J. G. Chen and P. Liu, Journal of Catalysis, 2016, *343*, 115-126.

[17] Y. Zhao, Y. Wei, X. Wu, H. Zheng, Z. Zhao,J. Liu and J. Li, Applied Catalysis B: Environmental, 2018, *226*, 360-372.

[18] Y.-H. Chung, K. Han, C.-Y. Lin, D. O'Neill, G. Mul, B. Mei and C.-M. Yang, Catalysis Today, 2019.

[19] K. Matsubara, M. Inoue, H. Hagiwara and T. Abe, Applied Catalysis B: Environmental, 2019, *254*, 7-14.

[20] G. Gao, Y. Jiao, E. R. Waclawik and A. Du, J Am Chem Soc, 2016, *138*, 6292-7.

[21] X. Liu, J. Iocozzia, Y. Wang,X. Cui,Y. Chen,S. Zhao,Z. Li and Z. Lin, Energy & Environmental Science, 2017, *10*, 402-434.

[22] A. Meng, L. Zhang, B. Cheng and J. Yu, ACS Appl Mater Interfaces, 2019, *11*, 5581-5589.

Chapter 6. Conclusions and outlooks

To summarize, in this thesis, the design of 2D-TiO_2 based nanomaterials for sustainable applications such as photocatalysis, electrocatalysis, rechargeable batteries and bio-inspired applications are discussed in detail. Three research works including "structure-induced charge unsaturation and wide-band light adsorption for enhanced photocatalytic performance", "strongly interfacial-coupled 2D-2D TiO_2/g-C_3N_4 heterostructure for enhanced visible-light induced synthesis and conversion" and "2D-TiO_2 nanosheets as substrates for Pt photocatalyst" are presented respectively.

In Chapter 3, a new strategy to modify the chemical state and electronic structure of metal oxide semiconductor realized by manipulating the crystal structure of homogeneous 2D-TiO_2 nanosheets is proposed, in which no foreign doping impurities nor inherent vacancy defects are included. The crystallized 2D-TiO_2 nanosheets exhibited unconventional electronic states compared to its bulk counterparts, aroused by the 2D derived lattice distortion in the nanosheet structures. The structure-induced charge transfer from O atoms to Ti atoms resulted in reduced chemical states of the Ti metals in the 2D-TiO_2 nanosheet structures, which presented extraordinary optical and catalytic properties compared to those with conventional bulk crystal structures. Moreover, this structure also maintained the salient surface physical and chemical properties of 2D materials, such as the enlarged surface area which is beneficial for creating abundant surface active sites, leading to a better catalytic performance in the photocatalytic oxidation reactions of benzyl alcohol and benzylamine.

In Chapter 4, 2D-2D TiO_2 nanosheet/g-C_3N_4 heterostructure with strongly interfacial coupling was synthesized by direct growth of ultrathin 2D-TiO_2 nanosheets on the 2D g-C_3N_4 templates. Different to the commonly used method for fabricating

weakly contact 2D-2D heterostructures through physically mixing two oppositely surface charged 2D nanosheets, this in-situ growth of 2D-TiO_2 nanosheet on 2D g-C_3N_4 allows the formation of strong chemical bonds between the nanosheets during the self-assembly. As a result we expected, much more significant charge transfer and stronger interfacial coupling occur of the in-situ grown, strongly bonded 2D-2D heterostructures than the corresponding physically mixed, weakly bonded 2D-2D heterostructures, and endorse the materials with much enhanced catalytic activities, particularly under visible light irradiations. We therefore proposed that the strongly coupled 2D-2D heterojunctions can further alter the interfacial electronic structure and much enhance visible light induced photosynthesis and photocatalysis activities, would provide us a new path for designing novel 2D based catalysts towards high-performance photocatalysis or electrochemical catalysis.

In Chapter 5, we demonstrated novel 2D-TiO2 nanosheets as the substrate to load noble metal Pt particles, which showed superb photocatalytic performance in a series of organic transforming reactions. When used for aerobic oxidation under visible light, the Pt loading on 2D-TiO_2 substrates (Pt/2D-TiO_2) promote the reaction more efficiently than the Pt loading on commercial P25 (Pt/P25). Such improvement could be attributed to the abundant surface active sites of 2D-TiO_2 aroused by its large surface area and the uniform distribution of noble metal particles on 2D surfaces. This research indicates the advantages of 2D nanomaterial as substrates in metal-loading catalysts, and could provide some beneficial reference for the field of visible-light driven photocatalyst.

Although some progress has been made in the field of 2D nanomaterials, the challenges and limitations still remain and yet to be overcame in this emerging research area. For example, the 2D-TiO_2 nanosheet with charge-unsaturation exhibited

enhanced photocatalytic activity compared to commercial P25 TiO_2 catalysts, however the catalytic performance is still far from practical requirement. Also, taking practicability into consideration, the productivity is another big challenge for the development of 2D nanomaterials. And the thermal stability of 2D-TiO_2 is another problem that the 2D morphology cannot maintain during high-temperature calcination. Further research and investigations are still required to improve the quality, productivity and property of 2D nanomaterials.

In the future work, more researches and investigations will be made in the field of 2D-TiO_2 based sustainable applications. For example, the 2D-TiO_2 derived $Li_2Ti_5O_{12}$ nanomaterials showed superior battery capacity compared to the P25 derived counterparts in our early-stage investigation, the transition temperature point from TiO_2 to $Li_2Ti_5O_{12}$ has been determined by the calcination experiments under various heating rates and temperatures, however, we still need more detailed investigations and characterizations to figure out the structural feature and mechanism of 2D-TiO_2 derived $Li_2Ti_5O_{12}$ nanomaterials in Li-ion rechargeable batteries. Meanwhile, study on other 2D nanomaterials such as 2D-Co_3O_4 and 2D-MnO_2 will also be focused in our future research due to their promising potential in energy storage areas including electrocatalysis and rechargeable batteries. As investigated in Chapter 3, the crystallized 2D-TiO_2 nanosheets exhibited unconventional electronic states compared to its bulk counterparts, aroused by the 2D derived lattice distortion in the nanosheet structures. The same features were also found in 2D-Co_3O_4 and 2D-MnO_2 which were synthesized via similar wet-chemistry self-assembly method. The chemical binding energy shift was determined by XPS characterization in both 2D-Co_3O_4 and 2D-MnO_2 heat-treated under various temperature and they showed different electrochemical activities in the corresponding OER tests. In future work, more systematic researches

are expected to carry on the characterizations of 2D-Co_3O_4 and 2D-MnO_2 as well as the related electrocatalytic tests. In addition, the exploration on other promising 2D nanomaterials such as graphene, g-C3N4, MXenes in sustainable applications including photocatalysis, electrocatalysis and rechargeable batteries will also be included in our future research plans. In a word, it is believed that the research and investigations on 2D nanomaterials based sustainable applications is of great significance for the further development of a green, sustainable and environmental society.